ETHANOL CONVERSION TO HIGHER ALCOHOLS OVER HYBRID $CuZn/SiO_2$ ¦ Mg-KNaX CATALYST

PITTAWAT SUKKEAW

A THESIS SUBMITTED IN PARTIAL FULFILLMENT OF THE REQUIREMENT FOR THE DEGREE OF MASTER OF SCIENCE IN APPLIED CHEMISTRY SCHOOL OF SCIENCE KING MONGKUT'S INSITUTE OF TECHNOLOGY LADKRABANG

2022

KMITL-2022-SC-M-050-065

Thesis Title	Ethanol conversion to higher alcohol over hybrid CuZn/SiO_2 ¦ Mg-KNaX catalyst
Students Name	Mr. Pittawat Sukkeaw
Student ID	60605032
Degree	Master of science (Applied Chemistry)
Department	Chemistry
Year	2022
Thesis Advisor	Assistant Professor Dr. Natthida Numwong
Thesis Co-advisor	Professor Dr. Tawan Sooknoi

Abstract

High conversion of ethanol to higher alcohols was obtained over hybrid CuZn/SiO_2 ¦ Mg-KNaX catalyst. CuZn/SiO_2 and a series of Mg-KNaX catalysts were prepared and characterized by XRF, N_2-physisorption, SEM-EDS, H_2-TPR, XRD, and TPD of NH_3 and CO_2. The CuZn/SiO_2 shown high activity with acetaldehyde selectivity up to 98%, particularly with the presence of H_2. Highly dispersed MgO species over Mg-KNaX provided both basic and acid sites for aldol condensation and hydrogen transfer. The increase in Mg content did not only enhance higher alcohol selectivity, but also decrease the dehydration of ethanol to ethylene. The hybrid CuZn/SiO_2 ¦ Mg-KNaX catalyst in physical mixed bed system provided up to 50% conversion with 66% total higher alcohol selectivity and higher stability. The synergistic effect between CuZn/SiO_2 and Mg-KNaX, observed in the physical mixed bed system with the ratio of 0.2, was derived from the balanced dehydrogenation, hydrogen transfer and aldol condensation rate.

Keywords: Ethanol, higher alcohols, hybrid catalyst, hydrogen transfer, aldol condensation, CuZn, Mg

Acknowledgement

The author desires to appreciatively thank my advisors, Professor Dr. Tawan Sooknoi and Assistant Professor Dr. Natthida Numwong for suggestions, inspiration, carefulness, reassurance, experimental instrument, and knowledge in catalysis throughout this research

I would like to gratefully acknowledge chairperson and committee, Assistant Professor Dr. Sabaithip Tungkamani and Associate Professor Dr. Karoon Sadorn for judgment and valuable comments.

Moreover, I would like to acknowledge the financial support from Research Grant for New Scholar (RGNS), Office of the Permanent Secretary, Ministry of Higher Education, Science, Research and Innovation (Grant No. RGNS 63 - 248) and SCG Chemicals Co. Ltd. In addition, I would like to thank Faculty of Science, King Mongkut's Institute of Technology Ladkrabang for the equipment, chemicals, and facilities.

Unforgettable, I would like to grateful to my friends, my brothers in Catalytic Chemistry Research Unit (CCR group) for their help, advice, support, and encouragement.

Finally, I deeply appreciate and thank our parents and family for their love and support.

Mr. Pittawat Sukkeaw

LIST OF CONTENTS

LIST OF TABLES

LIST OF FIGUERS

LIST OF SCHEMES

Chapter 1

Introduction

1.1 Motivation

In addition to fuel additives and solvent, bio-ethanol has become one of the most interesting renewable resources as a chemical building block, these days [1-2]. It can be typically produced from fermentation of various feedstock, i.e., sugarcane, starch, corn, or hydrolyzed lignocellulosic biomass [3]. Accordingly, conversion of ethanol to chemicals could be a promising approach to replace non-renewable fossil feedstock. This is particularly for production of higher alcohols, i.e., butanol, hexanol, and octanol, which were widely used in various industries such as medicines, cosmetics, detergents, etc. [4-5]. Moreover, compared to bio-ethanol, higher alcohols have high potential properties for additive in gasoline due to higher cetane number higher energy density and compression ignition quality and so on [6]. These advantages of higher alcohols make upgrading of bio-ethanol to higher alcohols very interesting.

Catalytic conversion of ethanol to higher alcohol involves a Guerbet reaction [7-8]. In this reaction, ethanol is dehydrogenated to acetaldehyde follows by aldol condensation of aldehydes to larger unsaturated one. The last step is hydrogen transfer forming higher alcohol. The main requirements of catalyst are optimal number of Lewis acid-base sites that provide comparable rate of aldol condensation and hydrogen transfer [9-11]. Excessive acid sites lead to a dehydration of ethanol to undesirable ethylene and diethyl ether, suppressing aldol condensation to higher alcohols. In addition, dehydrogenation of ethanol should be initially promoted otherwise small amount of higher molecular weight products would be obtained due to the lack of acetaldehyde. Accordingly, optimization between the rate of dehydrogenation/hydrogen transfer and aldol condensation is a key for higher alcohol production.

Various catalysts possessing both acid and basic sites were reported for Guerbet reaction, such as Mg/Al layered double hydroxides (Mg/Al LDHs) [12-14], hydroxyapatites [15-16], and MgO [17-18]. Even the Mg-Al LDHs had appropriately acid-base capacity for ethanol conversion, the

layered structure had a low water tolerance leading to the gradual decrease in activity and butanol selectivity [12]. Although hydroxyapatites provided high butanol selectivity with high stability, it offers low conversion due to relatively low surface area and difficulty in catalysts preparation [15-16]. Comparatively, the MgO, which had both weak Lewis acid site (surface Mg^{2+}) and strong Bronsted basic site (surface O^{2-}), shows high aldol condensation rate, providing higher butanol with lower ethylene yield [17]. However, low dehydrogenation rate was obtained from relatively low surface area of bulk MgO [18-21].

To improve MgO active surface, the MgO can be incorporated into zeolite supports via ion exchange followed by precipitation. This method provides high dispersion of MgO nanoparticles in zeolite cavity leads to an increase in proximate acid-base site capacity in definite form of zeolite framework. Zhang, et al. [22], reported that MgO incorporated faujasite catalyst (13X) provide 94.5% C4 aldehyde selectivity with 5.5% butanol selectivity for the conversion of acetaldehyde. In line with this observation, we have recently reported that aldol condensation rate depended on amounts of occluded $[Mg_4(OH)_4]^{4+}$ species in KNaX [23]. Moreover, the zeolite confinement can inhibit excessive condensation to coke precursors [22]. However, the catalyst still offers limited dehydrogenation activity leading a relatively low conversion of ethanol to higher alcohol. Accordingly, incorporation of dehydrogenation catalyst to the Mg-KNaX could improve dehydrogenation/hydrogen transfer activity to produce higher alcohol. With this regard, the copper base catalyst, such as Cu-SiO_2 [24], Cu-ZnO-Al_2O_3 [25], and Cu-ZnO catalysts [26], were widely used for ethanol dehydrogenation to acetaldehyde. M. Ohira et al. [27] reported that incorporation of ZnO into Cu/SiO_2 can improve the stability of ethanol dehydrogenation with high acetaldehyde yield (~80%). This is presumably due to strong interaction of Zn with Cu, which could limit the Cu sintering on the SiO_2 support.

Herein, CuZn/SiO_2 was incorporated with Mg-KNaX as a hybrid catalyst system in physical mixed bed and sequential bed. The conversion of ethanol to higher alcohols over the hybrid CuZn/SiO_2¦Mg-KNaX catalysts has been demonstrated in flow reactor at 380°C under atmospheric N_2 or H_2 pressure. The catalysts were characterized by XRD, XRF, N_2 adsorption, SEM-EDS, H_2-TPR. NH_3-TPD and CO_2 -TPD were also tested for acid-base properties of the catalysts. The effect of Mg loading, type of carrier gas and bed configuration on the catalytic activity and stability were investigated. The ratio between CuZn/SiO_2 and Mg-KNaX, that synergistically regulated the

dehydrogenation/hydrogen transfer and aldol condensation activity of the hybrid catalyst system, was also considered.

1.2 Objectives

1) To produce higher alcohols from ethanol via Guerbet reaction
2) To understand the effect of carrier gas on ethanol dehydrogenation to acetaldehyde over Cu-Zn/SiO_2 catalysts.
3) To understand the effect of MgO loading, acid-base properties, and contact time on the conversion of ethanol to higher alcohols over Mg-KNaX catalysts.
4) To study the effect of bed configuration: sequential bed and physical mixed bed on the conversion of ethanol to higher alcohols over hybrid CuZn/SiO_2 ¦ Mg-KNaX catalysts.

1.3 Scopes of study

1) Preparation of CuZn/SiO_2 catalyst by wetness impregnation.
2) Preparation of MgO incorporated Na zeolite catalysts via ion exchange and precipitation method
3) Characterization of catalyst by gas adsorption analysis (BET), scanning electron microscopy (SEM), scanning electron microscopy-energy dispersive X-ray spectroscopy (SEM-EDX), X-ray fluorescence (XRF), X-Ray diffraction spectroscopy (XRD), temperature-programmed reduction (TPR), temperature programmed desorption (TPD).
4) Testing activity of the reaction over dehydrogenation and Guerbet reaction in a continuous fixed- bed reactor.
5) Study the effect of carrier gas on ethanol dehydrogenation to acetaldehyde over Cu-Zn/SiO_2 catalysts.
6) Study the effect of MgO loading on ethanol conversion activity, selectivity, and stability over Mg-KNaX catalysts.
7) Study the effect of carrier gas, bed configuration system, contact time, and catalysts ratio on ethanol conversion over the hybrid CuZn/SiO_2 ¦ Mg-KNaX catalysts.

5). Analysis and quantification of liquid products from the reactions by online gas chromatograph equipped with a flame ionization detector (GC-FID).

1.4 Expected result

It is expected that this study could improve the value of bioethanol by the ethanol conversion to higher alcohols. The modified catalysts could provide higher activity, selectivity, and stability compared with the previous ones. Furthermore, the knowledge obtained from this study can be applied in chemical industry.

Chapter 2

Theory and Literature Reviews

2.1 Alcohol

In chemistry, an alcohol is an organic compound which a hydroxyl (-OH) functional group on an aliphatic carbon atom. Alcohols is known in the general formular ROH, which R is alkyl group (including aliphatic and aromatic). The mono alcohols are classified in 3 main types included primary, secondary (RCH_2OH), and tertiary (R_2CHOH) based upon the number of carbon atoms (number of R group) connected to the carbon atom that bears the hydroxyl functional group [28]. At ordinary, the hydroxyl group is a polar functional group, which can form an H-bond with other alcohol molecules. Hence, a small alcohol molecule (C_2-C_4) had a boiling point close to the water and higher than hydrocarbon as compared equally a carbon number.

The advantage of alcohol in physical properties in high polarity and high boiling point as mentioned above, it can be used for solvents and diluents for paints (mainly C_4-C_6 alcohols), as intermediates in the manufacture of esters and a whole range of organic compounds, as flotation agents, as lubricants, and in recent times increasingly as fuel or fuel additives, e.g. For industrial purposes, isomeric mixtures often are preferred because the pure alcohols are too expensive. Moreover, mixtures of alcohols with differing numbers of carbon atoms can be advantageous for certain purposes. Therefore, the amounts of alcohol mixtures available on the market are similar to the quantities of the pure, individual alcohols [29]. Industrially, the most important alcohols are methanol, ethanol, 1-propanol, 1-butanol, 2-methyl-1-propanol (isobutyl alcohol), the plasticizer alcohols (C6-C11), and the fatty alcohols (C_{12}-C_8), used for detergents. The mainly preparation of alcohols are synthesis gas (methanol), oxo synthesis, and Ziegler process.

Reactions of alcohols can be characterized by cleavage of the O-H bond or the C-O bond either homolytically or ionically. Under normal conditions, alcohols are stable [30]. Alcohols can undergo oxidation to give aldehydes, ketones, or carboxylic acids, or they can be dehydrated to alkenes. They can react to form ester compounds, and they can (if activated first) undergo nucleophilic substitution reactions. The lone pair electrons on the oxygen of the hydroxyl group

also make alcohols nucleophiles. Catalytic oxidation or dehydrogenation of primary and secondary alcohols on copper, silver, iron, molybdenum, etc., a catalyst leads to the formation of aldehydes and ketones. In the Oppenauer oxidation a secondary alcohol is dehydrogenated by an excess of a ketone [31].

2.2 Ethanol

Ethanol or ethyl alcohol, also called drinking alcohol, is the principal type of alcohol found in alcoholic beverages, produced by the fermentation of sugars by yeasts. It is a neurotoxic psychoactive drug and one of the oldest recreational drugs used by humans. It can cause alcohol intoxication when consumed in sufficient quantity. Its structural formula, $CH_3CH_2OH_3$ is often abbreviated as C_2H_5OH, C_2H_6O or EtOH [33].

Ethanol or ethyl alcohol (CH_3CH_2OH) is also referred to an alcohol spirit, spirit of wine, grain alcohol, absolute alcohol, and ethyl hydrate. Depending on its water content, preparation, and final use, several ethanol products exist on the market. The 99% alcohol (often referred to as absolute alcohol) is used extensively for tinctures and pharmaceutical preparations, as a solvent and preservative, as an antiseptic, and in perfume. Ethanol is an important functional component of alcoholic beverages, which are produced by fermentation of fermentable carbohydrates. The fermentation broth itself may constitute (after processing and aging) a beverage, e.g., in the case of beer or wine, or the alcohol can be concentrated from the broth to produce high-alcohol-containing spirits. If the alcohol is used for purposes other than as a beverage, it is denatured by the addition of substances such as methanol, pyridine, formaldehyde, or sublimate. The denatured alcohol is then used by industry and commerce, principally as a solvent, as a raw material for manufacturing chemicals, or as a fuel [34].

The chemical properties of ethanol are dominated by the OH-functional group, which can undergo many industrially important chemical reactions, e.g., dehydration, halogenation, ester formation, and oxidation. Because ethanol can be produced efficiently not only by chemical synthesis from petroleum and coal-based feedstock, but also by fermentation of abundantly available organic materials, its commercial role as a raw material for various chemicals is of increasing importance. Conversion of ethanol to "alkochemicals" is an entirely new approach to

producing familiar petrochemicals. Some of these routes are already being used industrially in large alcohol producing countries [34].

2.3 Higher alcohols

2.3.1 Butanol

Butanol (butyl alcohol) refers to a four-carbon alcohol with a formula of C_4H_9OH. There are four possible isomeric structures for butanol, from a straight-chain primary alcohol to a branched-chain tertiary alcohol [35]. It is primarily used as a solvent, as an intermediate in chemical synthesis, and as a fuel. It is sometimes also called biobutanol when produced biologically.

Butanol is considered as a potential biofuel (butanol fuel). Butanol at 85 % strength can be used in cars designed for gasoline (petrol) without any change to the engine (unlike 85% ethanol), and it contains more energy for a given volume than ethanol and almost as much as gasoline, so a vehicle using butanol would return fuel consumption more comparable to gasoline than ethanol. Butanol can also be used as a blended additive to diesel fuel to reduce soot emissions. It is used as a solvent for a wide variety of chemicals and textile processes, in organic synthesis and as a chemical intermediate. It is also used as paint thinner and a solvent in other coating applications, where it is used as a relatively slow evaporating latent solvent in lacquers and ambient-cured enamels. It finds other uses such as a component of hydraulic and brake fluids [36].

2.3.2 Hexanol

1-Hexanol $CH_3(CH_2)_4CH_2OH$, is prepared according to the Ziegler process from ethylene or is made from natural products derived from coconut or palm oils. It is used as a solvent, as a basic material for the perfume industry, and for the production of plasticizers (in this case usually as a mixture with higher n-alcohols). Nitrates of 1-hexanol are recommended as cetane number improvers. 2-Methyl-1-pentanol $CH_3(CH_2)_2CH(CH_3)CH_2OH$, is prepared by aldol condensation of propionaldehyde and subsequent hydrogenation of the intermediate 2-methyl-2-pentenal, it is used as a solvent [37].

2.3.4 Benzyl alcohol

Benzyl alcohol is the simplest and also the industrially most important aromatic alcohol. LIEBIG and WHLER-first prepared benzyl alcohol from bitter almond oil (benzaldehyde) in 1832. The structure of benzyl alcohol was determined in 1853 by CANNIZZARO. Can-nizzaro used the reaction named after him, in which benzaldehyde is disproportionated into benzoic acid and benzyl alcohol through the action of an alkali.

Benzyl alcohol occurs in nature both free and in combined forms. In the latter case it exists as esters of acetic, benzoic, salicylic, and cinnamic acids, among others. It is known to occur in the balsams of Peru and Tolu, in the flower oils of hyacinths and wallflowers, in ylang-ylang oil, and in other essential oils. It also occurs as a glucoside in maize [38].

2.4 Aldehyde

Aldehydes are represented by the general formula RCHO, where R can be hydrogen or an aliphatic, aromatic, or heterocyclic group. According to IUPAC nomenclature, aldehydes are identified by the ending "al." However, many of them still are called by their common names.

The polarity of the carbonyl group of aldehydes not only facilitates the typical aldehyde reactions-addition of nucleophiles, reduction, and oxidation but it also makes the α-hydrogen atom acidic. For these reasons, aldehydes can undergo a wide variety of reactions [39].

2.4.1 Acetaldehyde

Acetaldehyde (CH_3CHO) was observed in 1774 by SCHEELE during reaction of black manganese dioxide and sulfuric acid with alcohol. Its constitution was explained in 1835 by LIEBIG who prepared pure acetaldehyde by oxidation of ethanol with chromic acid and designated this product “aldehyde” a concentration of the term “alcohol dehydrogenation”.

Acetaldehyde is mobile, low-boiling, highly flammable liquid with a pungent odor. Because of its high chemical reactivity, acetaldehyde is an important intermediate in the production of acetic acid, acetic anhydride, ethyl acetate, piratic acid, butanol, 2-ethylhexnaol, pentaerythritol, chlorinated acetaldehyde (chloral), glyoxal, alkyl amines, pyridines and other chemicals.

Occurrence: Acetaldehyde is an intermediate in the metabolism of plant and animal organisms, in which it can be detected in small amounts. Lager amounts of acetaldehyde interfere with biological processes. As an intermediate in alcoholic fermentation processes it is present in small amounts in all alcoholic beverages, such as beer, wine, and spirits. Acetaldehyde also has been detected in plant juices and essential oils, roasted coffee, and tobacco smoke [40].

2.4.2 Butanal

Butanals are saturated aliphatic C4 aldehydes. C_4H_8O, there are two isomers straight-chain butyraldehyde (butanal) and the branched iso- butyraldehyde (2-methylpropanal, dimethyl acetaldehyde).

Both aldehydes have been found in small amounts in various essential oils, in plants as well as in the dry distillation products of various natural substances. Both, butyraldehyde and iso-butyraldehyde are highly reactive intermediate products for a large number of chemical syntheses, above all leading to the formation of compounds with four to eight carbon atoms.

The annual world production of butyraldehyde is several million tons; industrial-scale production is almost exclusively by hydroformylation [41].

2.4.3 Hexanal

The C6 aldehydes are colorless, mobile liquids. Hexanal occurs naturally, e.g., in lemon and orange oils [42], it can use in the flavor industry to produce fruity flavors.

2.5 Reaction

2.5.1 Dehydrogenation reaction

Dehydrogenation is a chemical reaction that involves the removal of hydrogen from a molecule. It is the reverse process of hydrogenation. The first step in this process is ethanol adsorption on the catalyst surface by O atom of hydroxyl group attached on the metal surface (such as Ag, Cu) to produce η^1 (O)-carbonyl species (a). After that, dissociation of O-H bond is generated alkoxide intermediate. Finally, the dehydrogenation of ethanol can occur via an alkoxide intermediate to produce acetaldehyde with a metal hydride (di-hydride). In addition, η 2 (C, O)-carbonyl species (b) can occur with alkoxide intermediate by α-C and O atom attached on metal surface (such as Ni) to form acyl intermediate (η^1 (C)-acyl)) that may well desorb as

acetaldehyde. However, yield of acetaldehyde obtained from η^2 (C, O)-carbonyl species is less than that from η^1 (O)-carbonyl species because formation of the acyl intermediate can lead to decarbonylation to CH_4 and CO (**Scheme 1**) [43].

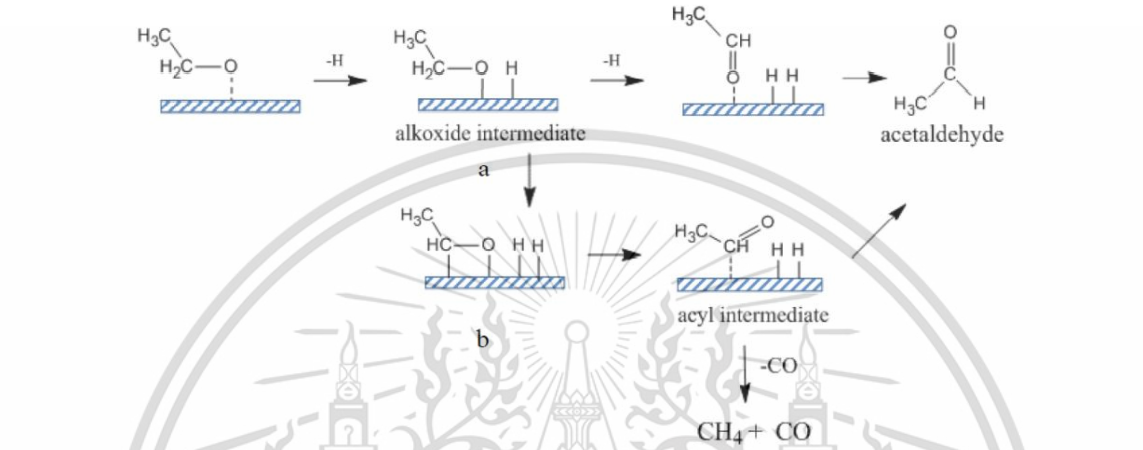

Scheme 1 Dehydrogenation of ethanol (a) η^1(O)-alcohol species, (b) η^2(C, O)-alcohol species.

2.5.2 Guerbet reaction

An important reaction to produce higher alcohols from ethanol is "Guerbet reaction". The Guerbet reaction of alcohols is the oldest and best understood material in the class of compounds first synthesized by Marcel Guerbet [11]. In this reaction, the ethanol was adsorbed on the catalyst surface and dehydrogenated to acetaldehyde, follows by aldol condensation trough coupling of two aldehydes molecule to larger unsaturated aldehyde and dehydration. Final step is hydrogen transfer, which promotes the formation of higher alcohol from unsaturated aldehyde. The reaction mechanism is considered pair of acid-base sites [11].

Dehydrogenation starts by alcohol chemisorption on acid-basic site pairs, which cleave O-H bonds to form surface alkoxide intermediates bound to the acid center (**Scheme 2**).

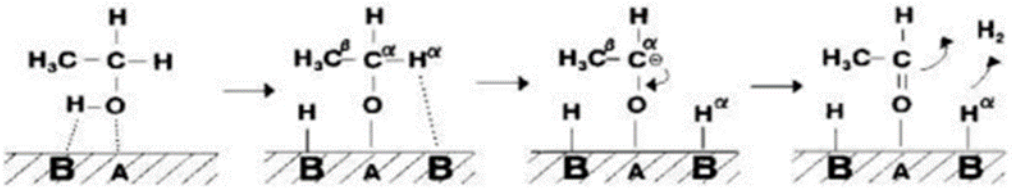

Scheme 2 Dehydrogenation of alcohols to the corresponding aldehydes [11].

The **α**-hydrogen in the alkoxide group is then abstracted by a neighboring basic site in order to form adsorbed aldehydes. Aldol condensation reactions on Mg_yAlO_x samples involved also the formation of a carbanion intermediate on Lewis acid-strong Brønsted base pair sites as shown in **Scheme 3**

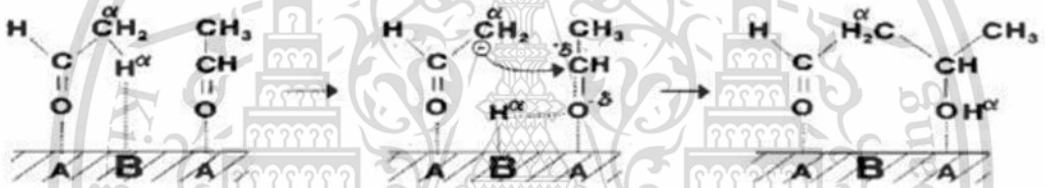

Scheme 3 Aldol condensation [11].

After aldol condensation, the product of aldol condensation will be dehydrated to crotonaldehyde. Finally, crotonaldehyde will be hydrogenated to 1-butanol as shown in **Scheme 4**

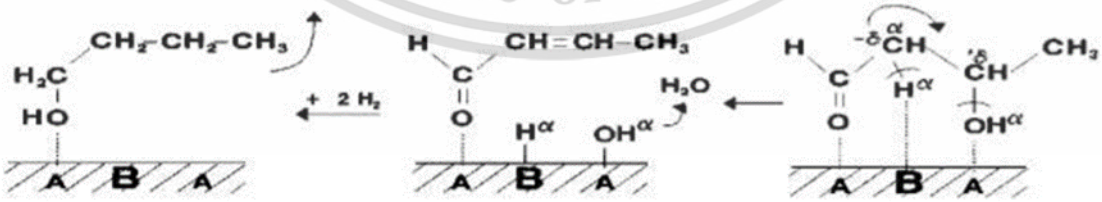

Scheme 4 Dehydration and hydrogenation of C4 aldehyde to C4 alcohol [11].

Hence, it can be seen there are many reactions that occurred in Guerbet reaction included dehydrogenation, aldol condensation, dehydration, and hydrogenation. It indicated that the catalyst for higher alcohol production from ethanol must had several functions or known in bifunctional catalysts.

2.6 Catalysts

2.6.1 Dehydrogenation catalyst

Dehydrogenation was one of the important processes in Guerbet reaction due to playing a role to generate acetaldehyde from ethanol. Acetaldehyde is an important intermediate for aldol condensation process, in which the rate of aldol condensation not only depends on a number of active sites over catalysts but also depends on acetaldehyde concentration in system [18]. Accordingly, high dehydrogenation activity catalysts will provide a chance to produce higher alcohols. The catalysts were often used to dehydrogenation of ethanol to acetaldehyde such as Cu-SiO_2 [24], Cu-ZnO-Al_2O_3 [25], and Cu-ZnO catalysts [26].

In 1991 N. Iwasa [25] studied ethanol dehydrogenation to acetaldehyde, it was carried out over copper-based catalysts in various supported (SiO_2, ZrO_2, Al_2O_2, MgO, ZnO). The reaction was investigated in flow reactor at 380-420 K. The result confirmed the ethyl acetate and butyraldehyde are formed via acetaldehyde. This is because does not ethyl acetate was detected, when swishing feed from ethanol to crotonaldehyde. Cu/ZrO_2 and Cu/ZnO provided high ethyl acetate selectivity, while coupling product and diethyl ether was obtained over Cu/Al_2O_3. This coupling product produced by the reactions over acid site. However, the ethyl acetate and coupling product was gradually decreased with a decrease in copper loading and lowest around 1 to 10 wt% of Cu (90 wt% to 1 wt%), which obtained at ethanol conversion of 35%. This suggested that the excess mount of acid site from Cu high loading over SiO_2 facilitated for C-C coupling of acetaldehyde. Accordingly, low Cu loading (~10%) may be provided high selectivity of acetaldehyde.

In 2001 S. Fujuta et al [26]. The ethanol dehydrogenation to acetaldehyde over Cu/ZnO was investigated as compared to Cu/SiO_2 in flow reactor. The Cu/ZnO was prepared by coprecipitation method. The reaction over Cu/ZnO mainly provided acetaldehyde selectivity

(~54%) from ethanol dehydrogenation with high ethyl acetate selectivity (~42%). This is because supported ZnO is active site for the transformation of acetaldehyde from dehydrogenation over Cu metal site to ethyl acetate. While Cu/SiO_2 provided higher acetaldehyde selectivity (~68%). Because the supported SiO_2 was inert lead to only Cu metal site for the reaction. Hence, the inert supported is suitable for high acetaldehyde selectivity, and reduce the side reaction as in supported SiO_2.

In 2018 M. Ohira et al [27]. The dehydrogenation of ethanol to acetaldehyde was studied over Cu/SiO_2 and ZnO/SiO_2 in vapor-phase. The 1 to 15 wt% loading of Cu and Zn over SiO_2 was prepared by the conventional impregnation method. The stability for ethanol dehydrogenation over 10 wt% Cu/SiO_2 was dropped at 350°C due to sintering of Cu metal over SiO_2 support. While the reaction over ZnO/SiO_2 provided high acetaldehyde selectivity with high stability at 350°C due to without sintering from tolerance against of impurities decomposition, or it may be that ZnO strong interacted with supported SiO_2. Additionally, founding 5, 10, and 15 wt% of ZnO gave same acetaldehyde yield (~25%). This is because conversion of ethanol to acetaldehyde was limited by ZnO dispersion and surface area of catalysts. Accordingly, the incorporated Cu with ZnO may be improve Cu sintering of catalysts at 10 wt% Cu with low amount of ZnO (5-15 wt%), which could provide high activity and stability for ethanol conversion to acetaldehyde.

2.6.2 Guerbet Catalysts

Acid-basic catalyst is a catalyst with both acid and basic functions in the structure so-called bifunctional catalyst. The catalytic mechanism can be categorized into two types depending on how the acid and basic interact with substrate. Both acid and basic can interact independently or step by step with different mechanisms, which are further categorized as simultaneous and successive acid–base interaction, respectively [13].

Simultaneous acid–base interaction can be further divided into two types. The first one is the simultaneous interaction that the acid and basic interact with the substrate in such a way that the basic pushes the electron pair to one part of the substrate and the acid pulls the electron pair from the other part of the substrate called “concerted mechanism”. Another one is the simultaneous interaction that the acidic site interacts with one substrate molecule and the basic site with a different substrate molecule. Both interactions occur simultaneously but

independently. For the successive interaction case, the substrate interacts with a certain catalytic site to form an intermediate, which interacts successively with the other type of catalytic site to form another intermediate or final product. The acid site and basic site take different roles successively in the catalytic process [12]. The acid-base catalysts widely used for Guerbet reaction such as basic zeolite [44-45], MgO [19-20], Ni-MgO [21], and etc.

The zeolites are microporous, aluminosilicate minerals commonly used as commercial adsorbents and catalysts. Zeolite can be classified from Si/Al ratio of each structure such faujasite, ZSM-5, MFI, BEA, LTA, etc. The faujasite is a mineral group in the zeolite family of silicate minerals. Faujasite zeolites are divided into X and Y zeolites. The Al/Si ratio in X zeolite is between 2 and 3, while in Y zeolites it is 3 or higher [46], which a low Si/Al ratio of these zeolite lead to low acid strength. In addition, the basic properties of faujasite depended on type of charge balancing cation such as of faujasite-Na, faujasite-Mg and faujasite-Ca form. They all share the same basic formula: (Na_2, Ca, Mg) $3.5[Al_7Si_{17}O_{48}]\cdot 32(H_2O)$ by varying the amounts of sodium, magnesium and calcium [47].

In 1992 C. Yang and Z. Meng [45] studied bimolecular condensation of ethanol to 1-butanol by using alkali cation zeolites catalyst in continuous-flow system at 400°C. The basic zeolites were prepared by ion exchange with alkali solution (Li, Na, and K) followed by impregnation of rubidium nitrate solution and calcination. The formation of C4 alcohol and C4 aldehyde over basic zeolite are decreased in the order of: Rb-LiX > Rb-NaX > Rb-KX. It was presumably due to occurring of basicity from exchanged Rb^+ lead to the enhanced aldol condensation activity, including with an increase in dehydrogenation rate of ethanol to acetaldehyde over Lewis acid site from the hard Li^+ cation. However, the C4 alcohol and acetaldehyde are main products, this suggests that aldol condensation is rate determining step in alkali zeolite due to lacking of basic site for C-C coupling of acetaldehyde to form higher molecular weight product.

In 2000, K. Gotoh., et al [44]. investigated Guerbet reaction between methanol and ethanol over supported alkali salt catalysts in fixed bed flow reactor at 350°C. The supported alkali salt catalysts were prepared by conventional impregnation using Na_2CO_3 on two types of zeolite support: NaX and NaY. Both NaX and NaY supported catalysts provided higher total alcohol selectivity (n-propanol and iso-butanol, ~94%) with lower selectivity towards dehydration product

as compared to SiO_2-Al_2O_3 and kaolinite catalysts. This is because basic site of Na_2CO_3 can promote aldol condensation, including low Si/Al ratio of NaX and NaY decreased dehydration activity. The effect of zeolite preparation with various Na salts (carbonate, nitrated, acetate, sulfate, and chloride) by ion-exchange method on catalytic activity was studied. Supported carbonate, nitrated, and acetate illustrated high conversion with high n-propanol and iso-butanol selectivity, while the Guerbet reaction was inhibited in both sulfate and chloride due to these salts were not decomposed at high temperature (600°C). The increasing of aldol condensation rate over CsKX can improve iso-butanol selectivity due to an increase of basic strength from Cs incorporation. Although basic zeolite can improve higher alcohol by alkali addition, dehydration still obtained from the retained acid site in zeolite cavity.

Magnesium oxide (MgO), or magnesia, is a white hygroscopic solid mineral that occurs naturally as periclase and is a source of magnesium. It has an empirical formula of MgO and consists of a lattice of Mg^{2+} ions and O^{2-} ions held together by ionic bonding. MgO has Brønsted basic site that can promote aldol condensation in Guerbet reaction. Magnesium oxide has been used as catalyst for numerous technological processes. It has been found to be the most active in the reaction of alcohols to aldehydes, esters, or olefins [12].

The isolated O^{2-} ion on MgO surface would be unable to from ethoxide intermediates. Thus, the incorporation of small amounts of metal cations to MgO drastically increased the acetaldehyde formation rate because of the generation of new surface Lewis acid-strong base pair sites [12]. However, MgO can be used in catalytic industry as base catalyst. For example, the activity for both the aldol condensation of citral with acetone and the glycerolysis of methyl oleate diminished with the MgO calcination temperature because these reactions were essentially promoted on strongly basic O^{2-} site.

In 2003, A. S. Ndou et al [19] investigated dimerization of ethanol to butanol over alkali earth metal oxides catalysts (MgO, CaO, and BaO). Higher alcohols are produced through Guerbet reaction (1 bar, 450°C) in fix bed reactor. The reaction shows high conversion (~34%) and high butanol yield (~18%) over MgO, while CaO provided lower activity with lower amount of butanol. On the other side, BaO does not present activity in butanol formation. This is because of the strong basic site and acid site of MgO (observed by CO_2 TPD), which can promote dehydrogenation and aldol condensation of ethanol to C4 aldehydes/C4 alcohols. In addition, the ethanol

conversion was also investigated over alkali earth metal loaded MgO. Even though the basicity of MgO was improved by loaded Ba and Ca but the decrease in selectivity of butanol due to a drop of condensation rate, from an increase in the basicity of oxygen anions in MgO. Thus, MgO alone can provide the highest rate of aldol condensation for butanol production.

In 2020 S. A. Susanto et al [20] studied the conversion of ethanol to 1-butanol in a batch reactor at 350°C using MgO prepared by various methods. The MgO(p) prepared by precipitation of $MgCl_2$ and NaOH, provided the highest 1-butanol yield comparing with MgO(m) (commercial) and MgO(k) (direct calcination of $Mg(NO_3)2.6H_2O$). This is because the smaller crystallite size, higher surface area, and higher amount of basic site over MgO(p) that can facilitate dehydrogenation and aldol condensation activity. From this result, it seems that the surface area and acid-base capacity are a key factor for increasing 1-butanol yield activity.

In 2020 H. Wang et al [21] investigated the effect of Ni loading (Ni/Mg at 0.1, 1, and 10 ratio) over supported MgO to improve dehydrogenation and aldol condensation for long chain-alcohols production. The reaction was tested in batch reactor (250°C, 2.5 MPa, 5 h under helium). Over the Ni supported on MgO, the conversion (up to ~45%) and C4 alcohol yield (up to ~23%) were increased and highest at Ni-MgO (ratio = 1) as compared to MgO alone. This is because the dehydrogenation of ethanol to acetaldehyde was facilitated by Ni species, which is the first step in the formation of 1-butanol. Additionally, the CO_2 and NH_3-TPD reveals that the highest of moderate basic and acidic site was obtained over Ni-MgO (ratio = 1), resulting in higher dehydrogenation and aldol condensation activity. Therefore, the incorporation of Ni can improve dehydrogenation rate from the increase acid-base capacity and provides higher C-C coupling activity for 1-butanol production. Nevertheless, the excessive Ni loading may cause large particle size of Ni over MgO lead to unfavorable catalytic activity from low the dispersion as in Ni10-MgO ratio.

In general, the metal oxide was incorporated on supported catalysts by impregnation using metal precursor. Nevertheless, the low dispersion of metal/metal oxide was often obtained and uneven from human error preparation. For this reason, the catalysts from impregnation method may not be suitable for the reaction that requires high active site or high surface area like the Guerbet reaction. In 2016, D.E. Resasco., et al [22] improved aldol condensation activity by increasing the dispersion of MgO on KNaX support. The KNaX catalyst was initiately prepared by

ion-exchange of NaX(13X) zeolite with K^+ solution. After that the exchanged catalyst was consequently exchange with Mg^{2+} solution. Finally, MgO-KNaX was obtained from the precipitation with KOH solution and calcination (Scheme 5). The activity in acetaldehyde/ethanol (mixed feed) conversion was investigated in a batch reactor at 290°C under pressure 300 psi. The ratio of K^+, Na^+, $2Mg^{2+}$: Al of the prepared catalyst was 0.99, 1.10, 1.14, 1.32. The MgO-KNaX-0.99 provided high C4 aldehyde selectivity (~94%) with low butanol selectivity (~5%), while MgO-KNaX-1.14 can increase the yield of higher MW aldehydes (C6-C8). This is because aldol condensation rate of aldehyde intermediate depended on MgO at extra-framework of zeolite; while size and shape selectivity of product was controlled by confinement in zeolite. Accordingly, the advantage of MgO-KNaX catalyst is that it can control basic density by amount of MgO nanoparticles incorporation. Additionally, the confinement can limit the over C-C coupling to higher long-chain alcohol.

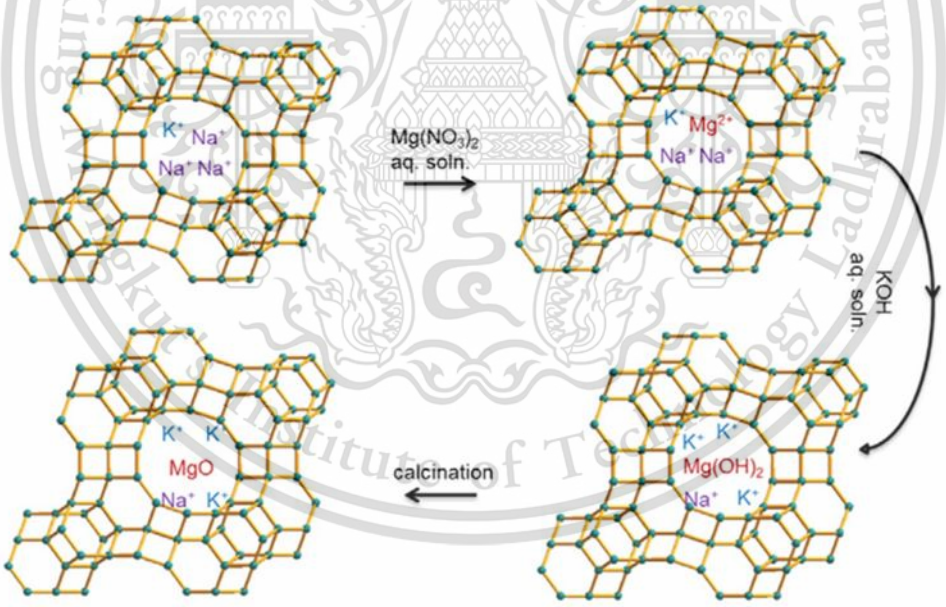

Scheme 5 The preparation of MgO incorporated faujasite zeolite [22].

Chapter 3

Experimental

3.1 Reagents

Table 3.1 Materials and Chemicals

Chemicals	Grade of purity	Manufactures
1. Magnesium acetate ($Mg(CH_3COO)_2$)	99%	CARLO ERBA
2. Potassium carbonate (K_2CO_3)	99%	CARLO ERBA
3. Potassium hydroxide (KOH)	85%	CARLO ERBA
4. Ethanol (C_2H_5OH)	99.9%	CARLO ERBA
5. Nitrogen gas	High purity (99.99%)	PRAXAIR
6. Hydrogen gas	High purity (99.99%)	PRAXAIR
7. Air	High purity (99.99%)	PRAXAIR
8. Distilled water	-	-
9. Copper nitrate trihydrate ($Cu(NO_3)_2•3H_2O$)	99.5%	CARLO ERBA
10. Zinc nitrate hexahydrate ($Zn(NO_3)_2.6H_2O$)	98%	TECHNICAL
11. Sillicon dioxide (SiO_2)	99%	CARLO ERBA
12. Molecular sieve 13X	-	Honeywell

3.2 Apparatus

1. Syringe (10 mL)
2. Syringe pump
3. Peristaltic pump

4. Mass flow controller
5. Catalytic testing rig
6. Gas chromatograph
7. Heating tape
8. Magnetic stirrer
9. Laboratory glassware
10. Laboratory plastic ware
11. Oven
12. Sieve
13. pH meter
14. Tube furnace with a programmable temperature controller
15. Temperature programmed reduction (TPR) system
16. Temperature programmed desorption (TPD) system
17. X-ray fluorescence spectrometer (Wavelength Dispersive, Philips, PW2400, Scientific and Technological Research Equipment Centre 2-3 Building, Chulalongkorn University and Energy Dispersive, Oxford, ED-2000, Scientific and Technological Research Equipment Centre 2-3 Building, Chulalongkorn University)
18. X-ray powder diffractometer (Rigaku, DMAX 2200/Ultima+, Faculty of Science, Chulalongkorn University)
19. Gas Chromatography with Flame Ionization Detector (GC-FID).

3.3 Experimental procedure

3.3.1 Catalyst Preparation

3.3.1.1 Cu-Zn/SiO_2 catalyst

The CuZn/SiO_2 was prepared by co-impregnation using mixture of 1.72 M of $Cu(NO_3)_2$ and 0.16 M of $Zn(NO_3)_2$ as precursors. Then, the sample was dried at 90°C overnight. After that the catalysts were calcined under air (30 mL/min) at 450°C for 3 h. The CuZn/SiO_2 catalyst was reduced under H_2 (30 mL/min) at 550°C for 2 h before activity test.

3.3.1.2 Mg-KNaX catalyst

KNaX was prepared by ion exchange the commercially available molecular sieve 13X (3 g) with 100 mL of 0.1 M K_2CO_3 at 80˚C for 24 h. Then, the solid was filtered and dried overnight at 120˚C. After that the catalysts were calcined under air (30 mL/min) at 450˚C for 3 h.

Mg-KNaX was prepared by ion exchange the obtained KNaX (3g) with $Mg(CH_3COO)_2$ solution (100 mL) at 80˚C for 24 h. To modify the Mg^{2+}content, the $Mg(CH_3COO)_2$ concentration was varied from 0.5, 0.7, 0.8, 0.9, and 1 M. Then the solid was filtered and dried overnight at 120˚C. After that the sample (3 g) was mixed with 1.0 M KOH solution (100 mL) under stirring at room temperature for 20 min, then filtered, and dried over night at 120˚C. The Mg-KNaX catalysts were calcined under air (30 mL/min) at 450˚C for 3 h before activity testing.

3.3.2 Catalyst Characterization

3.3.2.1 Structural analysis using X-ray Diffraction (XRD)

The crystalline phase of the prepared materials can be identified, using XRD measurement. The sample was ground before it is packed on the sample holder. Analysis was done employing Bruker diffractometer (Cu K α radiation, 40 kV, 30 mA), covering the range of 2θ = 5-90˚ for CuZn/SiO_2 and 5-60˚for zeolite (0.02˚/step). A scanning rate was 1s/step.

3.3.2.2 Quantitative elemental composition analysis by X-ray Fluorescence (XRF)

X-ray fluorescence is a surface composition determination that is results from bombarding the sample with high-energy X-rays to releases characteristic secondary X-ray. This technique can be performed according to the procedure: the 0.5 g of catalyst sample and 4.5 g of boric acid were mixed and grinded together and compressed into alumina pan before bring into the XRF sample holder in XRF instrument.

3.3.2.3 Determination of specific surface area by nitrogen adsorption

Surface area of the catalysts can be determined by a gas adsorption analyzer (Autosorb-1C, Quantachrome). Approximately 0.01-0.05 g of the sample was loaded into the cell, which is attached to the outgassing station equipped with a heating mantle. The temperature was raised

to 350°C during outgassing process. After that, nitrogen gas was introduced to the sample cell where the adsorption can be measured at the range of the partial pressure (P/P0) from 10-6 to 1.0. The adsorption isotherm and the corresponding surface area was analyzed using BET **equation** as shown in **Equation 3.1.**

$$\frac{1}{\upsilon\,[(p_0/p)-1]} = \frac{c-1}{\upsilon_m c}\left(\frac{p}{p_0}\right) + \frac{1}{\upsilon_m c} \qquad \textbf{Equation 3.1}$$

Where p and p0 are the equilibrium and the saturation pressure of adsorbents at the temperature of adsorption, υ_m is the adsorbed gas quantity (for example, in volume units), υ_m is the monolayer adsorbed gas quantity, and C is the BET constant. The concept of the theory is an extension of the Langmuir theory, which is a theory for monolayer molecular adsorption to multilayer adsorption with the following hypotheses: (a) gas molecules physically adsorb on a solid in layers infinitely; (b) there is no interaction between each adsorption layer; and (c) the Langmuir theory can be applied to each layer.

3.3.2.4 Determination of basicity of the catalyst by CO_2-Temperature Programmed Desorption (CO_2-TPD)

The basic function of the catalyst was identified using CO_2-TPD measurement. Sample (0.2 g) was packed in quartz tube reactor and was covered with quartz. The catalyst was preheated under the flowing of airzero at 450°C for 2 h and evacuated and then it was exposed to 20 kPa of pure CO_2 gas at 30˚C until saturation coverage was reached for 1 h. After that the sample was flushed with He at room temperature for 1 h. The physisorbed CO_2 was performed at this temperature, the temperature was then increased at a linear rate of 10˚C/min from 50 to 500˚C under vacuum

3.3.2.5 Determination of acidity of the catalysts by NH_3-Temperature Programmed Desorption (NH_3-TPD)

The acid function of the catalyst was identified using NH_3-TPD measurement. Sample (0.2 g) was packed in quartz tube reactor and was covered with quartz. The catalyst was preheated under the flowing of airzero at 450˚C for 2 h and evacuated and then it was exposed to 20 kPa of pure 1% NH_3/He gas at 30˚C until saturation coverage was reached for 1 h. After that the

sample was flushed with, He at room temperature for 1 h. The physisorbed NH_3 was performed at this temperature, the temperature was then increased at a linear rate of 10˚C/min from 50 to 500˚C under vacuum

3.3.2.6 Temperature programmed reduction

Temperature-programmed reduction (TPR) was used to identify the active site species of the catalysts by monitoring their reducibility. Temperature programmed reduction was measured using thermal conductivity detector (TCD). The sample weighed 2.5 mg was placed into a quartz tube reactor, which was located inside a temperature-regulated furnace. Prior to the H_2-TPR, each sample was heated to its activation temperature in air zero (30 ml/min) for 1 h with 10°C /min and was cooled down to below 40°C. The catalyst was investigated from temperature range of 100 to 600 ˚C The heating rate of 10°C/min, 30 ml/min of 10% H_2 in Ar was applied for TPR analysis. Water production during the reduction process was removed in a U-shape glass trap at -196°C (liquid nitrogen) before entering the TCD detector.

3.3.2.7 Determination of scanning electron microscope

A scanning electron microscope (SEM) is commonly applied for studying surface of catalysts. It is used to investigate the morphology, structure and dispersion of metal in the catalysts by scanning the surface beam of electrons and signal form SEM depending on the number of secondary electrons. The SEM technique can achieve resolution better than 1 nanometer.

3.3.3 Catalytic activity testing

The catalyst was pressed, crushed, and sieved into particle size of 600-850 μm. After that, it was packed in a glass tube reactor and covered with both glass wool and glass bead, the scheme of catalytic testing rig and bed configuration are shown in **Scheme 6** and **Scheme 7, respectively**. The conversion of ethanol was studied in a fixed-bed reactor at atmospheric pressure in the temperature 380˚C. Nitrogen and hydrogen were used as carrier gas. Flow rate of the gases was controlled by a mass flow controller and checked by a bubble flow meter. Before activity testing, the catalyst was activated by heating from room temperature to 450˚C (5˚C/min) and held at 450˚C for 2 h under air zero and/or H_2 at a flow rate of 30 mL/min. The conditions for activation, reduction, and reaction of each catalyst are shown in **Table 1.** Then, 99.99%

ethanol was fed into the reactor by a syringe pump at a flow rate of 1.0 mL/h. The catalytic testing was conducted for a total time on stream (TOS) of 3 h. The product effluents were analyzed using an online gas chromatograph equipped with Rt®-Q-BOND capillary column.

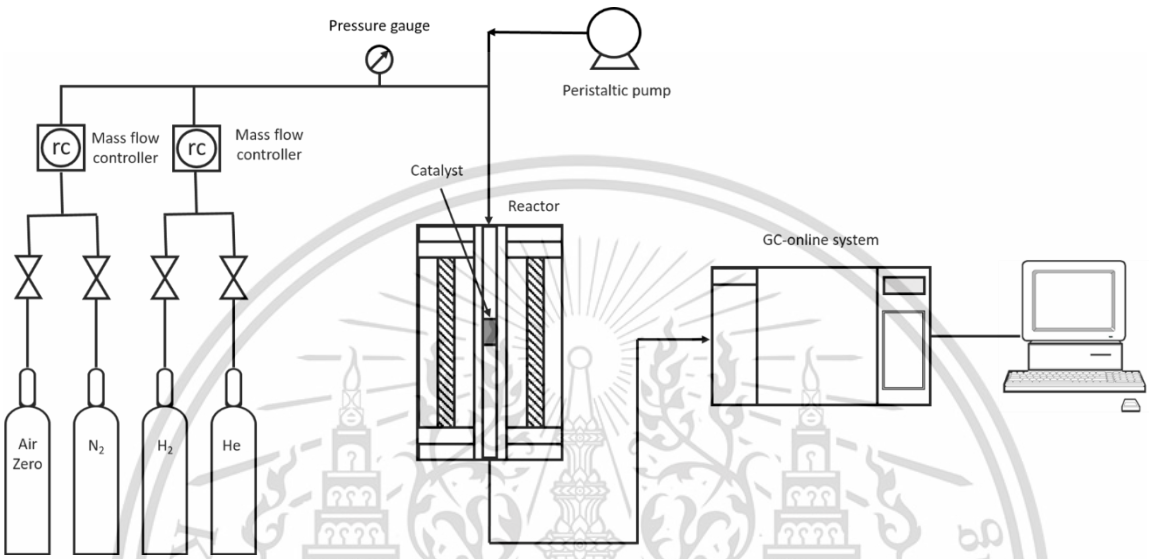

Scheme 6 Catalytic activity testing rig.

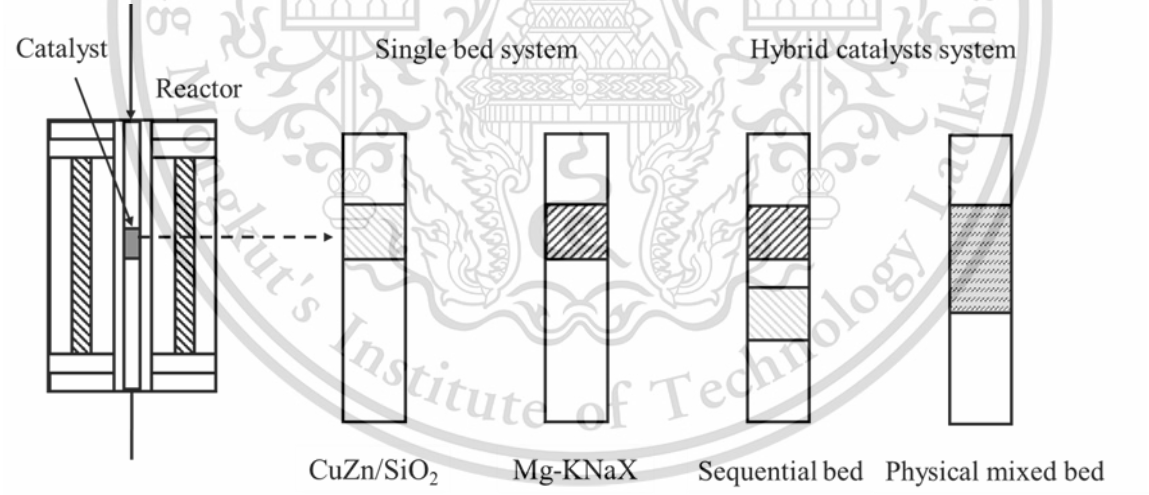

Scheme 7 Bed configuration of catalysts.

Table 1 The catalytic condition for activation, reduction, and reaction.

Entry	Catalyst	Activation		Reduction		Reaction	
		Temperature (˚C)	Carrier gas	Temperature (˚C)	Carrier gas	Temperature (˚C)	Carrier gas
Dehydrogenation catalysts							
1	$CuZn/SiO_2$	450	Air	550	H_2	380	N_2
2	$CuZn/SiO_2$						H_2
Guerbet catalysts							
3	NaX	450	Air	-	-	380	N_2
4	KNaX						
5	3.1Mg-KNaX						
6	3.3Mg-KNaX						
7	3.4Mg-KNaX						
8	3.9Mg-KNaX						
9	4.3Mg-KNaX						
Hybrid catalysts (S) Sequential bed							
10	(5+10)[a]	450	Air	550	H_2	380	N_2
11	(5+10)[a]						H_2
Hybrid catalysts (P) Physical mixed bed							
12	(5+10)[a]	450	Air	550	H_2	380	N_2
13	(5+10)[a]						H_2
14	(0+15)[a]						H_2
15	(3+12)[a]						H_2
16	(7.5+7.5)[a]						H_2
17	(10+5)[a]						H_2

[a] catalysts ratio of $CuZn/SiO_2$ + Mg-KNaX (g.h/mol)

3.3.4 Products analysis

The products were analyzed using an online BUCK Scientific 910 gas chromatograph equipped with a flame ionized detector (GC-FID, Agilent). The products were collected in gas sampling loop, and then periodically injected into GC column with an inert carrier nitrogen gas. The temperature of the injection port was set at 250°C, 35°C for column oven, and 250°C for FID detector. The GC temperature condition was started at 35°C, hold for 2 min and heat up to 200 (heating rate 15°C/min), hold for 2 min. Pressure of the carrier gas was fixed to 6.35 psi at all time. The products were recorded as a chromatogram. Each peak areas from the chromatogram were measured and calculated. Compared with standard peak areas, the species and composition of each product were determined.

Chapter 4

Results and Discussion

4.1 Characterization of catalysts

4.1.1 Characterization of catalysts

The elemental composition and the surface area of the $CuZn/SiO_2$ and zeolite X catalysts were shown in **Table 2.** It can be seen that Cu (0.13 mol/g) and Zn (0.03 mol/g) content of the bimetallic catalyst is closed to the expected loading: that is 0.16 mol/g Cu (10 wt.%), and 0.03 mol/g Zn (2 wt.%). The variation of the loading obtained may be accounted for the deviated concentration of the metal precursor during preparation.

Table 2 Elemental composition and surface characteristics of catalysts.

Entry	Catalysts	Alkaline wash	Si/Al[a]	Metal content (mol/g)							S_{BET} (m^2/g)	Pore volume (cm^3/g)
				Cu[a]	Zn[a]	Na[a(b)]	K[a(b)]	Mg[a(b)]	Na+K/Al[a(b)]	Total cation/Al [a(b)]		
1	$CuZn/SiO_2$	N/A	N/A	0.13	0.03	N/A	N/A	N/A	N/A	N/A	245	0.908
2	NaX	N/A	1.30	-	-	0.57(N/A)	-	-	1.14(N/A)	1.14(N/A)	457	0.068
3	KNaX	N/A	1.30	-	-	0.55(0.35)	0.32(0.19)	-	1.80(1.00)	1.80(1.00)	358	0.058
4	3.1Mg-KNaX	KOH	1.24	-	-	0.06(0.08)	0.38(0.38)	0.13(0.14)	0.97(0.86)	1.25(1.13)	535	0.065
5	3.3Mg-KNaX	KOH	1.25	-	-	0.04(0.06)	0.38(0.38)	0.14(0.15)	0.98(0.75)	1.30(1.05)	479	0.058
6	3.4Mg-KNaX	KOH	1.23	-	-	0.05(0.07)	0.41(0.38)	0.14(0.14)	1.03(0.87)	1.34(1.16)	444	0.054
7	3.9Mg-KNaX	KOH	1.23	-	-	0.05(0.05)	0.41(0.38)	0.16(0.17)	1.01(0.81)	1.37(1.16)	402	0.059
8	4.3Mg-KNaX	KOH	1.19	-	-	0.04(0.05)	0.40(0.38)	0.18(0.18)	0.97(0.81)	1.36(1.16)	244	0.042

[a] Total composition determined by XRF

[b] Surface composition determined by SEM-EDS

The surface area and pore volume of the $CuZn/SiO_2$ were derived from the typical SiO_2 supports. XRD of the catalyst exhibits typical CuO-ZnO phase at 2θ = 35.5°, 38.7°, and 48.7° as shown in **Figure 1**. H_2-TPR (**Figure 2**) shows two reduction peaks at 302 °C, attributed to the reduction of a small particle of CuO, and at 357 °C for the reduction of CuO-ZnO to the bimetallic

CuZn [48]. A higher reduction temperature of the catalyst, as compared to CuO (~250 °C), is presumably due to the increase electron density of the mixed oxide when ZnO is incorporated.

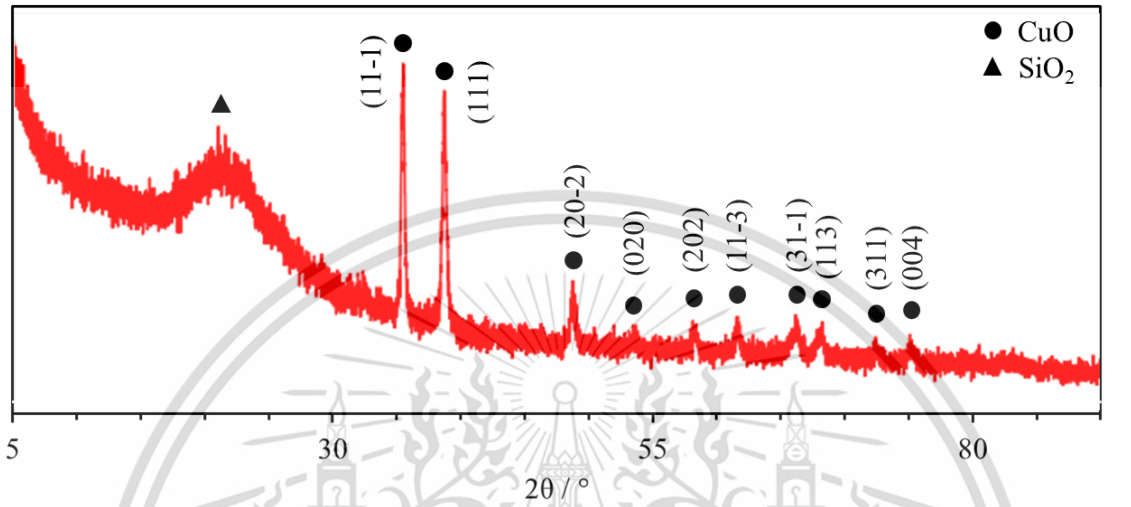

Figure 1 XRD patterns of Cu-Zn/SiO_2.

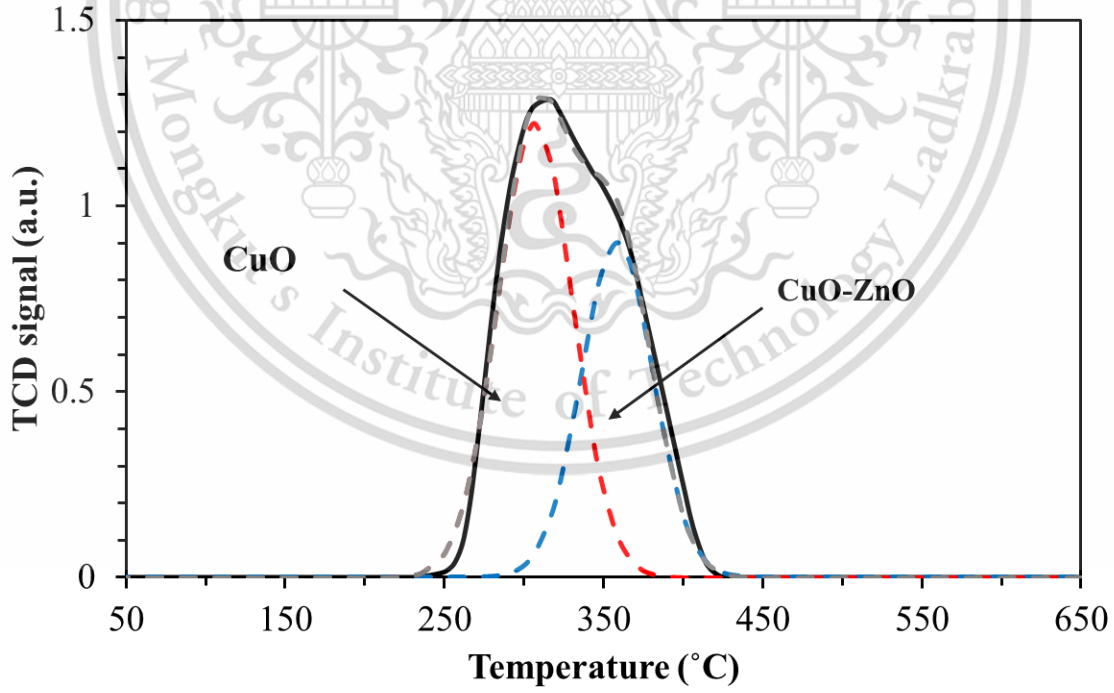

Figure 2 H_2-TPD profile of 10Cu-2Zn/SiO_2 catalyst.

For the zeolite X catalysts, when K^+ was exchanged with NaX, the total cations/Al is noticeably higher than one (**Table 2**, **entry 2**). The Na^+ content remains similar to that of the parent NaX. It is suggested that K^+ does not readily exchange with Na^+, but possibly exist as occluded salts in the pore of the sample. This is because $K_2(CO_3)$ solution may well retain in the pore after ion exchange without washing. Accordingly, the $K_2(CO_3)$ salt would be left inside after calcination. In support with this view, a decrease in surface area and pore volume of KNaX, together with a lower Na+K/Al content on the surface were evidenced.

Unlike exchange with K^+, the amount of Na^+ significantly dropped after exchange with 0.5 M of $Mg(CH_3COO)_2$ (**Table 2, entry 3**). This is because the Mg^{2+} are harder than the Na^+ and strongly interact with the hard framework of the zeolite X. As Na^+ was replaced by Mg^{2+}, the surface area and pore volume of catalysts was increased. The amount of K^+ slightly increased after the sample was washed by KOH solution. This is because the KOH washing precipitate the exchangeable Mg^{2+} into $Mg(OH)_2$, bearing only K^+ as charge balancing cation of the framework. Accordingly, (Na+K)/Al ratio becomes closed to 1, while the total cations/Al is higher than one and increased with Mg loadings (**Table 2, entry 3-7**). This suggests that the MgO species may well be distributed as occluded $[Mg_4(OH)_4]^{4+}$ species in the zeolite cavity [23], and on the external surface as evidenced by SEM (**Figure 3**).

It is clear that external surface of all Mg loaded samples was covered by petal-like structure, (**Figure 3b-1f**), when compared to that of the parent KNaX (Figure 1a). This petal-like structure was previously seen and suggested to be MgO nanoparticles formed on the FAU surface [23]. That additional texture notably increases the surface area of 3.1Mg-KNaX (535 m^2/g), as compared to KNaX (358 m^2/g). The elemental analysis by EDX (**Figure 3a**) suggests that the MgO nanoparticle was highly dispersed on the zeolite surface. As the surface composition of Mg is similar to total Mg composition (as seen by XRF, Table 1), it is likely that MgO would also exist in the zeolite cavities as occluded $[Mg_4(OH)_4]^{4+}$ species mentioned earlier. Accordingly, the surface area and pore volume of Mg loaded samples were dropped when Mg content is increased.

It is worth noting that, the Si/Al ratio slightly decreased with incorporation of MgO. This is possibly due to some desilication after washing with 1M KOH. Nevertheless, the crystallinity was retained as the XRD of all samples appeared similar (**Figure 4**), except for 4.3Mg-KNaX. The XRD intensity and surface area of this sample were notably drop. This indicates a partial collapse of

FAU structures, presumably due to an ion exchange with relatively high concentration (1 M) of acidic $Mg(CH_3COO)_2$ solution.

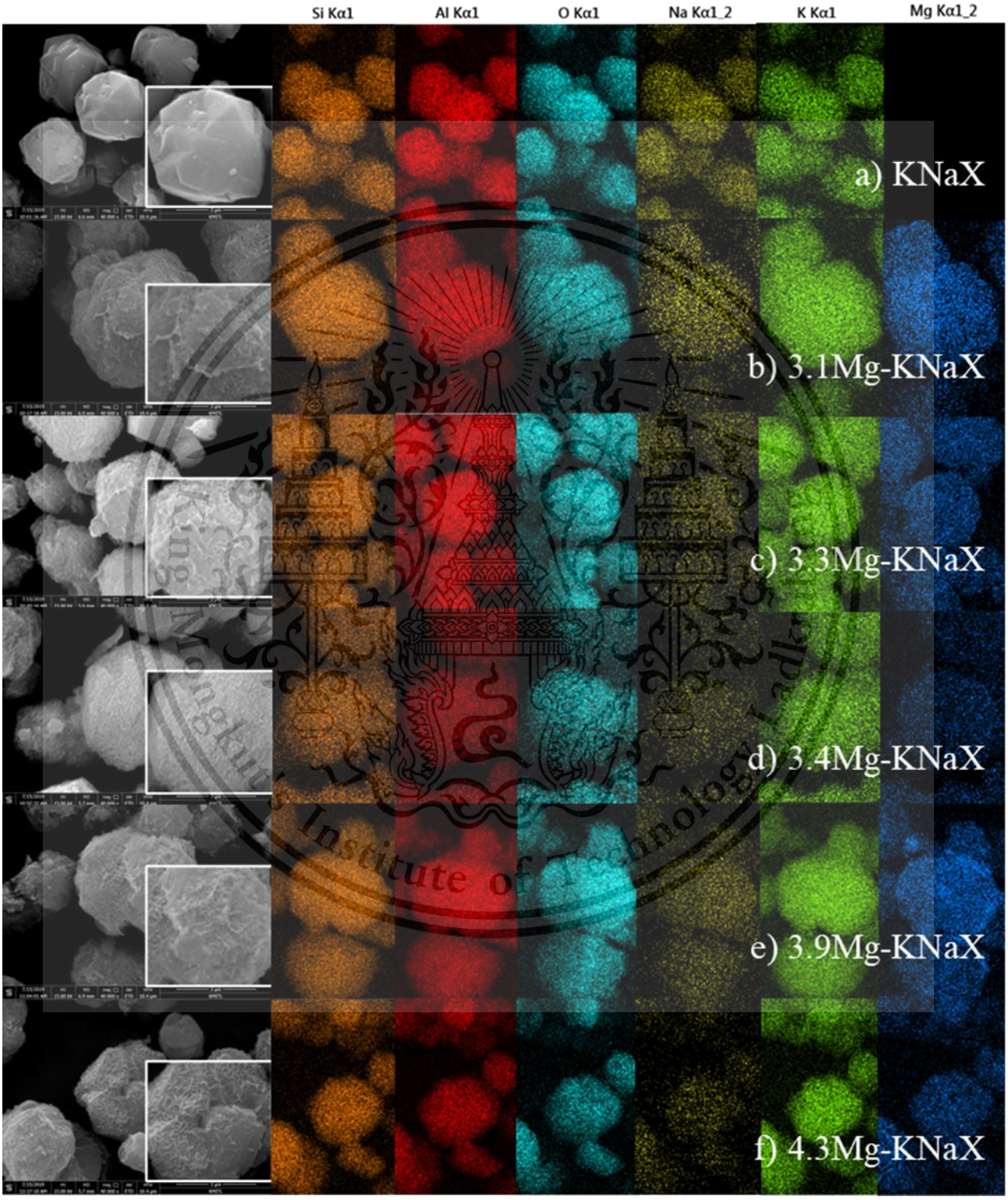

Figure 3 SEM images and elemental dispersion of a) KNaX, b) 3.1Mg-KNaX, c) 3.3Mg-KNaX, d) 3.4Mg-KNaX, e) 3.9Mg-KNaX and f) 4.3Mg-KNaX.

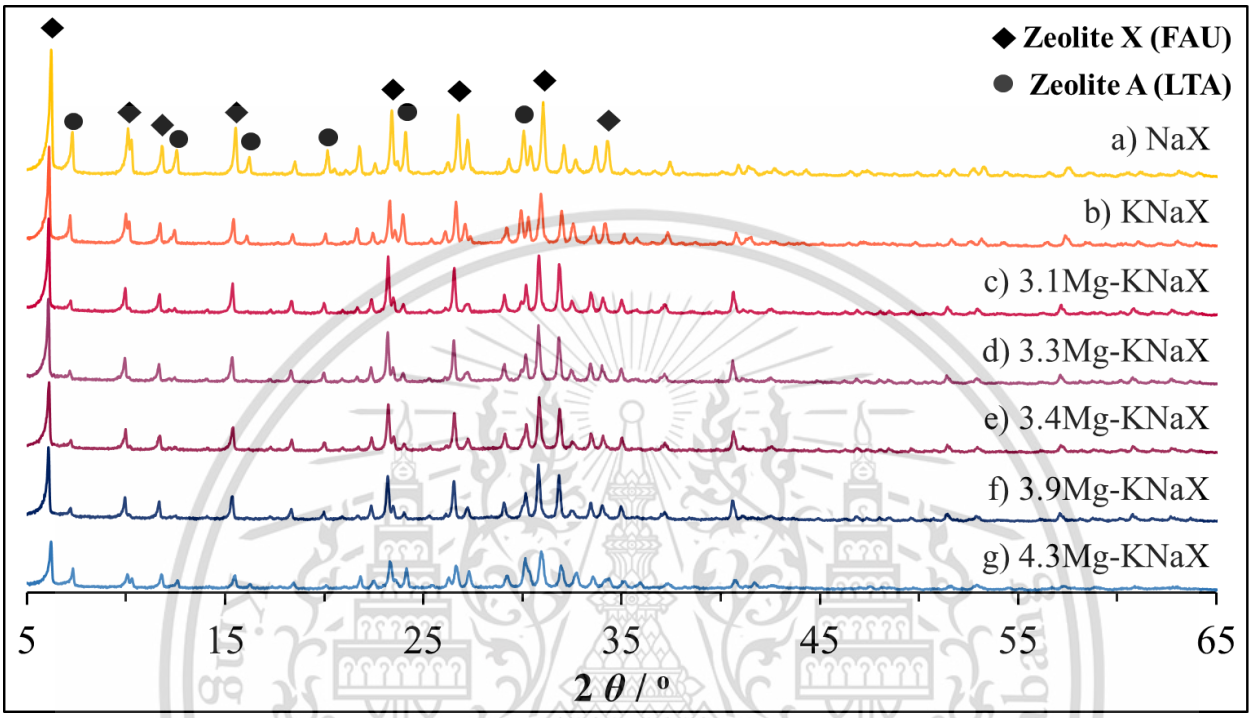

Figure 4 XRD patterns of a) NaX b) KNaX, c) 3.1Mg-KNaX, d) 3.3Mg-KNaX, e) 3.4Mg-KNaX, f) 3.9Mg-KNaX and h) 4.3Mg-KNaX.

Total basicity and acidity of Mg-KNaX catalysts was evaluated by temperature-programmed desorption of CO_2 (CO_2-TPD) and NH_3 (NH_3-TPD) as displayed in **Figure 5**. It can be seen that the NaX demonstrated NH_3 desorption peaks at 350°C. This suggests that most of the acid sites of NaX was medium Lewis acid site. Since Na^+ is a relatively hard alkaline cation, it can well interact with Lewis base (NH_3) [49]. Accordingly, physically adsorbed CO_2 was mainly observed for NaX at 50-250°C. Nevertheless, the peak at 450-550°C does not represent the basic site of this sample, but rather derived from decomposition of the bicarbonate species retained the NaX [50] after calcination at 450°C.

The weaker acid site (~150°C) was observed over KNaX, with a noticeable decrease in medium acid sites (~350°C). These weak Lewis acid sites could be attributed from the occluded salts of K^+ in pore of zeolite since K^+ is much softer than the Na^+ [51]. Moreover, the smaller Na^+

could be obscured by larger K^+ salt in the pore, resulting in decreases in surface area and pore volume. Accordingly, both NH_3 and CO_2 adsorption is suppressed in KNaX, as compared to those on NaX (**Table 3, entry 1-2**).

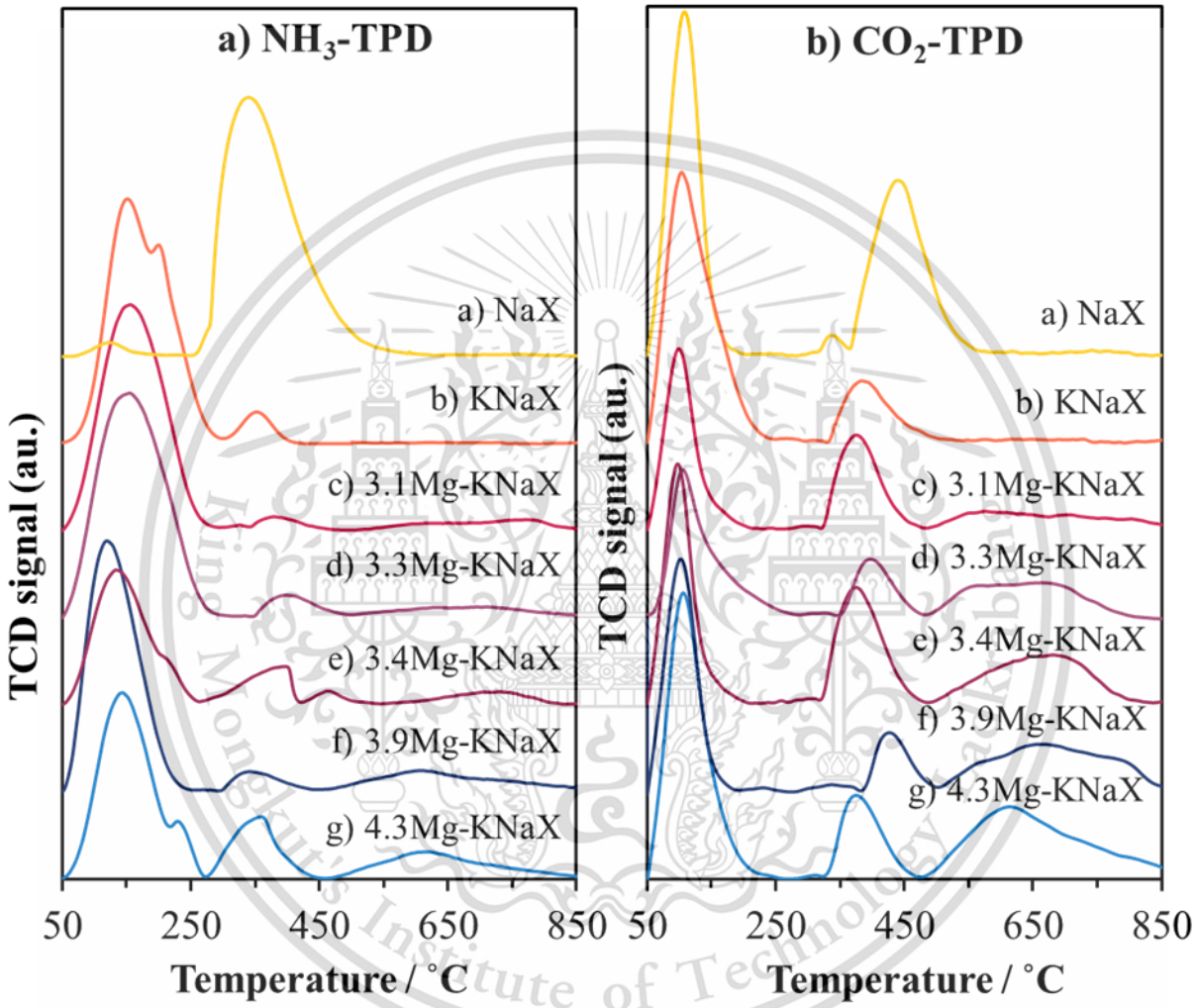

Figure 5 (a) NH3-TPD and (b) CO_2-TPD profile of zeolite catalysts.

Table 3 Acid/Base properties of catalysts.

Entry	Catalysts	[a]Acidity (mmol/g)		[b]Basicity (mmol/g)		[ac]Acidity x10³ (mmol/m²)		[bc]Basicity x10³ (mmol/m²)	
		total	450-850˚C	total	450-850˚C	total	450-850˚C	total	450-850˚C
1	NaX	3.9	-	0.5	-	8.5	-	1.1	-
2	KNaX	3.4	-	0.2	-	9.5	-	0.6	-
3	3.1Mg-KNaX	3.3	0.3	0.3	0.1	6.2	0.5	0.6	0.1
4	3.2Mg-KNaX	3.7	0.3	0.3	0.1	7.6	0.7	0.6	0.2
5	3.4Mg-KNaX	2.3	0.4	0.4	0.1	5.1	0.8	1.0	0.3
6	3.9Mg-KNaX	3.3	0.5	0.4	0.2	8.1	1.4	0.9	0.4
7	4.3Mg-KNaX	3.3	0.6	0.5	0.2	13.5	2.4	2.2	0.8

[a] Determined by NH_3-TPD

[b] Determined by CO_2-TPD

[c] Determined by BET

The CO_2-TPD and NH_3-TPD of Mg-KNaX displayed similar profiles as the KNaX, except unobvious peaks at 500-700˚C for both NH_3 and CO_2 adsorption. The desorption peak at high temperature for NH_3, represent strong Lewis acid site of Mg^{2+} from the occluded $[Mg_4(OH)_4]^{4+}$ species [23] and incorporated MgO nanoparticles [52-53]. While the desorption peak at a high temperature for CO_2 represent a strong basic site [54], presumably chemisorbed CO_2 on the occluded $[Mg_4(OH)_4]^{4+}$ species [23] or the decomposition of $MgCO_3$ formed by the reaction of CO_2 with the MgO nanoparticles [55-58]. In other words, the Mg^{2+} and O^{2-} of the occluded $[Mg_4(OH)_4]^{4+}$ species and the incorporated MgO nanoparticles are responsible for the strong Lewis acid site and Bronsted base site, respectively. As Mg loading increases, the number of acidity and basicity was raised along Mg content as show in **Figure 6 (Table 2, entry 3-7)**. However, acidity/surface area and basicity/surface area were significantly increased for 4.3 Mg-KNaX sample. This is a result of a significant drop in surface area due to the partial collapse of FAU structure, as mentioned earlier.

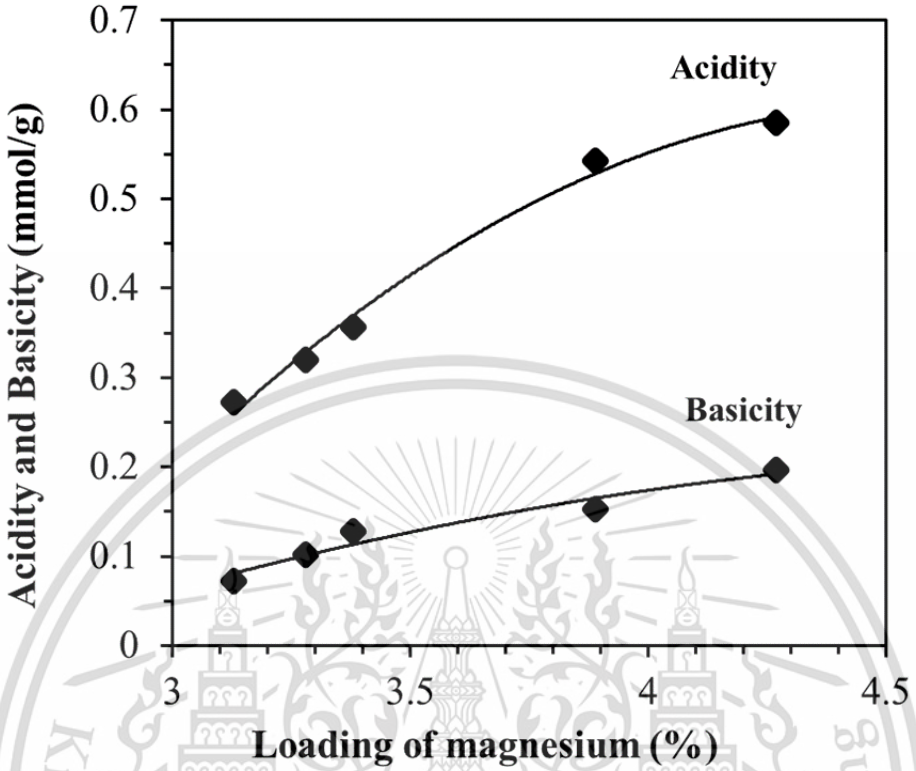

Figure 6 Relation of Magnesium loading with acidity and basicity of catalysts. (Desorption peak over 500°C)

4.2 Catalytic testing

4.2.1 Dehydrogenation of ethanol to acetaldehyde over $CuZn/SiO_2$ catalysts

The vapor-phase dehydrogenation of ethanol was primarily studied over $CuZn/SiO_2$ catalysts under N_2 and H_2 flow, as shown in **Table 4**. The reaction under H_2 provides higher conversion (65.8%), as compared to that under N_2 (41.8%). It is suggested that ethanol can be readily dehydrogenated to acetaldehyde that adsorbed as η^1-(O)-carbonyl species [59] on CuZn metal surface (Species (I) in **Scheme 8**). The carbonyl group of ethanol can dissociate over both Cu and Zn. The desorption of such species can be facilitated by an increased electron density of the metal surface, due to the dissociative adsorption of H_2 from the gas phase. While under N_2, the strong interaction of acetaldehyde (η^1-(O)-carbonyl species) with the electron-deficient CuZn surface can lead to formation of η^2-(C=O)- carbonyl species, as also shown in Scheme 1 (Species (II)). This strong adsorption mode limits accessible sites for further ethanol dehydrogenation, leading to lower activity under N_2, as compared to that in the presence of H_2. Accordingly, catalyst deactivation was observed, from a lower conversion after 240 min on stream (Table 4), particularly for the reaction under N_2. This again supports the hypothesis that strong product adsorption takes place in the absence of H_2.

Table 4 Conversion of ethanol to acetaldehyde over $CuZn/SiO_2$ catalysts

Entry	Catalysts	W/F (g.h/mol)	Carrier gas	Conversion (%) at 40 min	Conversion (%) at 240 min	Selectivity (%)			
						Ethylene	Acetaldehyde	Acetone	C4 aldehyde
1	$CuZn/SiO_2$	5	N_2	41.8	19.5	0.9	98	0.1	0.9
2	$CuZn/SiO_2$	5	H_2	65.8	44.4	0.4	97.6	1.3	0.8

(Reaction condition; temperature: 380°C, pressure: atmospheric pressure., flow rate of carrier gas: 160 mL/min, reaction at 40 min on stream)

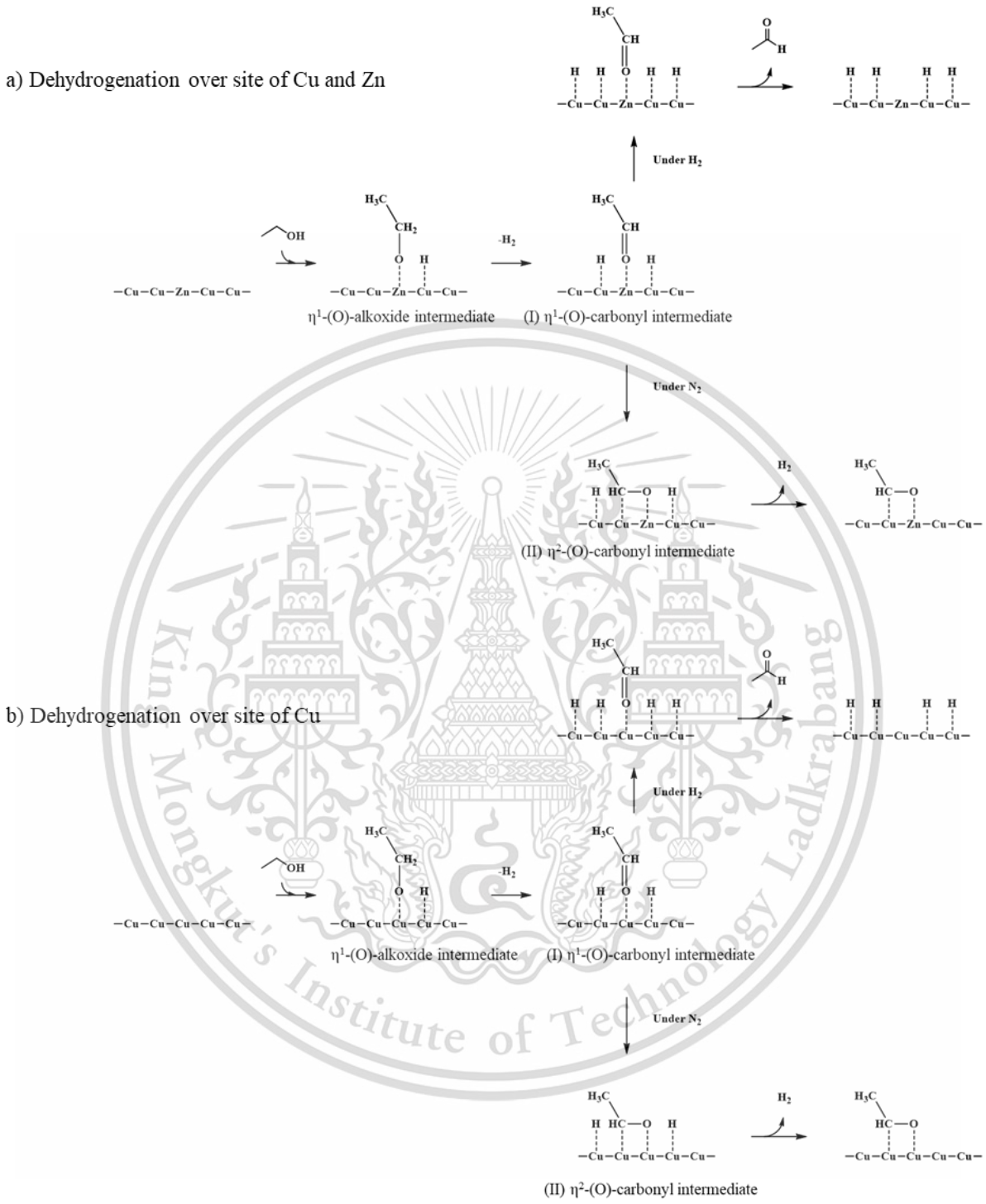

Scheme 8 Possible reaction pathway for dehydrogenation of ethanol over $CuZn/SiO_2$ catalyst.

Nevertheless, high selectivity of acetaldehyde was obtained for both reactions under H_2 and N_2. Small amounts of other products included C4 aldehyde, acetone, and ethylene. These

products were typically promoted by the Lewis acid sites [60], retained from incomplete reduction of CuO-ZnO. Over the bifunctional catalyst (CuZn/CuO-ZnO), C4 aldehyde was produced by aldol condensation of the acetaldehydes as shown in **Scheme 8**. Acetone may well be generated by the decarbonylation of 3-oxobutanal intermediate. In addition, ethylene can be promoted by the dehydration of ethanol as also shown in **Figure 7**. With highly selective acetaldehyde production, this $CuZn/SiO_2$ was later included in the hybrid catalyst system. As the acetaldehyde is a precursor for aldol condensation step, C-C coupling would be enhanced for Guerbet reaction. In addition, H-transfer may also be facilitated by the in situ produced hydrogen from the increased dehydrogenation activity of the $CuZn/SiO_2$. Such improved H-transfer would increase higher alcohol selectivity and suppress the formation of high MW products that causes catalyst deactivation for typical zeolite-based catalysts.

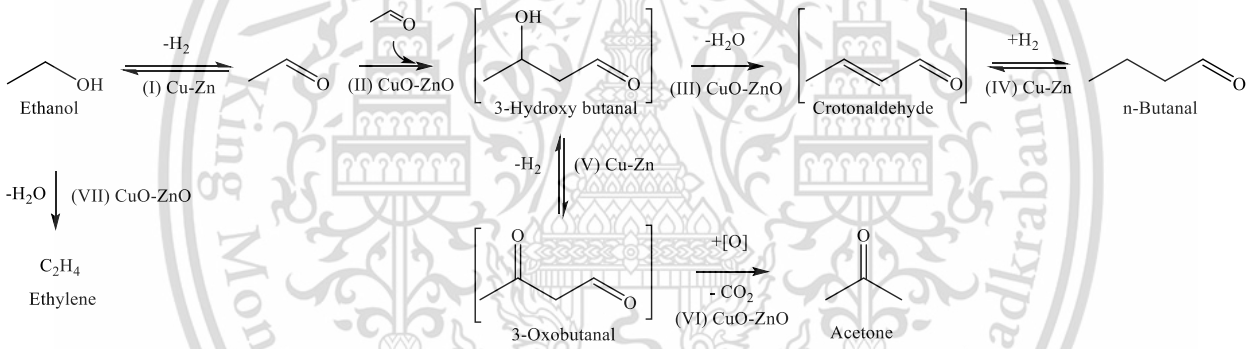

Figure 7 The reaction pathway of ethanol over $Cu-Zn/SiO_2$.

4.2.2 Conversion of ethanol over zeolite catalysts

The catalysts performance of various zeolite catalysts for ethanol conversion was shown in **Table 5**. NaX catalyst provides 33.4% conversion with only small amounts of higher alcohols. Most of ethanol was dehydrated to undesirable ethylene (~76% selectivity) because high amounts of residual acid site remained on the NaX catalyst [45], as observed in NH_3-TPD (**Figure 5a**). Incorporation of K^+ (KNaX) leads to lower conversion (11.1%) and ethylene selectivity (~58%) since medium acid sites is decreased due to obscuring of occlude K^+ salt (see **Figure 5a**, **Table 2**). However, only trace amounts of higher alcohols were obtained (~3% selectivity), presumably due to the lack of strong basic sites (see **Figure 5b**).

Table 5 Product distributions from ethanol conversion overs zeolite catalysts.

Entry	Catalysts	% Conversion	% Yield						
			Acetaldehyde	C4 aldehyde	C4 alcohol	Ethylene	Diethyl ether	Butadiene	Acetone
1	NaX	33.4	1.6	1.4	1.0	25.2	2.0	2.2	-
2	KNaX	11.1	1.1	0.8	0.3	6.4	2.5	-	-
3	3.1Mg-KNaX	16.9	1.9	0.7	3.1	6.3	2.0	1.1	1.8
4	3.3Mg-KNaX	14.1	3.2	1.2	3.3	3.3	1.9	0.9	1.4
5	3.4Mg-KNaX	15.8	2.1	1.6	4.3	3.4	1.8	1.0	1.6
6	3.9Mg-KNaX	14.7	2.4	1.2	4.1	2.8	1.7	1.2	1.2
7	4.3Mg-KNaX	15.0	2.9	1.6	3.9	2.0	1.7	1.1	1.7

(Reaction condition; contact time 16.75 g.h./mol, temperature: 380°C, pressure: atmospheric pressure., flow rate of N_2 carrier gas: 160 mL/min, reaction at 40 min time on stream)

After 3.1wt% of Mg was incorporated into KNaX, C4 alcohol was observed. As Mg loading increased from 3.1 to 4.3 wt%, selectivity of Guerbet products (acetaldehyde, C4 aldehyde, and C4 alcohol) were readily increased, which provide highest C4 alcohol selectivity (~28%) at 3.9 wt% of Mg as shown in **Figure 8**. This is because the presence of Lewis acid site, Mg^{2+}, of the occluded $[Mg_4(OH)_4]^{4+}$ species or the incorporated MgO nanoparticles can promote dehydrogenation/ hydrogen transfer of ethanol to acetaldehyde. While the strong basic site from O^{2-} of the occluded $[Mg_4(OH)_4]^{4+}$ species or the MgO nanoparticles can catalyze aldol condensation of the acetaldehyde to C4 aldehyde. As the Lewis acid and basic sites are in closed proximity, hydrogen transfer (MPV reaction [60-62]) from ethanol to the forming C4 aldehyde can be readily facilitated, yielding C4 alcohol as observed (**Scheme 9**). Accordingly, the more the MgO incorporated, the higher the Guerbet products. However, at 4.3 wt% MgO loading, selectivity to aldol products was somewhat declined. This is presumably due to an excessive increase in dehydrogenation activity, as compared to the condensation activity, for this catalyst.

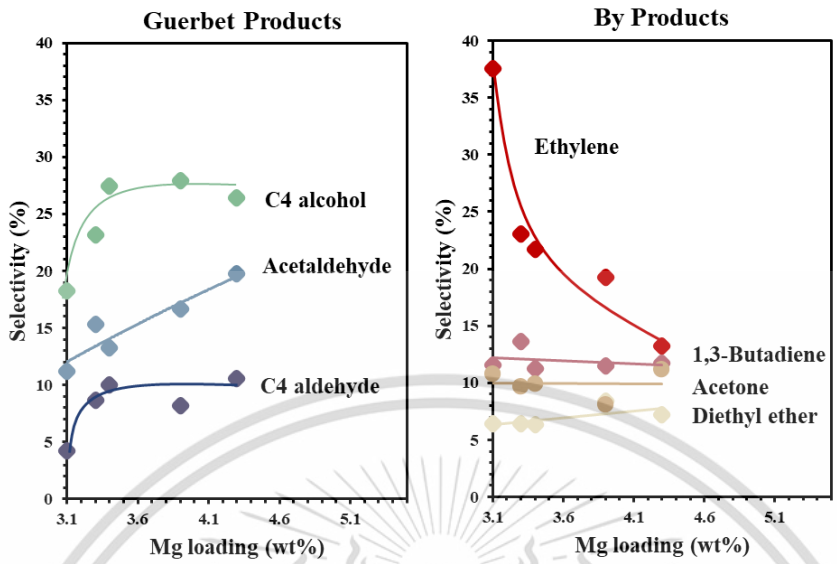

Figure 8 Product selectivity at similar conversion (~15%) at various Mg loading over KNaX. (Reaction condition; contact time 16.75 g.h./mol, temperature: 380°C, pressure: atmospheric pressure., flow rate of N_2 gas: 160 mL/min, selectivity at 40 min on stream)

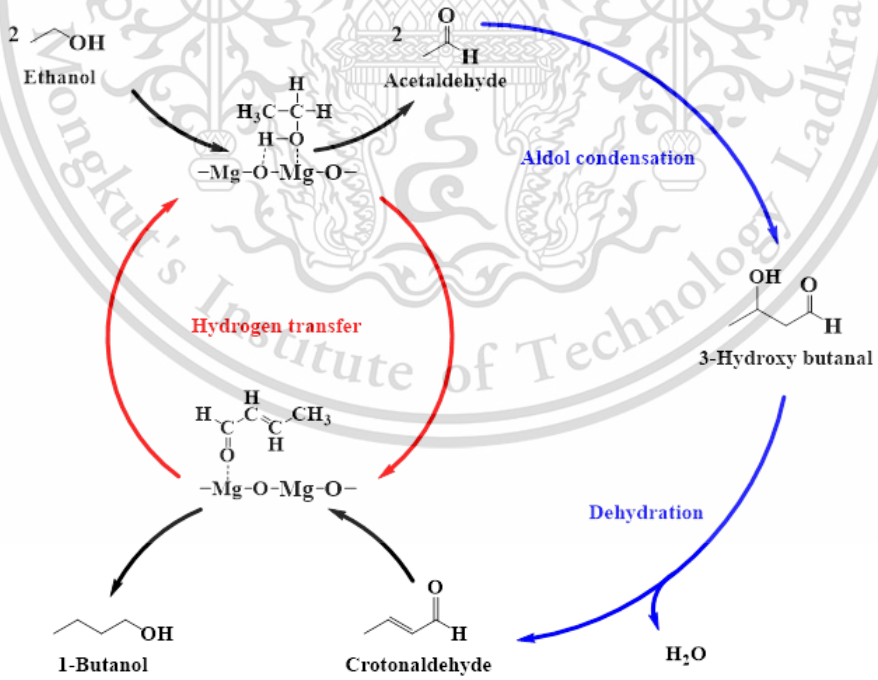

Scheme 9 Proposed reaction pathway for ethanol conversion over Mg-KNaX catalysts.

In the opposite manner, ethylene selectivity sharply decreased with Mg loading. This is because the dehydration activity is decreased due to loss of medium acid sites by formation of the occluded $[Mg_4(OH)_4]^{4+}$ species in the zeolite cavities as seen from **Figure 5a**. However, the selectivity of diethyl ether (~7%), 1,3-butadiene (~12%), and acetone (~10%) remain similar for all Mg loading. This suggested that these products were not promoted by the occluded $[Mg_4(OH)_4]^{4+}$ species or the incorporated MgO nanoparticles, but rather by the KNaX support. Over the exchangeable cation of the zeolites, diethyl ether can be produced via bimolecular dehydration of ethanol, while 1,3-butadiene was produced via dehydration of 3-hydroxy butenal [43-65]. Decarbonylation of 3-oxobutanal intermediate can be also promoted with the alkali zeolite cavities [47], as shown in **Figure 9**.

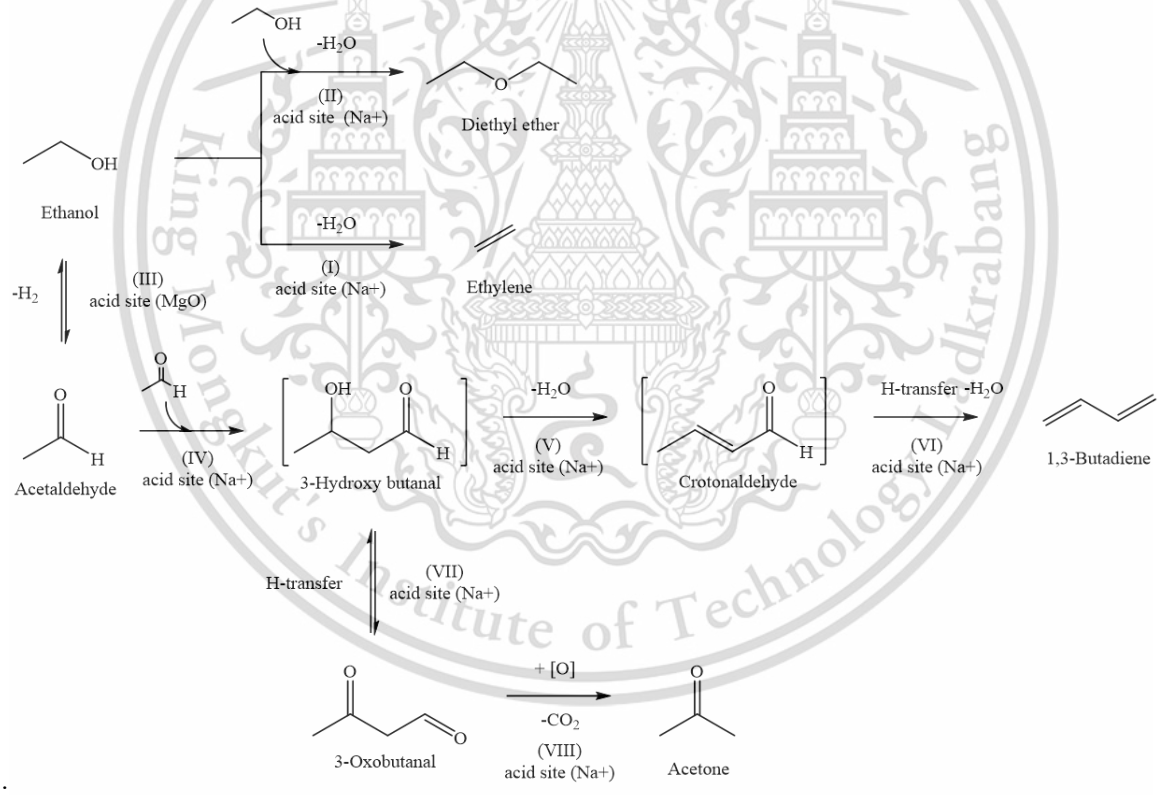

Figure 9 Possible reaction pathway for ethanol conversion of by-product over Mg-KNaX catalyst.

From the above results, it seems that a balance between the Lewis acid and base sites for Guerbet reaction is highly sensitive to the amounts of Mg^{2+} incorporated on KNaX. A catalyst with relatively low Mg^{2+} (3.1wt.%) provides a limited aldol condensation activity but enhances the dehydration of ethanol to ethylene by-products. On the other hand, dehydrogenation is excessively promoted to acetaldehyde over a catalyst with high Mg^{2+} (4.3 wt.%). This is presumably because the proximate Lewis acid-base sites would be obtained only from the occluded $[Mg_4(OH)_4]^{4+}$ species or the highly dispersed MgO nanoparticles that interacts with either internal or external surface of the zeolites. According to the result in **Figure 8**, 3.9Mg-KNaX appears to offer appropriate Lewis acid-base sites for high selectivity to C4-alcohol, and was selected as a hybrid catalyst component.

4.2.3 Conversion of ethanol over hybrid $CuZn/SiO_2$ + 3.9Mg-KNaX catalysts

To improve conversion and higher alcohol yields, a hybrid catalyst system, containing $CuZn/SiO_2$ (for dehydrogenation) and 3.9Mg-KNaX (for Guerbet reaction), was investigated and the results are shown in **Table 6**. For the sequential bed configuration under N_2, the reaction over $CuZn/SiO_2$ + 3.9Mg-KNaX provided a similar conversion to that of the single bed $CuZn/SiO_2$ (~42% conversion, **Figure 10a** and **10b**). It is suggested that ethanol is dehydrogenated over the first bed ($CuZn/SiO_2$) with relatively the same rate, producing acetaldehyde and H_2. As entering the second bed (3.9Mg-KNaX), aldol condensation of acetaldehyde is then promoted to higher alcohol, likely with hydrogen transfer from H_2 produced from the first bed. The hydrogen transfer from gas phase H_2 have been evidenced by D_2 exchange over zeolites with low Si/Al [67]. It is suggested that negligible hydrogen transfer from ethanol took places in the second bed, otherwise higher conversion of ethanol would have been observed. As the conversion is relatively high, selectivity of C4 alcohol is lower than that over 3.9Mg-KNaX catalysts (**Table 5**, **entry 6**). Nevertheless, a higher yield of C4 alcohol yield (7.4%) was observed as compared to that over 3.9Mg-KNaX catalysts alone (4.1%). This suggests that the increased amounts of acetaldehyde by ethanol dehydrogenation over the first bed ($CuZn/SiO_2$), lead to an increase in aldol condensation/ hydrogen transfer to C4 alcohol over the second bed (3.9Mg-KNaX).

Table 6 Product distributions over hybrid $CuZn/SiO_2$ + 3.9Mg-KNaX catalysts.

Entry	W/F $CuZn/SiO_2$+ 3.9Mg-KNaX (g.h./mol)	Catalyst ratio	Bed configuration	Carrier Gas	Conversion (%)	Selectivity (%)									
						Acetaldehyde	C4 aldehyde	C4 alcohol	C6 aldehyde	C6 alcohol	Ethylene	Diethyl Ether	Butadiene	Acetone	Total Higher Alcohols
1	5 + 10	0.5	S	N_2	42.0	75.0	4.3	17.6	-	-	2.1	0	0	1.1	17.6
2	5 + 10	0.5	S	H_2	65.4	78.1	4.7	15.5	-	-	0.5	0	0	1.1	15.5
3	5 + 10	0.5	P	N_2	23.1	36.2	4.1	28.9	-	15.5	7.6	0	7.7	0	44.4
4	5 + 10	0.5	P	H_2	23.5	42.1	4.6	27.1	-	15.4	5.2	0	5.5	0	42.5
5	0 + 15	0.0	P	N_2	14.4	15.1	7.1	28.9	-	-	18.6	12.5	7.9	1.5	28.9
6	2.6 + 12.4	0.2	P	N_2	22.0	27.3	3.6	33.1	2.5	17.6	6.8	0	9.2	0	50.7
7	7.5 + 7.5	1.0	P	N_2	22.0	52.8	4.1	20.6	-	9.2	7.8	0	5.5	0	29.8
8	10 + 5	2.0	P	N_2	25.2	64.7	3.5	15.9	-	6.6	6.4	0	2.9	0	22.5

(Reaction condition; temperature: 380˚C, pressure: atmospheric pressure., flow rate of N_2 carrier gas: 160 mL/min, conversion and selectivity at 40 min time on stream)

A higher conversion (65.4%) over hybrid catalyst system was obtained under H_2 (**Figure 10b'**) since ethanol dehydrogenation rate is increased over $CuZn/SiO_2$ as discussed in 2.1. The C4 alcohol yield (10.1%) increases with the conversion with similar selectivity to that under N2 (**Table 6, entry 1** vs **2**). This suggests that the presence of H_2 have an impact only on the $CuZn/SiO_2$ bed, no effect of H_2 on C4 alcohol production over 3.9Mg-KNaX bed. This is because aldol condensation of acetaldehyde, produced from the first bed, is the rate determining step for C-C coupling. Even though H_2 is abundant for H-transfer, the reaction is still limited by number of active sites in the second bed. Accordingly, the sequential bed configuration cannot readily be improved to higher alcohol production. Moreover, the catalyst deactivation is observed both under N_2 and H_2 (**Figure 10b** and **10b'**) due to product adsorption over $CuZn/SiO_2$ catalyst, as previously discussed in 2.1.

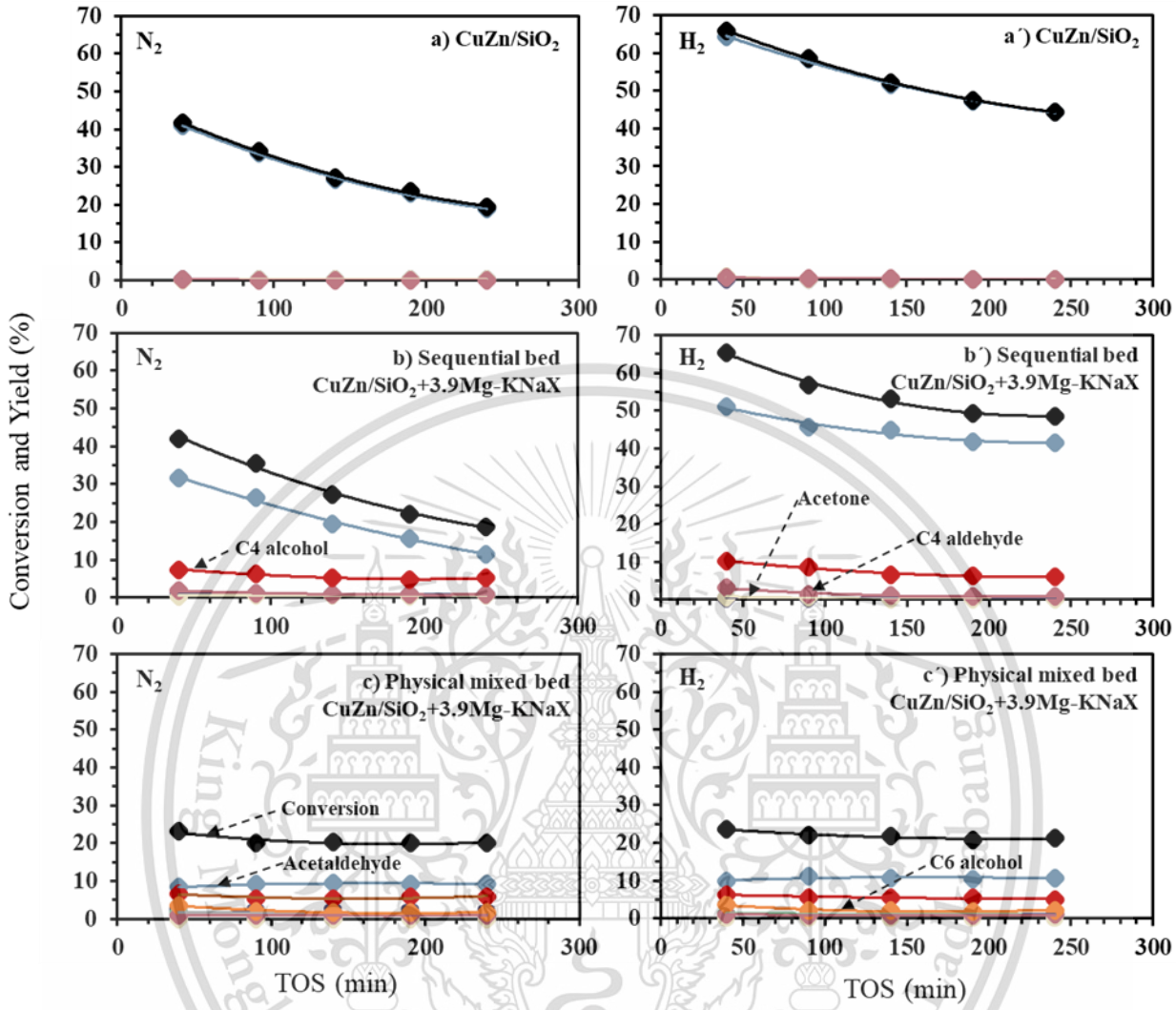

Figure 10 Conversion and yield with time on steam of hybrid catalysts a) $CuZn/SiO_2$ under N_2, a′) $CuZn/SiO_2$ under H_2, b) Sequential bed under N_2, b′) Sequential bed under H_2, c) Physical mixed bed under N_2, and c′) Physical mixed bed under H_2.

(Reaction condition; temperature: 380°C, pressure: atmospheric pressure., flow rate of carrier gas: 160 mL/min, reaction at 40 min time on stream, catalyst ratio of $CuZn/SiO_2$+3.9Mg-KNaX = 5+10 g.h/mol)

For the physical mixed bed system under N_2 (**Figure 10c**), a lower conversion was obtained, as compared to the sequential bed system (**Figure 10b**). This is because when ethanol entering in the bed, $CuZn/SiO_2$ is dispersed with Mg-KNaX leading to a decrease in the dehydrogenation activity to acetaldehyde and H_2. The acetaldehyde formed over $CuZn/SiO_2$ can

be readily coupling to higher MW products over the adjacent Mg-KNaX, which can be re-adsorbed on some of the neighboring CuZn/SiO_2. The competitive adsorption of such high MW products limits accessible sites for ethanol, leading to a lower dehydrogenation over the physical mixed bed system.

However, such lower dehydrogenation activity is somewhat beneficial the significant increase in total higher alcohols selectivity (C4 alcohol and C6 alcohol, ~44%), especially the C6 alcohol (**Table 6**, **entry 3**). This is because, as lower amount of H_2 is produced over CuZn/SO_2, the rate of hydrogen transfer over Mg-KNaX is limited in physical mixed bed system. Hence, relatively less C4 aldehyde intermediates could be hydrogenated/ hydrogen transfer to C4 alcohol over Mg-KNaX, but rather undergo aldol condensation with acetaldehyde from the near-by CuZn/SiO_2, to produced C6 aldehydes and eventually C6 alcohol as illustrated in **Scheme 10**. The lower hydrogen transfer activity in the physical mixed bed system also leads to formation of butadiene. This is because a limited hydrogen transfer to C4 aldehyde could result in crotyl alcohol that is an intermediate for butadiene over Mg-KNaX as shown in **Scheme 9** and **Scheme 10**.

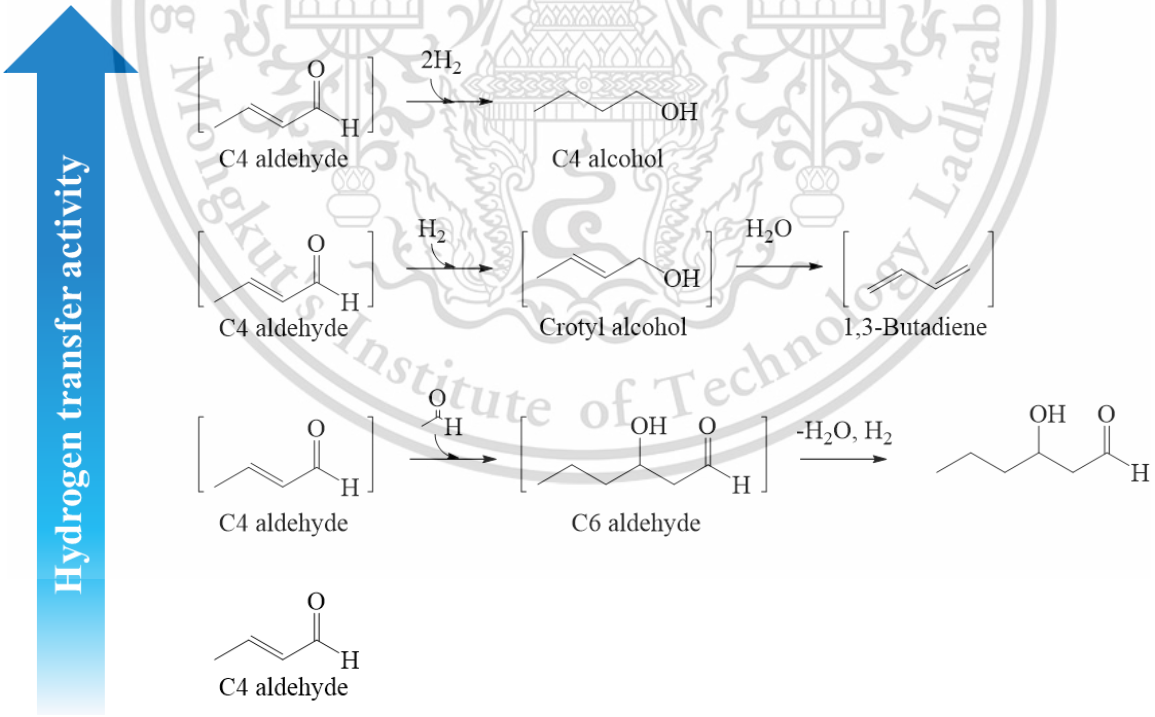

Scheme 10 Dependence of product distribution on H-transfer activity.

Moreover, the catalytic stability of the physical mixed bed is superior to that in the sequential bed one. This is because acetaldehyde can be readily desorbed from CuZn/SiO_2 surface by the water produced over the neighboring Mg-KNaX. As the aldol condensation of aldehydes over Mg-KNaX takes place concurrently with the ethanol dehydrogenation over CuZn/SiO_2, water and coupling products from Mg-KNaX can re-adsorbed on neighboring CuZn/SiO_2. This would facilitate the desorption of acetaldehyde from the CuZn/SiO_2 surface, suppressing the catalysts deactivation. Accordingly, such synergic effect between CuZn/SiO_2 and Mg-KNaX in the physical mixed bed system can improve the catalyst stability, when compared to the sequential bed system.

The reaction under H_2 in the physical mixed bed system provided the same conversion and total higher alcohol selectivity as that under N_2 (**Table 6**, **entry 4**). This is probably because the accessible site for ethanol dehydrogenation over CuZn/SiO_2 in this case, was virtually governed by competitive adsorption of H_2O and coupling product from the near-by Mg-KNaX, as discussed above. Hence, the presence of H_2 would play no role on dehydrogenation rate as in the sequential bed system.

Comparing hybrid CuZn/SiO_2 ¦ Mg-KNaX catalyst in physical mixed bed system with 3.9Mg-KNaX single bed (Figure 8a and 8b**)**, much higher conversion (up to ~50%) was obtained with higher selectivity of higher alcohols as shown in **Figure 11**. This is because the presence of CuZn/SiO_2 in the hybrid catalyst can provide a higher rate of dehydrogenation/ hydrogen transfer, as compared to Mg-KNaX alone. The formation of acetaldehyde and H_2 were readily enhanced leading to a significant increase in higher alcohol yields (C4 alcohol and C6 alcohol). It is suggested that the aldol condensation rate in hybrid catalyst system is higher than that in Mg-KNaX single bed despite the lower Mg content in the hybrid catalyst system. This is due to the presence of CuZn/SiO_2 as dehydrogenation catalysts that provides a greater amount of acetaldehyde and H_2, as compared to the Mg-KNaX single bed. Hence, aldol condensation of acetaldehydes over Mg-KNaX in the hybrid catalyst to higher aldehyde intermediates would be enhanced. Moreover, the hydrogenation/ hydrogen transfer from the neighboring CuZn/SiO_2 to higher alcohol would be promoted, suppressing adsorption of higher MW intermediates/products on the Mg-KNaX in the hybrid catalyst. In contrast, lower acetaldehyde and limited hydrogen transfer of the Mg-KNaX single bed led to relatively lower aldol condensation activity but more product adsorption,

resulting in lower yields of higher alcohol as observed. With an appropriate bed configuration (physical mixed), the synergy of $CuZn/SiO_2$ and Mg-KNaX in the hybrid catalyst play important role in the improved activity and stability for Guerbet reaction.

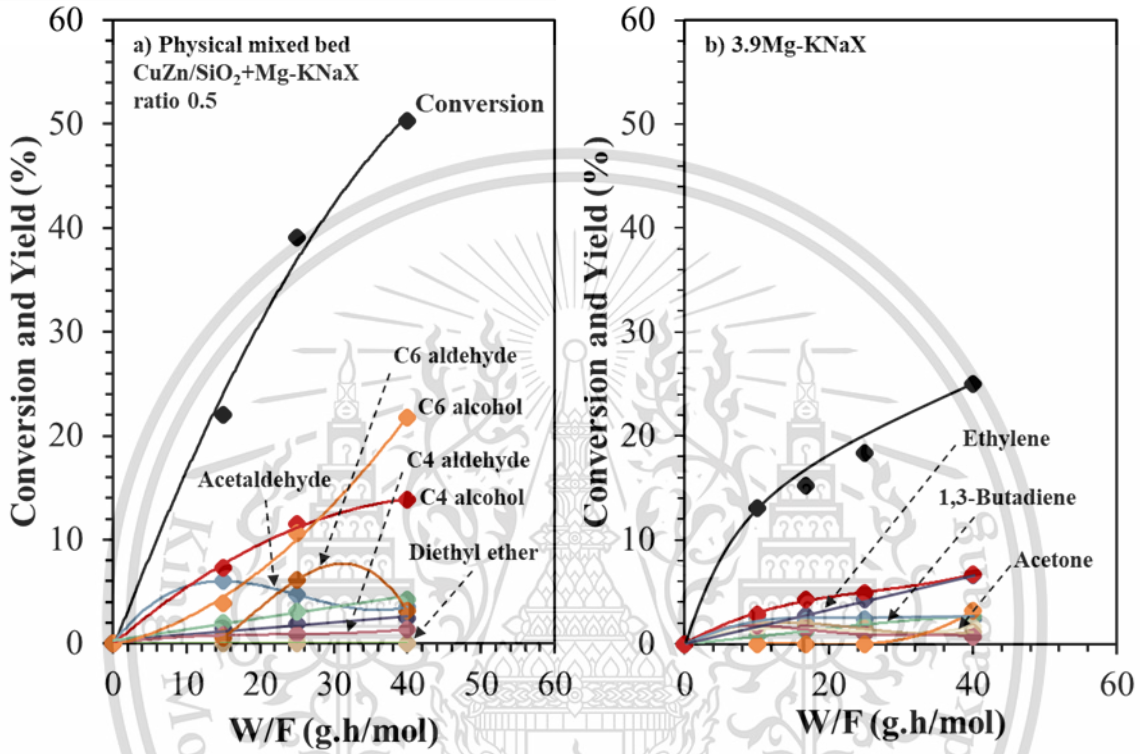

Figure 11 Conversion and yield over a) hybrid catalyst in physical mixed system compared to b) 3.9Mg-KNaX.

(Reaction condition; temperature: 380 °C, pressure: atmospheric pressure., flow rate of carrier gas: 160 mL/min)

In addition to the bed configuration, the synergy between $CuZn/SiO_2$ and Mg-KNaX would essentially depend on the composition of the hybrid catalyst as shown in **Figure 12**. When $CuZn/SiO_2$ is incorporated at the $CuZn/SiO_2$:Mg-KNaX ratio of 0.2, the conversion and higher alcohol yields were significantly increased, as discussed earlier. With the same contact time, an increase in $CuZn/SiO_2$:Mg-KNaX ratio from 0.2 to 1.0 provided continual rises in conversion and acetaldehyde yields. This is because the ethanol dehydrogenation rate was readily promoted by an increased $CuZn/SiO_2$ in the bed. However, the C4 alcohols and C6 alcohols were gradually

decreased. This is derived from a limited aldol condensation of acetaldehyde due to a decrease in number of basic sites from Mg-KNaX fraction. Further increase in $CuZn/SiO_2$:Mg-KNaX ratio to 2.0 leads to a proportional increase in acetaldehyde yield. Nevertheless, no significant change in higher alcohols yields can be observed. This suggested that the increasingly produced acetaldehyde cannot be further coupled to higher MW products, bearing more acetaldehyde and hydrogen in the product stream. Hence, the conversion is slightly increase, presumably due to a thermodynamic limitation. It is suggested from this study that an improved synergy between $CuZn/SiO_2$ and Mg-KNaX can be obtained with the ratio of 0.2, where the rate of dehydrogenation/H-transfer and aldol condensation can be optimized for higher alcohol production.

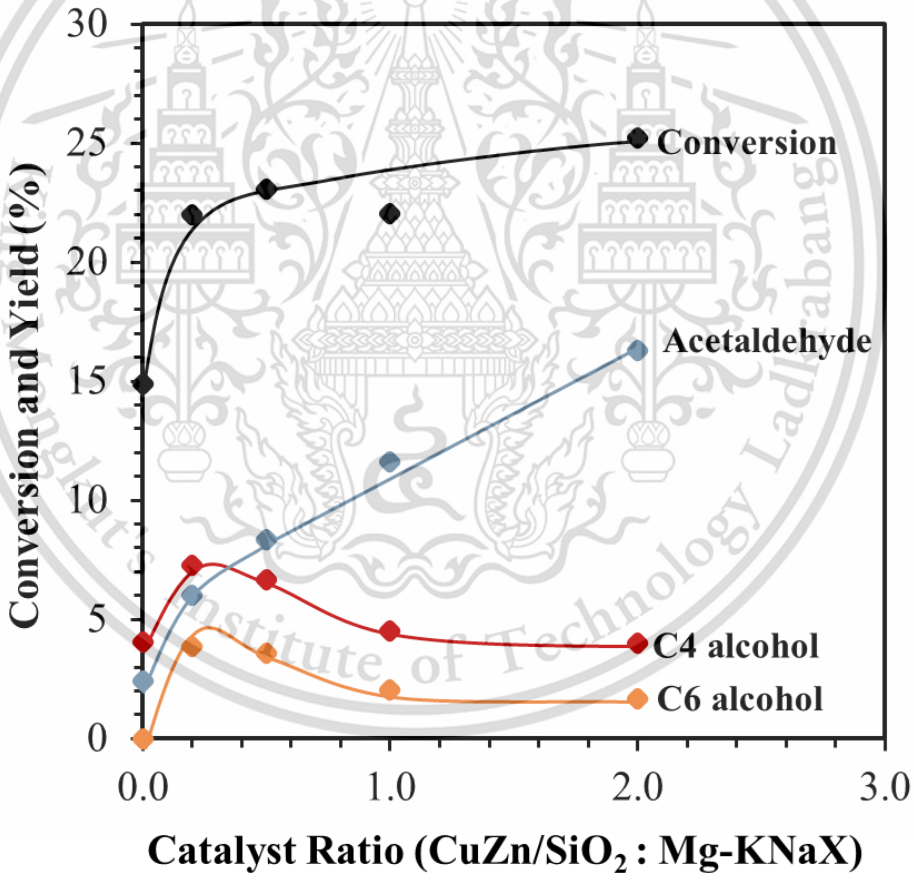

Figure 12 Conversion and yield of physical mixed bed under H_2 Gas.

(Reaction condition; temperature: 380°C, pressure: atmospheric pressure., flow rate of H_2: 160 mL/min)

Chapter 5

Conclusions and suggestions

5.1 Conclusions

The incorporation of Zn into $CuZn/SiO_2$ catalyst provided high activity with acetaldehyde selectivity up to ~97% under H_2 atmosphere, presumably due to a weaker acetaldehyde adsorption of the metal surface. Ion exchange of NaX with K^+ can significantly decrease the medium acid site and dehydration activity. The incorporated MgO species are highly dispersed as the occluded $[Mg_4(OH)_4]^{4+}$ species in zeolite cavities and as MgO nanoparticles on external surface, providing additional strong basic and acid sites. The increase in Mg loading readily enhances C4 alcohol selectivity by suppressing the undesirable ethanol dehydration to ethylene. The dehydrogenation/hydrogen transfer rate is significantly improved over the hybrid $CuZn/SiO_2$ ¦ Mg-KNaX catalyst in sequential bed system. However, the higher alcohol selectivity is decreased with rapid deactivation, due to the large amounts of acetaldehyde present. In a different manner, the physical mixed bed containing $CuZn/SiO_2$:Mg-KNaX ratio of 0.2 allows a synergistic effect between the two catalysts, leading to a balance between dehydrogenation/hydrogen transfer and aldol condensation rate. The hybrid $CuZn/SiO_2$ ¦ Mg-KNaX catalyst provided up to 50% conversion with 66% higher alcohol selectivity and an improved stability. This is due to the water and high MW product produced over Mg-KNaX can inhibit acetaldehyde adsorption on the neighboring $CuZn/SiO_2$.

5.2 Suggestions

1. The catalytic stability, cause of deactivation, and catalyst regenerating should be investigated.

2. The activity of CuZn-KNaX catalyst prepared by impregnation method should be studied and compared with the hybrid catalyst.

References

1 J. Scalbert, F. Thibault-Starzyk, R. Jacquot, D. Morvan, F. Meunier. 2014. “Ethanol condensation to butanol at high temperatures over a basic heterogeneous catalyst: How relevant is acetaldehyde self-aldolization.” Journal of Catalysis. vol. 311. pp. 28–32.

2 Y. Van, D. Meer. 2017. “Sustainable bio-based materials: opportunities and challenges” Biotech France.

3 Hanspal, Sabra, dissertation. 2016. University of Virginia.

4 B. Ndaba, S. Chiyanzu, I. Marx. 2015. “n-Butanol derived from biochemical and chemical” Biotechnology Reports.

5 E.V. Makshina, W. Janssens, B.F. Sels, P.A. Jacobs. 2012. “Catalytic study of the conversion of ethanol into 1,3-butadiene.” Catalysis Today. vol. 198. pp. 338-44.

6 DY. Chen, Y. Wang, Y. Liu, K. Cen, X. Cao, Z. Ma, et al. 2019. “Chemistries and processes for the conversion of ethanol into middle-distillate fuels” Nat Rev Chem. 3. 223-49.

7 Clark, R. T. 1976. “Vapor-phase conversion of methanol and ethanol to higher linear primary alcohols by heterogeneous catalysis”. U.S. Patent. 3. 972. 952.

8 Gines, M. J. L. “Iglesia, E. 1998 “Bifunctional condensation reactions of alcohols on basic oxides modified by copper and potassium” J. Catal. 176. 155–172.

9 D.Gabriels, W. Y. Hernandez, B. Sels, P. V. D. Voort, A. Verberckmoes. 2013. “Review of catalytic systems and thermodynamics for the Guerbet condensation reaction and challenges for biomass balorization” Catalysts Science & Technology. vol. 1. number 1. pp-100.

10 Di Cosimo, J.I. Apesteguin, C.R, Gine M.J.L. and lglesa, E. 1998. “Structural Requirements and Reaction Pathways in Condensaton Reaction of Alcohol on MgyAlOx Catalyst” Journal Catalysis. 190. 261-275.

11 S. Ogo, A. Onda, K. Yanagisawa “Selective synthesis of 1-butanol from ethanol over strontium phosphate hydroxyapatite catalysts” Applied Catalysis A, pp.188-195

12 Jorge Quesada, Laura Faba, Eva Díaz, Salvador Ordóñez. 2018. “Enhancement of the 1-butanol productivity in the ethanol condensation catalyzed by noble metal nanoparticles supported on Mg-Al mixed oxide.” Applied Catalysis A. General 563. pp. 64-72

13 O. V. Larina, P. I. Kyriienko, N. D. Shcherban, P. S. Yaremov, D. Y. Balakin, I. Khalakhan, K. Veltruska, S. O. Soloviev, S. M. Orlyk. 2021. “Carbon-Supported Mg–Al Oxide Hybrid Catalysts for Aqueous Ethanol Conversion into 1-Butanol in a Flow Reactor” American Chemical Society. Ind. Eng. Chem. Res. 60. pp.11964-11976.

14 I. C. Marcu, N. Tanchoux, F. Fajula, D. Tichit. 2012. “Catalytic Conversion of Ethanol into Butanol over M–Mg–Al Mixed Oxide Catalysts (M 5 Pd, Ag, Mn, Fe, Cu, Sm, Yb) Obtained from LDH Precursors” Springer Science+Business Media New York.

15 H. Brasil, A. F. B. BittencourtK, K. C. E. S. Yokoo, P. C. D. Mendes, L. G. Verga, K. F. Andriani, R. Landers, J. L. F. D. Silva, G. P. Valenca. 2021. “Synthesis Modification of Hydroxyapatite Surface for Ethanol Conversion: The Role of the Acidic/Basic Sites Ratio” Journal of Catalysis.

16 L. Silvester, J. F. Lamonier, J. Faye, M. Capron, R. N. Vannier, C. Lamonier, J. L. Dubois, J. L. Couturier, C. Calais, F. Dumeignil. 2015. “Reactivity of ethanol over hydroxyapatite-based Ca-enriched catalysts with various carbonate contents†” Catalyssis Science & Technology. The Royal Society of Chemistry.

17 B. Szabo, G. Novodarszki, Z. May, J. Valyon, J. Hancsok, R. Barthos. 2020. “Conversion of ethanol to butadiene over mesoporous In_2O_3-promoted MgO-SiO_2 catalysts” Molecular Catalysis 491.

18 D. Fan, et al., 2017. “DFT study on aldol condensation reaction on MgO in the process of ethanol to 1,3-butadiene: Understanding the structure-activity relationship” Phys. Chem. Chem. Phys.

19 A. S. S. A. Susanto, N. Plint, N.J. Covill. 2003. “Dimerisation of ethanol to butanol over solid-base catalysts” Applied Catalystsis A. General 251. pp 337-345.

20 S. A. Susanto, R. T. Yunarti, R. R. Widjaya, Y. Maryati, A. A. Dwiatmoko, F. Aulia, N. Rinaldi. 2020. “Catalytic conversion of ethanol to butanol over magnesium oxide catalysts” Materials Science and Engineering.

21 H. Wang, et al. 2020. “Efficient One-pot Valorization of Ethanol to 1-Butanol over Earthabundant Ni-MgO Catalyst under Mild Conditions” Sustainable Energy & Fuels.

22 L. Zhang, T. N. Pham, et al. 2016. “Synthesis of C4 and C8 Chemicals from Ethanol on MgO Incorporated Faujasite Catalysts with Balanced Confinement Effects and Basicity” CHEMSUSCHEM. 9. 739-748.

23 N. Yotkkham, K. Choojun, P. Promchana, X. Fan, T. Sooknoi. 2022. “Higher alcohol production from ethanol over occluded $[Mg_4(OH)_4]^{4+}$ clusters in MgO/KNaX” Applied Catalysis A. General 632.

24 G. Garbarino, P. Riani, M. V. Garcia, E. Finocchil, V. S. Escribano, G. Busca. 2019. “A study of ethanol dehydrogenation to acetaldehyde over copper/zinc aluminate catalysts” Catalysis Today.

25 N. Iwasa, N. Takezawa. 1991. “Reforming of Ethanol Dehydrogenation to Ethyl Acetate and Steam Reforming to Acetic Acid over Copper-Based Catalysts” Bull. Chem. Soc. Jpn. 64. pp. 2619-2623.

26 S. Fujita, N. Iwasa, H. Tani, W. Nomura, M. Arai, N. Takezawa. 2001. “Dehydrogenation of Ethanol over Cu/ZnO Catalysts Prepared Form Various Coprecipitated Precursors” React. Kinet. Catal. Lett. Vol. 73. No. 2. pp. 367-372.

27 M. Ohira, H. Liu, D. he, Y. Hirata, M. Sano, T. Suzuki, T. Miyake. 2018. “Successive vapour phase Guerbet condensation of ethanol and 1-butanol over Mg-Al oxide catalysts in a flow reactor” Journal of the Japan Petroleum Institute. 61. (4). pp. 205-212.

28 “Alcohols” [Online]. Available: http://goldbook.iupac.org/A00204.html.

29 I. Majerz, I. Natkaniec. 2006. “Experimental and theoretical IR, R, and INS spectra of 2,2,4,4-tetramethyl-3-t-butyl-pentane-3-ol.” Journal of Molecular Structure., vol. 788, pp. 93-101.

30 W. Gerhartz, Y. Stephen Yamamoto, F. Thomas Campbell, R. Pfefferkorn and F. Rounsaville. (1999). Abrasives to Aluminum Oxide. Ullmmann’s Encyclopedia of Industrial Chemistry (vol. A1, pp. 279-282). German: Boschstrasse 12.

31 “Reactions of Alcohols” [Online]. Available: http://2012books.lardbucket.org.

32 “Ethanol” [Online]. Available: http://en.wikipedia.org.

33 W. Gerhartz, Y. Stephen Yamamoto, F. Thomas Campbell, R. Pfefferkorn and F. Rounsaville. (1999). Dithiocarbamic Acid to Ethanol. Ullmmann's Encyclopedia of Industrial Chemistry (vol. A9, pp. 588-590). German: Boschstrasse 12.

34 Atsumi, S.; Hanai, T.; Liao, J. C. 2008. "Non-fermentative pathways for synthesis of branched-chain higher alcohols as biofuels". Nature 451 (7174). pp. 86–9.

35 "Butanol" [Online]. Available: http://en.wikipedia.org.

36 W. Gerhartz, Y. Stephen Yamamoto, F. Thomas Campbell, R. Pfefferkorn and F. Rounsaville. 1999. Alcohol to Calcium Sulfate. Ullmmann's Encyclopedia of Industrial Chemistry (vol. A4, pp. 451-454). German: Boschstrasse 12.

37 W. Gerhartz, Y. Stephen Yamamoto, F. Thomas Campbell, R. Pfefferkorn and F. Rounsaville. 1999. Benzyl alcohol to Calcium Sulfate. Ullmmann's Encyclopedia of Industrial Chemistry (vol. A4, pp. 290). German: Boschstrasse 12.

38 W. Gerhartz, Y. Stephen Yamamoto, F. Thomas Campbell, R. Pfefferkorn and F. Rounsaville. 1999. Abrasives to Aluminum Oxide. Ullmmann's Encyclopedia of Industrial Chemistry (vol. A1, pp. 322). German: Boschstrasse 12.

39 Sitthisa, S., Pham, T., Prasomsri, T., Sooknoi, T., Mallinson, R., & Resasco, D. 2011. "Conversion of furfural and 2-methylpentanal on Pd/SiO_2 and $Pd–Cu/SiO_2$ catalysts." Journal Of Catalysis. 280(1). 17-27.

40 Sitthisa, S., Sooknoi, T., Ma, Y., Balbuena, P., & Resasco, D. 2011. Kinetics and mechanism of hydrogenation of furfural on Cu/SiO_2 catalysts. Journal of Catalysis, 277(1), 1-13.

41 Anthony, J. 2001 "Guerbet Chemistry." Journal of Surfactants and Detergents." 4. 311-315.

42 Di Cosimo, J.I. Apesteguin, C.R, Gine M.J.L. and lglesa, E. 1998. "Structural Requirements and Reaction Pathways in Condensation Reaction of Alcohol on Mg_yAlO_x Catalyst." Journal Catalysis. 190: 261-275.

43 56 Ji, D., Zhu, W., Wang, Z., Wang, G. 2007. "Dehydrogenation of cyclohexanol on $Cu–ZnO/SiO_2$ catalysts: The role of copper species." Catalysis Communications, 8(12), 1891-1895

44 K. Gotoh, S.Nakamura, T. Mori and Y. Morikawa. “Supperted alkali salt catalysts active for the guerbet reaction between methanol and ethanol.” Studies in surface science and catalysis 130. Pp. 2669-2674.

45 C. Yang and Z. Meng. 1993. “Bimolecular condensation of ethanol to 1-butnaol Catalyzed by alkali cation zeolites.” Journal of catalysis. 142. pp. 37-44.

46 “Zeolite” [Online Available]: https://en.wikipedia.org/wiki/Zeolite

47 C. Yang and Z. Meng. 1993. “Bimoclucular Condensation of Ethanol to 1-Butanol Catalyzed by Alkali Cation Zeolite” Journal of Catalysis 142. pp. 37-44.

48 Ji D., Zhu, W., Wang, Z., Wang, G. 2007. “Dehydrogenation of cyclohexanol on Cu–ZnO/SiO_2 catalysts: The role of copper species.” Catalysis Communications. 8(12). 1891-1895.

49 H. Han, M. Liu, X. Nie, F. Ding, Y. Wang, J. Li, X. Guo, Chus Song “The promoting effects of alkali metal oxide in side-chain alkylation of toluene with methanol over basic zeolite X” Microporous and Mesoporous Material 234. 61-72. 2016.

50 F. Benaliouche, Y. Boucheffa, P. Ayrault, S. Mignard, P. Magnoux. 2008. “NH_3-TPD and FTIR spectroscopy of pyridine adsorption studies for characterization of Ag- and Cu-exchanged X zeolites” Microporous and Mesoporous Materials 111. 80-88.

51 E. Diaz, E. Munoz, A. Vega, S. Wrdonez. 2008. “Enhancement of the CO_2 retention capacity of X zeolites by Na- and Cs-treatments” Chemosphere 70. 1375-1382.

52 E. Diaz, E. Munoz, A. Bega, S. Ordonez, Chemosphere 70 (2008) 1375-1382.

53 N. Skoglund 2014. “Ash chemistry and fuel design focusing on combustion of phosphorus-rich biomass” Doctoral thesis.

54 S. Jeong, G. L. Sudibya, J.Jeon, Y. Kim 2019. “The Use of a γ-Al_2O_3 and MgO Mixture in the Catalytic Conversion of 1,1,1,2-Tetrafluoroethane (HFC-134a)” Catalysts. 9. 901.

55 A. Nagu, K. Vasikerappa, P. Gidyonu, Ch. Prathap, M. Venkata Rao, K. S. Rama Rao, B. David Raju 2020. “Additive-free vapour-phase hydrogenation of benzonitrile over MgO-supported Ni catalysts” Springer Nature B.V.

56 G. Gravogl, et al. 2018. “Cycle Stability and Hydration Behavior of Magnesium Oxide and Its Dependence on the Precursor-Related Particle Morphology” Nanomaterials. 8. 795.

57 D. Fan, X. Dong, Y. Yu, M. Zhang 2017. “A DFT study on aldol condensation reaction on MgO in the process of ethanol to 1,3-butadiene: Understanding the structure-activity relationship” Physical Chemistry Chemical Physics.

58 L. Z. Kong, H. Iuo, Y. Zhang, X. Zhao, S. Li, Y. Sun “Efficient One-pot Valorization of Ethanol to 1-Butanol over Earthabundant Ni-MgO Catalyst under Mild Conditions” 2020. Sustainable Energy Fuels.

59 Lisiane V. Mattos, Gary Jacobs, Burtron H. Davis, and Fabio B. Noronha 2012. “Production of Hydrogen from Ethanol: Review of Reaction Mechanism and Catalyst Deactivation” Chemical reviews 112. 4094-4123.

60 P. A. Kots, A. V. Zabilska, Yu. V. Grigor’ev, I. I. Ivanova 2019. “Ethanol to Butanol Conversion over Bifunctional Zeotype Catalysts Containing Palladium and Zirconium” Peroleum Chemistry, vol. 59. No 8. pp. 925-934.

61 S. Yacob, B. A. Kilos, D. G. Barton, J. M. Notestein. 2016. “Vapor phase ethanol carbonylation over Rh supported on zeolite 13X” Applied Catalystsis A, General 520. pp. 122-131.

62 D. Gabriels, W. Y. Hernandez, B. Sels, P. V. D. Voort, A. Verberckmoes. 2013. “Review of catalytic systems and thermodynamics for the Guerbet condensation reaction and challenges for biomass valorization” Catalysis Science & Technology. vol.1. Number 1. pp. 1-100.

63 V. L. Sushkevich, I. I. Ivanova 2017. “Mechanistic Study of Ethanol Conversion into Butadiene over Silver promoted Zirconia Catalysts” Applied Catalysis B: Environmental.

64 J. T. Prillaman, N. Miyake, R. J. Davis. 2020. “Calcium Phosphate Catalysts for Ethanol Coupling to Butanol and Butadiene” Springer Science. Business Media.

65 H. Wang, G. Miao, L. Kong, H. Luo, Y. Zhang, X. Zhao, S. Li, Y. Sun. 2017. “Calcium Phosphate Catalysts for Ethanol Coupling to Butanol and Butadiene” Sustainble Energy & Fuels. vol. 1. Number 3. pp. 399-666.

66 M. A. Peralta, T. Sooknoi, T. Danuthai, D. E. Resasco. 2009. “Deoxygenation of benzaldehyde over CsNaX zeolites” Journal of Molecular Catalysis A: Chemical 312. pp. 78-86.

67 J. Lu, P. Serna, B. C. Gates. 2011. “Zeolite- and MgO-Supported Molecular Iridium Complexes: Support and Ligand Effects in Catalysis of Ethene Hydrogenation and H-D Exchange in the Conversion of H_2 + D_2” ACS Catal. 1. 1549-1561.

APPENDICES

APPENDIX A

CALCULATION

Contact time, W/F

Calculation of catalytic parameter

$$\frac{W}{F} = \frac{Weight\ of\ catalyst\ (g)}{Molar\ feed\ rate\ (mol/h)}$$

In the reaction using 0.7 mol/h of ethanol in feed and using 0.3 grams of catalysts the W/F is calculated as follow:

$$\frac{W}{F} = \frac{[0.2876\ g\ cat][46\ g\frac{EtOH}{mol}]}{\left[1\frac{mL}{h}\right][0.789\ g\frac{EtOH}{mL}]}$$

$$= 16.7675\ g.h/mol$$

In similar manner; W/F of catalysts with different catalyst weight and different feed rate are calculated.

Calculation of % yield of products from gas chromatography

Table A1 The summation of the peak area of products

Product	Peak area
Ethylene	4847.5
propylene	514.5
Acetaldehyde	338.6
butadiene	476.6
diethyl ether	418.2
C4 aldehyde	292.7
C4 alcohol	217.7
Ethanol (Feed)	14170.8
Total	21276.9

*Information of ethanol conversion over MgO, contact time = 16.75 g.h/mol, time on stream = 40 minutes, flow rate of carrier gas: N_2 at 160 mL/min

In normalization method, the aras of all eluted peak were computed areas for differences int the detector response to different compound types. The concentration of the analyszed was found from the ratio of its area to the total area of all peaks.

Calculate the percent yield of each componenet int smple as follows:

$$\%Yield\ of\ each\ product = \frac{Peak\ area\ of\ A\ \times 100}{Total\ area}$$

Where A is each product.

For example;

$$\%Yield\ of\ Ehylene = \frac{4847.5 \times 100}{21276.8}$$

$$= 22.7$$

The percent yield of each product obtained from above calculation is shown in **Table A2.**

Table A2 Yield of product derived from normalization method.

Product	Yield (%)
Ethylene	22.8
propylene	2.4
Acetaldehyde	1.6
butadiene	2.2
diethyl ether	2.0
C4 aldehyde	1.4
C4 alcohol	1.0
Ethanol (Feed)	66.6
Total	100.0

Conversion

%Conversion can be calculated from the following equation:

$$\%Conversion = \frac{(Total\ area - Area\ of\ feed) \times 100}{Total\ area}$$

For example;

$$\%Conversion = \frac{(21276.9 - 14170.8) \times 100}{21276.9}$$
$$= 33.3$$

Selectivity

%Selectivity can be obtained from the following equation:

$$\%Selectivity\ of\ each\ product = \frac{\%Yield\ of\ each\ product \times 100}{\%Conversion}$$

For example;

$$\%Selectivity\ of\ Ethylene = \frac{22.8 \times 100}{33.3}$$
$$= 68.4$$

APPENDIX B

GAS CHROMATOGRAM

Analysis of gas product from gas chromatography

Prior to analysis, the structure of each product in the sample is identified the by GC-MS (gas chromatography with mass spectrometer detector). Then, the quantitative analysis of each product was carried out by GC-FID (gas chromatography with flame ionization detector) with the condition expressed in **Table B1.**

Table B1 The GC condition for quantitative analysis

Column	RT Q BOND
Temperature program	35°C hold 2 min, ramp to 200°C 5°C/min hold 15 min
Carrier gas	Nitrogen at 160 mL/min
Injection	250 °C
Detector	FID

The chromatogram of gas products were identified using reference standard for comparison in **Table B2.**

Table B2 Chromatogram data of standard product distribution and feed

Product distribution	Retention time (min)
Ethylene	2.43
Acetoldehyde	9.41
butadiene	N/A
Ethanol	11.72
Acetone	N/A
diethyl ether	13.77
C4 aldehyde	N/A
C4 alchol	16.60
C6 aldehyde	N/A
C6 alcohol	22.19

Figure B1 Chromatogram of product of product over hybrid catalysts

Product distribution	Retention time (min)
Ethylene	2.42
Acetaldehyde	9.67
butadiene	11.48
Ethanol	11.97
Acetone	13.21
diethyl ether	13.80
C4 aldehyde	15.44
C4 alcohol	16.44
C6 aldehyde	19.39
C6 alcohol	22.32

APPENDIX C

CATALYTIC ACTIVITY DATA

1. Ethanol dehydrogenation over $CuZn/SiO_2$

1.1 Ethanol dehydrogenation over $CuZn/SiO_2$ under N_2

Table C1 Ethanol conversion and yield of products at contact time 15 g.h/mol

Time on stream (min)	40	90	140	190	240
Conversion (%)	41.8	34.2	27.3	23.5	19.5
Yield of product (%)					
Ethylene	0.4	0.3	0.3	0.3	0.3
Acetaldehyde	41.0	33.6	26.7	22.9	18.9
butadiene	0.0	0.0	0.0	0.0	0.0
Acetone	0.0	0.3	0.2	0.3	0.3
diethyl ether	0.0	0.0	0.0	0.0	0.0
C4 aldehyde	0.4	0.0	0.0	0.0	0.0
C4 alcohol	0.0	0.0	0.0	0.0	0.0
C6 aldehyde	0.0	0.0	0.0	0.0	0.0
C6 alcohol	0.0	0.0	0.0	0.0	0.0

(Reaction condition; temperature: 380˚C, pressure: atmospheric pressure, contact time: 15 g.h/mol, flow rate of N_2 carrier gas: 160 mL/min)

1.2 Ethanol dehydrogenation over $CuZn/SiO_2$ under H_2

Table C2 Ethanol conversion and yield of products at contact time 15 g.h/mol

Time on stream (min)	40	90	140	190	240

Conversion (%)	65.8	58.7	52.2	47.5	44.4
Yield of product (%)					
Ethylene	0.2	0.1	0.1	0.2	0.0
Acetaldehyde	64.2	58.2	51.7	47.3	44.4
butadiene	0.0	0.0	0.0	0.0	0.0
Acetone	0.8	0.0	0.0	0.0	0.0
diethyl ehter	0.0	0.0	0.0	0.0	0.0
C4 aldehyde	0.5	0.3	0.3	0.0	0.0
C4 alcohol	0.0	0.0	0.0	0.0	0.0
C6 aldehyde	0.0	0.0	0.0	0.0	0.0
C6 alcohol	0.0	0.0	0.0	0.0	0.0

(Reaction condition; temperature: 380˚C, pressure: atmospheric pressure, contact time: 15 g.h/mol, flow rate of H_2 carrier gas: 160 mL/min)

2. Conversion of ethanol to higher alcohols over basic zeolite catalysts

2.1 Ethanol conversion over NaX(13X)

Table C3 Ethanol conversion and yield of products over NaX

Time on stream (min)	40	90	140	190	240
Conversion (%)	33.4	28.1	26.2	25.1	24.4
Yield of product (%)					
Ethylene	22.8	18.6	16.9	15.9	15.2
propylene	2.4	2.3	2.2	2.3	2.2
Acetaldehyde	1.6	1.6	1.6	1.6	1.7
butadiene	2.2	1.8	1.7	1.6	1.6
diethyl ether	2.0	1.5	1.3	1.3	1.3
C4 aldehyde	1.4	1.7	1.9	1.9	2.1
C4 alcohol	1.0	0.6	0.5	0.5	0.3

(Reaction condition; temperature: 380°C, pressure: atmospheric pressure, contact time: 16.75 g.h/mol, flow rate of N_2 carrier gas: 160 mL/min)

2.2 Ethanol conversion over KNaX

Table C4 Ethanol conversion and yield of products over KNaX

Time on stream (min)	40	90	140	190	240
Conversion (%)	11.1	11.3	11.3	10.4	10.3
Yield of product (%)					
Ethylene	6.4	4.9	4.8	4.1	4.3
propylene	0.0	0.0	0.0	0.0	0.0
Acetaldehyde	1.1	1.1	1.2	1.2	1.2
butadiene	0.0	0.0	0.0	0.0	0.0
diethyl ether	2.5	2.2	2.2	2.0	2.0
C4 aldehyde	0.8	2.6	2.7	2.6	2.3
C4 alcohol	0.3	0.5	0.5	0.6	0.5

(Reaction condition; temperature: 380˚C, pressure: atmospheric pressure, contact time: 16.75 g.h/mol, flow rate of N_2 carrier gas: 160 mL/min)

3. Conversion of ethanol to higher alcohols over MgO modified by zeolites.

3.1 Ethanol conversion over 3.1%Mg-KNaX

Table C5 Ethanol conversion and yield of products over 3.13%Mg-KNaX

Time on stream (min)	40	90	140	190	240
Conversion (%)	16.9	17.5	17.1	17.2	15.9
Yield of product (%)					
Ethylene	6.3	5.9	5.1	4.9	4.2
butadiene	1.9	2.3	2.3	2.4	2.3
Acetaldehyde	1.1	1.1	1.2	1.2	1.2
Acetone	1.8	2.2	2.3	2.5	1.9
diethyl ether	2.0	1.7	1.7	1.6	1.8
C4 aldehyde	0.7	1.1	1.2	1.1	1.1
C4 alcohol	3.1	3.3	3.3	3.4	3.3

(Reaction condition; temperature: 380°C, pressure: atmospheric pressure, contact time: 16.75 g.h/mol, flow rate of N_2 carrier gas: 160 mL/min)

3.2 Conversion over 3.3%Mg-KNaX

Table C6 Ethanol conversion and yield of products over 3.3%Mg-KNaX

Time on stream (min)	40	90	140	190	240
Conversion (%)	14.1	14.2	14.9	15.0	14.2
Yield of product (%)					
Ethylene	3.3	2.8	2.8	2.6	2.3
butadiene	2.2	2.4	2.6	2.8	2.7
Acetaldehyde	0.9	0.9	1.0	1.0	0.9
Acetone	1.4	1.5	1.6	1.8	1.5
diethyl ether	1.9	1.9	1.8	1.7	1.8
C4 aldehyde	1.2	1.4	1.5	1.5	1.5
C4 alcohol	3.3	3.4	3.6	3.5	3.5

(Reaction condition; temperature: 380˚C, pressure: atmospheric pressure, contact time: 16.75 g.h/mol, flow rate of N_2 carrier gas: 160 mL/min)

3.3 Ethanol conversion over 3.4%Mg-KNaX

Table C7 Ethanol conversion and yield of products over 3.4%Mg-KNaX

Time on stream (min)	40	90	140	190	240
Conversion (%)	15.8	14.8	15.8	15.6	15.1
Yield of product (%)					
Ethylene	3.4	3.2	3.0	2.8	2.6
propylene	2.1	2.3	2.5	2.7	2.6
Acetaldehyde	1.0	0.9	1.0	1.1	1.1
Acetone	1.6	2.0	2.6	2.2	2.0
diethyl ether	1.8	1.8	1.7	1.7	1.8
C4 aldehyde	1.6	1.4	1.5	1.5	1.5
C4 alcohol	4.3	3.2	3.5	3.6	3.6

(Reaction condition; temperature: 380˚C, pressure: atmospheric pressure, contact time: 16.75 g.h/mol, flow rate of N_2 carrier gas: 160 mL/min)

3.4 Ethanol conversion over 3.9%Mg-KNaX

Table C8 Ethanol conversion and yield of products over 3.9%Mg-KNaX

Time on stream (min)	40	90	140	190	240
Conversion (%)	14.7	15.1	15.2	15.6	15.3
Yield of product (%)					
Ethylene	2.8	2.6	2.3	2.3	2.3
butadiene	2.4	2.8	2.9	3.0	3.1
Acetaldehyde	1.2	1.3	1.4	1.4	1.3
Acetone	1.2	1.6	1.5	1.6	1.6
diethyl ether	1.7	1.5	1.7	1.6	1.6
C4 aldehyde	1.2	1.3	1.4	1.5	1.5
C4 alcohol	4.1	4.1	4.1	4.2	4.0

(Reaction condition; temperature: 380˚C, pressure: atmospheric pressure, contact time: 16.75 g.h/mol, flow rate of N_2 carrier gas: 160 mL/min)

3.5 Ethanol conversion over 4.3%Mg-KNaX

Table C9 Ethanol conversion and yield of products over 4.3%Mg-KNaX

Time on stream (min)	40	90	140	190	240
Conversion (%)	14.9	15.0	14.8	14.5	14.2
Yield of product (%)					
Ethylene	2.0	1.7	1.6	1.5	1.4
propylene	2.9	3.3	3.4	3.3	3.3
Acetaldehyde	1.1	1.1	1.1	1.0	1.0
Acetone	1.7	1.8	1.8	1.6	1.5
diethyl ether	1.7	1.7	1.7	1.7	1.7
C4 aldehyde	1.6	1.6	1.7	1.8	1.8
C4 alcohol	3.9	3.7	3.5	3.5	3.6

(Reaction condition; temperature: 380˚C, pressure: atmospheric pressure, contact time: 16.75 g.h/mol, flow rate of N_2 carrier gas: 160 mL/min)

4. Conversion of ethanol to higher alcohols over MgO modified by zeolites.

4.1 Effect of contact time over 3.9%Mg-KNaX catalysts

Table C10 Ethanol conversion and yield of products at contact time 10 g.h/mol

Time on stream (min)	40	90	140	190	240
Conversion (%)	13.1	13.1	13.1	13.3	13.4
Yield of product (%)					
Ethylene	1.8	1.5	1.4	1.3	1.2
butadiene	2.4	2.6	2.7	2.8	2.8
Acetaldehyde	0.7	0.8	0.8	0.8	0.8
Acetone	1.4	1.4	1.5	1.7	1.6
diethyl ether	2.0	2.0	2.0	1.9	1.9
C4 aldehyde	1.8	1.8	1.8	1.8	1.9
C4 alcohol	2.9	3.0	3.0	3.0	3.1
C6 aldehyde	0.0	0.0	0.0	0.0	0.0
C6 alcohol	0.0	0.0	0.0	0.0	0.0

(Reaction condition; temperature: 380˚C, pressure: atmospheric pressure, contact time: 10 g.h/mol, flow rate of N_2 carrier gas: 160 mL/min)

Table C11 Ethanol conversion and yield of products at contact time 25 g.h/mol

Time on stream (min)	40	90	140	190	240
Conversion (%)	18.4	18.4	18.5	18.2	18.4
Yield of product (%)					
Ethylene	4.3	3.6	3.2	2.8	2.7
butadiene	2.4	2.6	3.0	3.0	2.8
Acetaldehyde	1.9	1.9	2.0	1.9	1.9
Acetone	2.5	2.5	2.4	2.3	2.2
diethyl ether	1.5	1.5	1.5	1.5	1.4
C4 aldehyde	0.9	1.2	1.2	1.3	1.3
C4 alcohol	4.9	5.1	5.2	5.4	6.1
C4 alcohol	0.0	0.0	0.0	0.0	0.0
C6 aldehyde	0.0	0.0	0.0	0.0	0.0

(Reaction condition; temperature: 380°C, pressure: atmospheric pressure, contact time: 25 g.h/mol, flow rate of N_2 carrier gas: 160 mL/min)

Table C12 Ethanol conversion and yield of products at contact time 40 g.h/mol

Time on stream (min)	40	90	140	190	240
Conversion (%)	25.0	21.3	21.6	20.9	21.3
Yield of product (%)					
Ethylene	6.6	5.6	4.7	4.1	4.0
butadiene	2.4	2.6	2.8	2.9	3.2
Acetaldehyde	2.6	2.7	2.8	2.9	2.3
Acetone	1.6	1.9	2.2	1.8	2.4
diethyl ether	1.1	1.3	1.3	1.3	1.1
C4 aldehyde	0.7	1.0	1.1	1.1	1.3
C4 alcohol	6.7	6.2	6.7	6.7	7.1
C4 alcohol	0.0	0.0	0.0	0.0	0.0
C6 aldehyde	3.2	0.0	0.0	0.0	0.0

(Reaction condition; temperature: 380°C, pressure: atmospheric pressure, contact time: 40 g.h/mol, flow rate of N_2 carrier gas: 160 mL/min)

5. Conversion of ethanol to higher alcohols over hybrid catalysts in sequential bed and physical mixed system under N_2

5.1 Hybrid catalysts in sequential bed system

Table C13 Ethanol conversion and yield of products at total contact time 15 g.h/mol

Time on stream (min)	40	90	140	190	240
Conversion (%)	42.0	35.7	27.2	22.1	18.8
Yield of product (%)					
Ethylene	0.9	1.0	1.0	0.8	0.8
Acetaldehyde	31.5	26.6	19.5	15.5	11.6
butadiene	0.0	0.0	0.0	0.0	0.0
Acetone	0.5	0.6	0.5	0.4	0.5
diethyl ether	0.0	0.0	0.0	0.0	0.0
C4 aldehyde	1.8	1.1	1.0	0.7	0.8
C4 alcohol	7.4	6.3	5.3	4.6	5.1
C6 aldehyde	0.0	0.0	0.0	0.0	0.0
C6 alcohol	0.0	0.0	0.0	0.0	0.0

(Reaction condition; temperature: 380˚C, pressure: atmospheric pressure, contact time of $CuZn/SiO_2$: 5 g.h/mol, contact time of 3.9%Mg-KNaX: 10 g.h/mol, flow rate of N_2 carrier gas: 160 mL/min)

5.2 Effect of physical mixed

Table C14 Ethanol conversion and yield of products at total contact time 15 g.h/mol

Time on stream (min)	40	90	140	190	240
Conversion (%)	23.1	20.2	20.2	20.2	20.0
Yield of product (%)					
Ethylene	1.8	1.5	1.5	1.4	1.3
Acetaldehyde	8.3	9.1	9.5	9.2	9.2
butadiene	1.8	1.5	1.4	1.3	1.2
Acetone	0.0	0.0	0.0	0.0	0.0
diethyl ether	0.0	0.0	0.0	0.0	0.0
C4 aldehyde	1.0	0.8	0.8	0.8	0.8
C4 alcohol	6.7	5.4	5.2	5.9	5.8
C6 aldehyde	0.0	0.0	0.0	0.0	0.0
C6 alcohol	3.6	1.9	1.8	1.7	1.6

(Reaction condition; temperature: 380°C, pressure: atmospheric pressure, contact time of $CuZn/SiO_2$: 5 g.h/mol, contact time of 3.9%Mg-KNaX: 10 g.h/mol, flow rate of N_2 carrier gas: 160 mL/min)

6. Conversion of ethanol to higher alcohols in double bed and physical mixed system in flow of H_2 carrier gas

6.1 Effect of double bed system

Table C15 Ethanol conversion and yield of products at total contact time 15 g.h/mol

Time on stream (min)	40	90	140	190	240
Conversion (%)	65.4	56.7	53.2	49.2	48.6
Yield of product (%)					
Ethylene	0.3	0.3	0.3	0.3	0.4
Acetaldehyde	51.1	45.6	44.9	41.7	41.4
butadiene	0.0	0.0	0.0	0.0	0.0
Acetone	0.8	0.6	0.0	0.0	0.0
diethyl ehther	0.0	0.0	0.0	0.0	0.0
C4 aldehyde	3.1	1.5	1.2	1.0	0.8
C4 alcohol	10.1	8.7	6.7	6.3	6.0
C6 aldehyde	0.0	0.0	0.0	0.0	0.0
C6 alcohol	0.0	0.0	0.0	0.0	0.0

(Reaction condition; temperature: 380˚C, pressure: atmospheric pressure, contact time of $CuZn/SiO_2$: 5 g.h/mol, contact time of 3.9%Mg-KNaX: 10 g.h/mol, flow rate of H_2 carrier gas: 160 mL/min)

6.2 Effect of physical mixed

Table C16 Ethanol conversion and yield of products at total contact time 15 g.h/mol

Time on stream (min)	40	90	140	190	240
Conversion (%)	23.5	22.2	21.8	20.9	21.2
Yield of product (%)					
Ethylene	1.2	1.2	1.2	1.0	1.2
Acetaldehyde	9.9	11.2	10.8	10.6	10.7
butadiene	1.3	1.2	1.2	1.1	0.9
Acetone	0.0	0.0	0.0	0.0	0.0
diethyl ether	0.0	0.0	0.0	0.0	0.0
C4 aldehyde	1.1	0.9	0.9	0.8	1.0
C4 alcohol	6.4	5.6	5.6	5.5	5.0
C6 aldehyde	0.0	0.0	0.0	0.0	0.0
C6 alcohol	3.6	2.1	2.1	1.9	2.3

(Reaction condition; temperature: 380°C, pressure: atmospheric pressure, contact time of CuZn/SiO_2: 5 g.h/mol, contact time of 3.9%Mg-KNaX: 10 g.h/mol, flow rate of H_2 carrier gas: 160 mL/min)

7. Conversion of ethanol to higher alcohols in physical mixed system

7.1 Effect ratio of $CuZn/SiO_2$ to 3.9%Mg-KNaX (0)

Table C17 Ethanol conversion and yield of products at ratio 0

Time on stream (min)	40	90	140	190	240
Conversion (%)	14.4	14.7	14.8	14.9	14.8
Yield of product (%)					
Ethylene	2.7	2.6	2.4	2.3	2.4
Acetaldehyde	2.3	2.7	2.7	3.0	2.8
butadiene	1.2	1.1	1.2	1.1	1.4
Acetone	1.2	1.6	1.6	1.4	1.5
diethyl ether	1.7	1.5	1.5	1.6	1.4
C4 aldehyde	1.2	1.1	1.5	1.5	1.5
C4 alcohol	4.1	4.0	3.9	4.0	3.8
C6 aldehyde	-	-	-	-	-
C6 alcohol	-	-	-	-	-

7.2 Effect ratio of $CuZn/SiO_2$ to 3.89%Mg-KNaX (0.2)

Table C18 Ethanol conversion and yield of products at ratio 1:5

Time on stream (min)	40	90	140	190	240
Conversion (%)	22.0	19.8	19.1	20.0	19.8
Yield of product (%)					
Ethylene	1.5	1.5	1.4	1.4	1.9
Acetaldehyde	6.0	7.0	6.7	7.4	7.0
butadiene	2.0	1.8	1.4	1.5	1.7
Acetone	0.0	0.0	0.0	0.0	0.0
diethyl ehter	0.0	0.0	0.0	0.0	0.0
C4 aldehyde	0.8	0.8	0.8	0.8	0.8
C4 alcohol	7.3	6.0	5.6	6.3	6.2
C6 aldehyde	0.5	0.0	0.0	0.0	0.0
C6 alcohol	3.9	2.8	3.2	2.5	2.2

(Reaction condition; temperature: 380°C, pressure: atmospheric pressure, contact time of $CuZn/SiO_2$: 3 g.h/mol, contact time of 3.9%Mg-KNaX: 12 g.h/mol, flow rate of H_2 carrier gas: 160 mL/min)

7.3 Effect ratio of $CuZn/SiO_2$ to 3.9%Mg-KNaX (1)

Table C19 Ethanol conversion and yield of products at ratio 1

Time on stream (min)	40	90	140	190	240
Conversion (%)	22.0	18.8	18.6	18.7	18.5
Yield of product (%)					
Ethylene	6.4	1.4	1.3	1.2	1.2
Acetaldehyde	64.7	16.4	15.6	15.3	16.2
butadiene	2.9	0.7	0.6	0.6	0.7
Acetone	0.0	0.0	0.0	0.0	0.0
diethyl ether	0.0	0.0	0.0	0.0	0.0
C4 aldehyde	0.9	0.8	0.8	0.8	0.8
C4 alcohol	4.5	3.9	3.8	3.7	3.7
C6 aldehyde	0.0	0.0	0.0	0.0	0.0
C6 alcohol	2.0	0.0	0.0	0.0	0.0

(Reaction condition; temperature: 380°C, pressure: atmospheric pressure, contact time of $CuZn/SiO_2$: 7.5 g.h/mol, contact time of 3.89%Mg-KNaX: 7.5 g.h/mol, flow rate of H_2 carrier gas: 160 mL/min)

7.4 Effect ratio of $CuZn/SiO_2$ to 3.9%Mg-KNaX (2)

Table C20 Ethanol conversion and yield of products at ratio 2

Time on stream (min)	40	90	140	190	240
Conversion (%)	22.0	18.8	18.6	18.7	18.5
Yield of product (%)					
Ethylene	1.7	1.5	1.4	1.3	1.4
Acetaldehyde	11.6	11.6	11.7	12.0	11.7
butadiene	1.2	1.1	1.0	1.0	0.9
Acetone	0.0	0.0	0.0	0.0	0.0
diethyl ether	0.0	0.0	0.0	0.0	0.0
C4 aldehyde	0.9	0.8	0.8	0.8	0.8
C4 alcohol	4.5	3.9	3.8	3.7	3.7
C6 aldehyde	0.0	0.0	0.0	0.0	0.0
C6 alcohol	2.0	0.0	0.0	0.0	0.0

(Reaction condition; temperature: 380°C, pressure: atmospheric pressure, contact time of $CuZn/SiO_2$: 10 g.h/mol, contact time of 3.9%Mg-KNaX: 5 g.h/mol, flow rate of H_2 carrier gas: 160 mL/min)

8. Conversion of ethanol to higher alcohols in physical mixed system

8.1 Effect of contact time in physical mixed

Table C21 Ethanol conversion and yield of products at total contact time 25 g.h/mol

Time on stream (min)	40	90	140	190	240
Conversion (%)	39.1	35.7	35.7	35.5	33.9
Yield of product (%)					
Ethylene	1.9	1.7	1.8	1.9	1.7
Acetaldehyde	4.7	5.5	6.4	7.1	7.1
butadiene	3.0	2.4	2.4	2.8	2.3
Acetone	0.2	0.3	0.3	0.3	0.3
diethyl ehter	0.0	0.0	0.0	0.0	0.0
C4 aldehyde	0.9	0.9	0.9	2.0	1.7
C4 alcohol	11.5	9.9	10.5	8.7	9.4
C6 aldehyde	6.1	5.6	4.1	3.9	3.3
C6 alcohol	10.6	9.5	9.3	8.8	8.1

(Reaction condition; temperature: 380˚C, pressure: atmospheric pressure, contact time of CuZn/SiO_2: 4.2 g.h/mol, contact time of 3.9%Mg-KNaX: 20.8 g.h/mol, flow rate of H_2 carrier gas: 160 mL/min)

Table C22 Ethanol conversion and yield of products at total contact time 40 g.h/mol

Time on stream (min)	40	90	140	190	240
Conversion (%)	50.3	41.2	36.0	34.6	34.9
Yield of product (%)					
Ethylene	2.5	2.1	2.1	2.1	2.1
Acetaldehyde	3.5	5.0	5.7	6.3	6.3
butadiene	4.3	2.8	3.0	2.9	2.8
Acetone	0.0	0.0	0.0	0.0	0.0
diethyl ether	0.0	0.0	0.0	0.0	0.0
C4 aldehyde	1.4	1.3	1.0	1.1	1.1
C4 alcohol	13.8	12.3	11.3	10.5	12.2
C6 aldehyde	3.2	2.0	1.7	1.6	1.1
C6 alcohol	21.7	15.7	11.2	10.1	9.2

(Reaction condition; temperature: 380°C, pressure: atmospheric pressure, contact time of CuZn/SiO_2: 6.7 g.h/mol, contact time of 3.9%Mg-KNaX: 33.3 g.h/mol, flow rate of H_2 carrier gas: 160 mL/min)

APPENDIX D

CATALYST CHARACTERIZATION

1. XRD diffraction pattern of $CuZn/SiO_2$ catatslyst

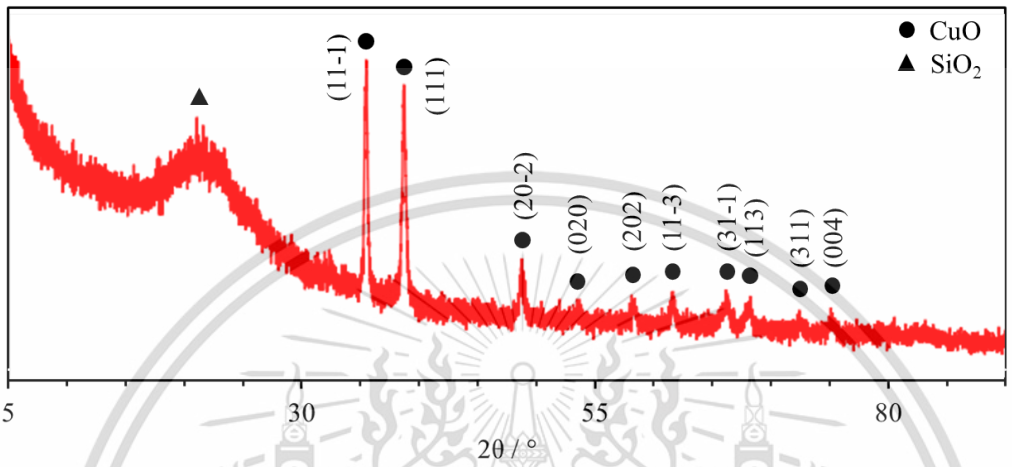

Figure D1 XRD patterns of $Cu-Zn/SiO_2$

2. XRD diffraction pattern of zeolite catalysts

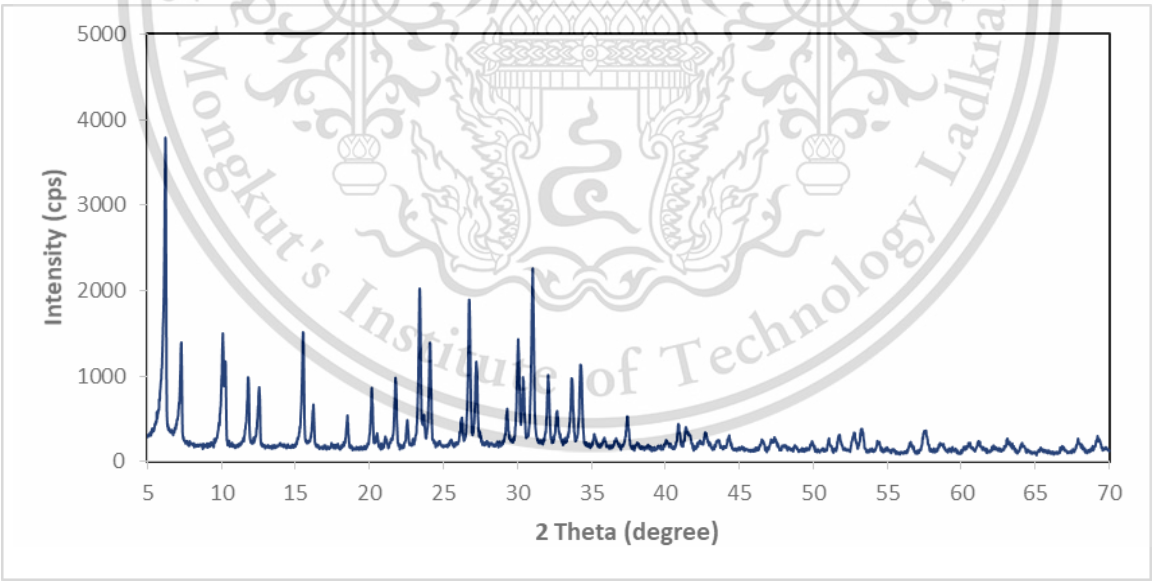

Figure D2 X-ray diffraction pattern of NaX

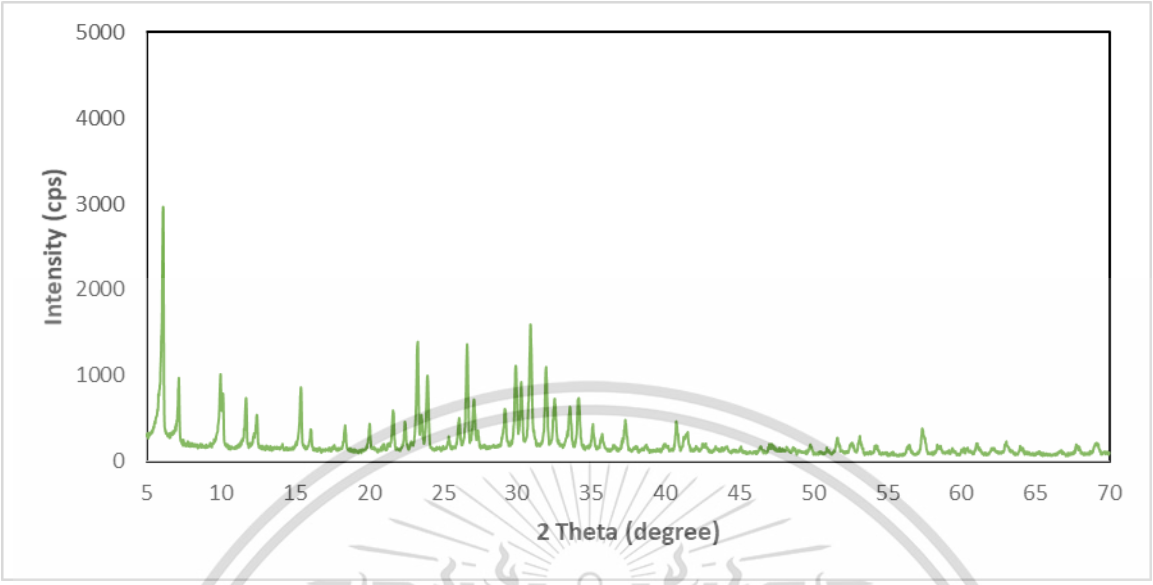

Figure D3 X-ray diffraction pattern of KNaX

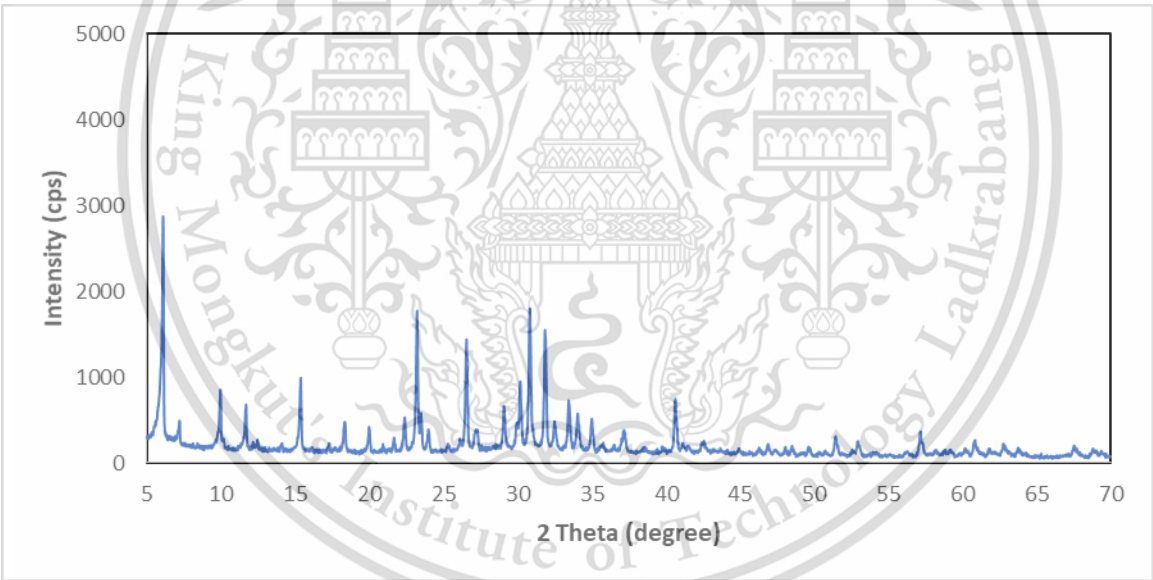

Figure D4 X-ray diffraction pattern of 3.1%MgO-KNaX

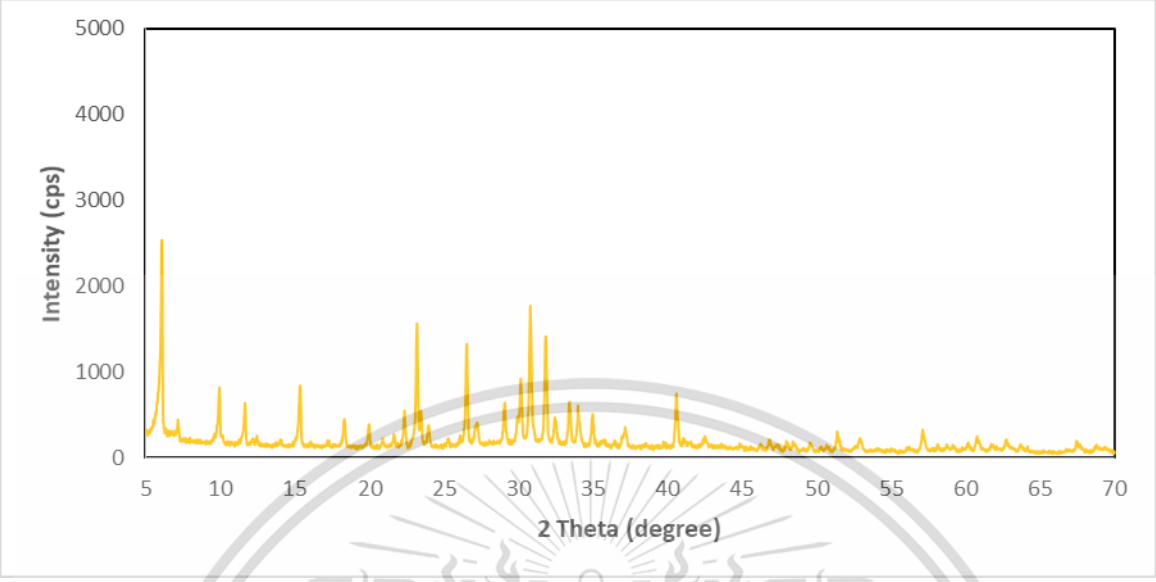

Figure D5 X-ray diffraction pattern of 3.3%MgO-KNaX

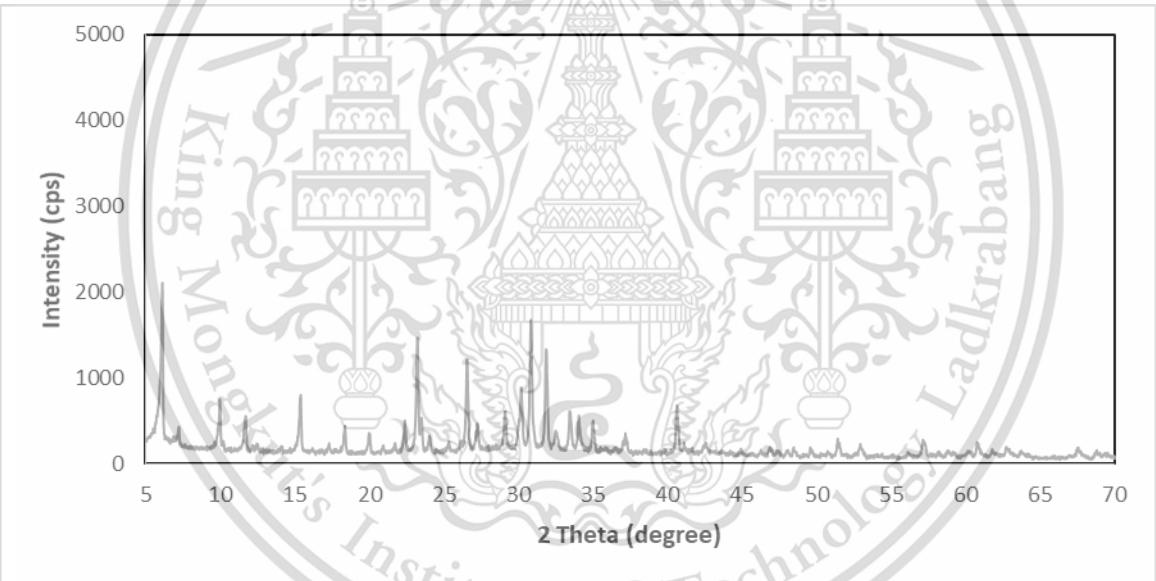

Figure D6 X-ray diffraction pattern of 3.4%MgO-KNaX

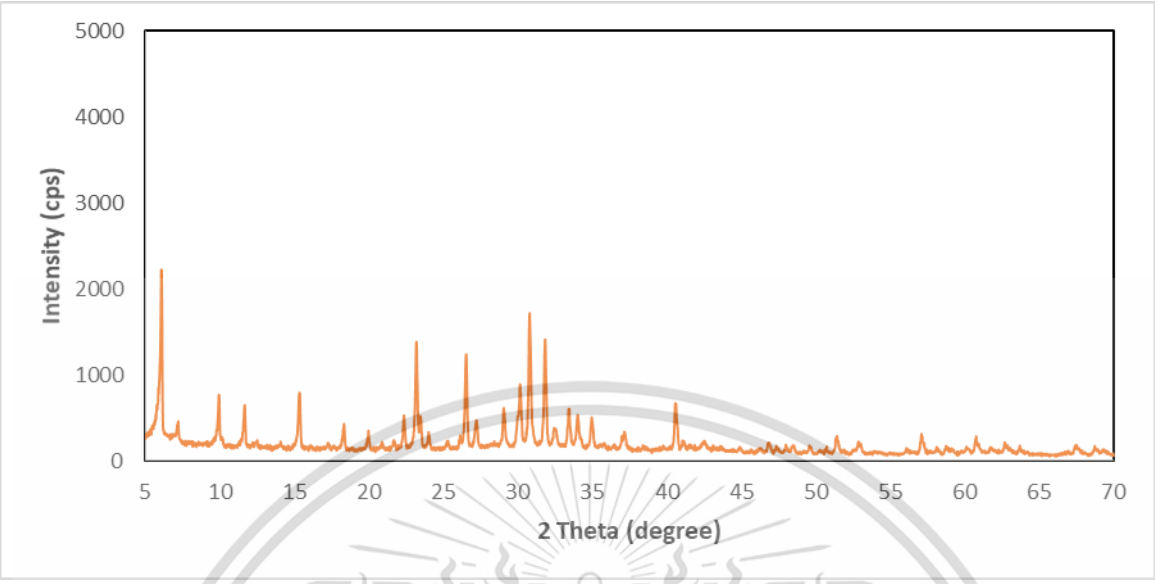

Figure D7 X-ray diffraction pattern of 3.9%MgO-KNaX

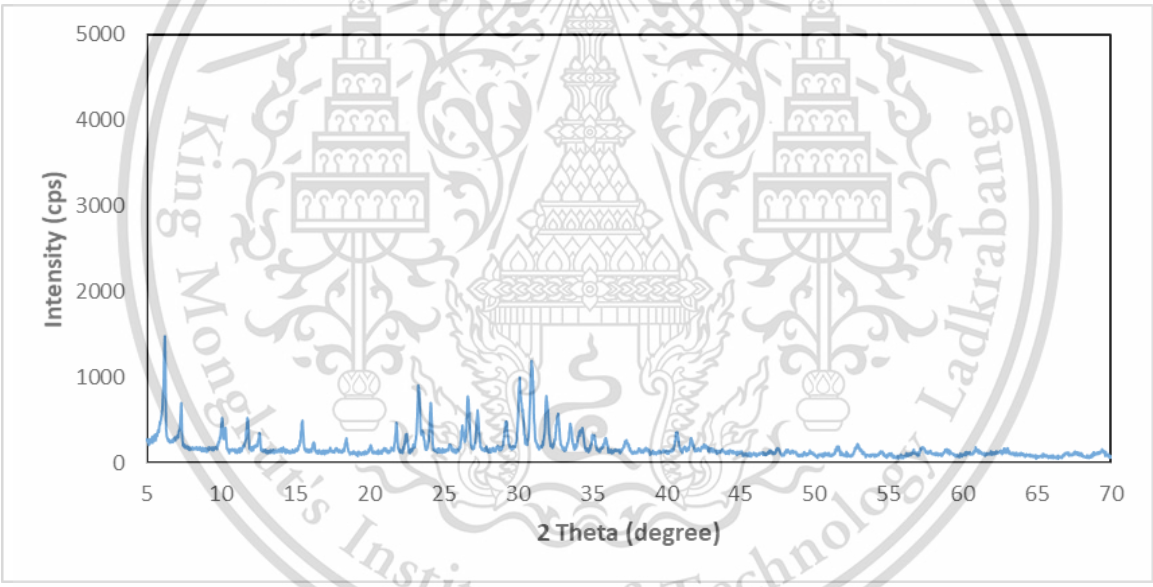

Figure D8 X-ray diffraction pattern of 4.3%MgO-KNaX

3. Adsorption-desorption isotherm

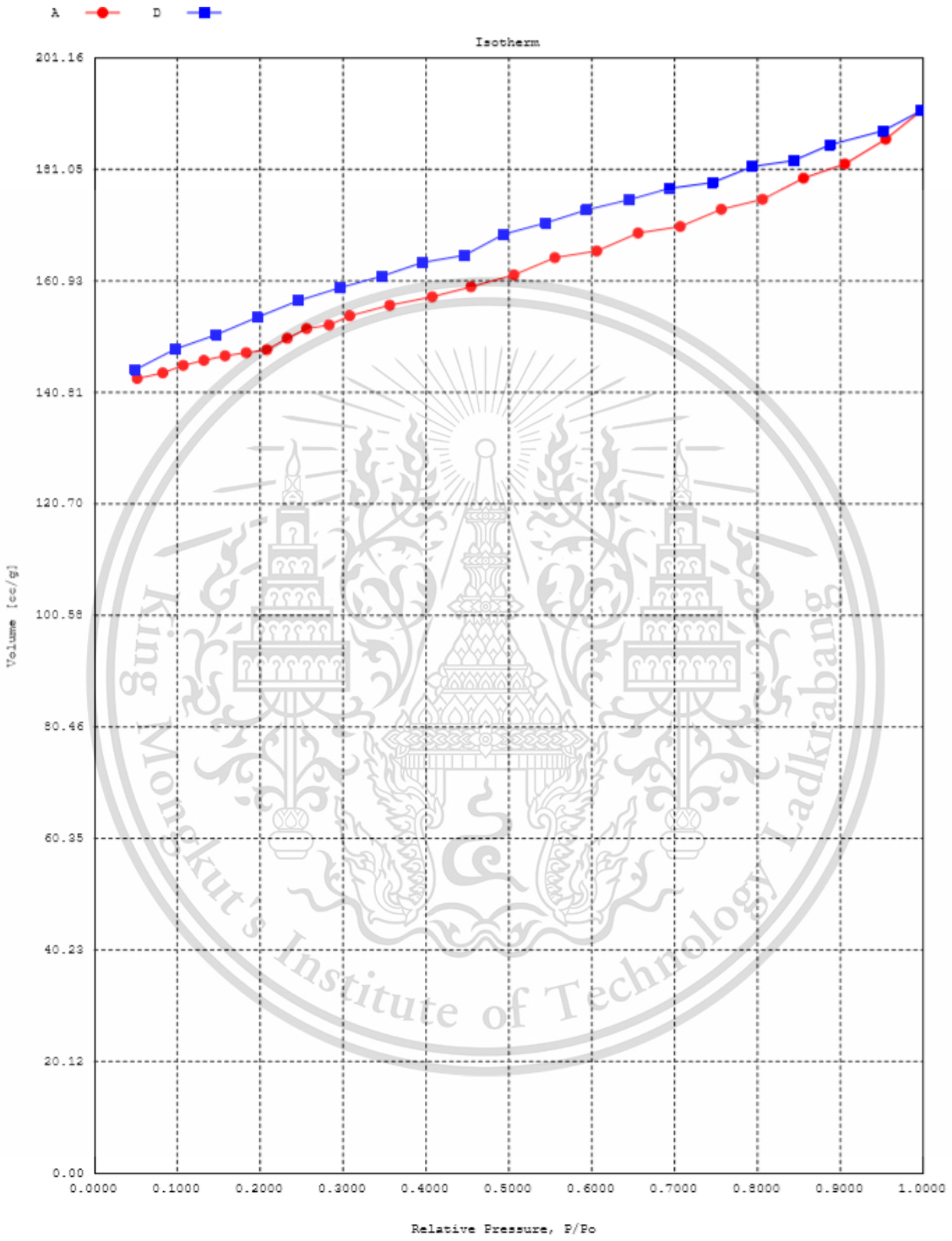

Figure D9 N_2 adsorption-desorption isotherm of NaX commercial.

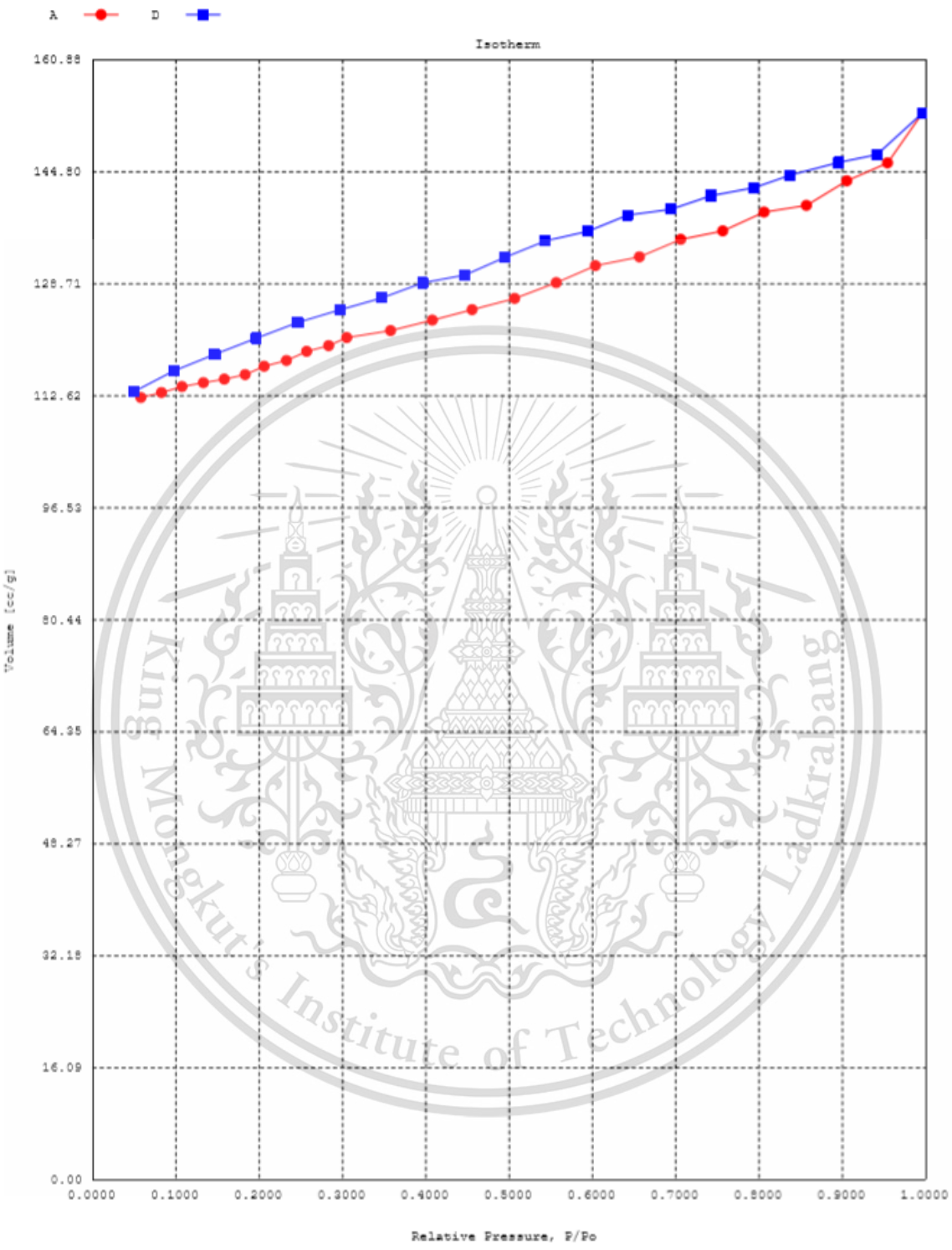

Figure D10 N_2 adsorption-desorption isotherm of KNaX commercial.

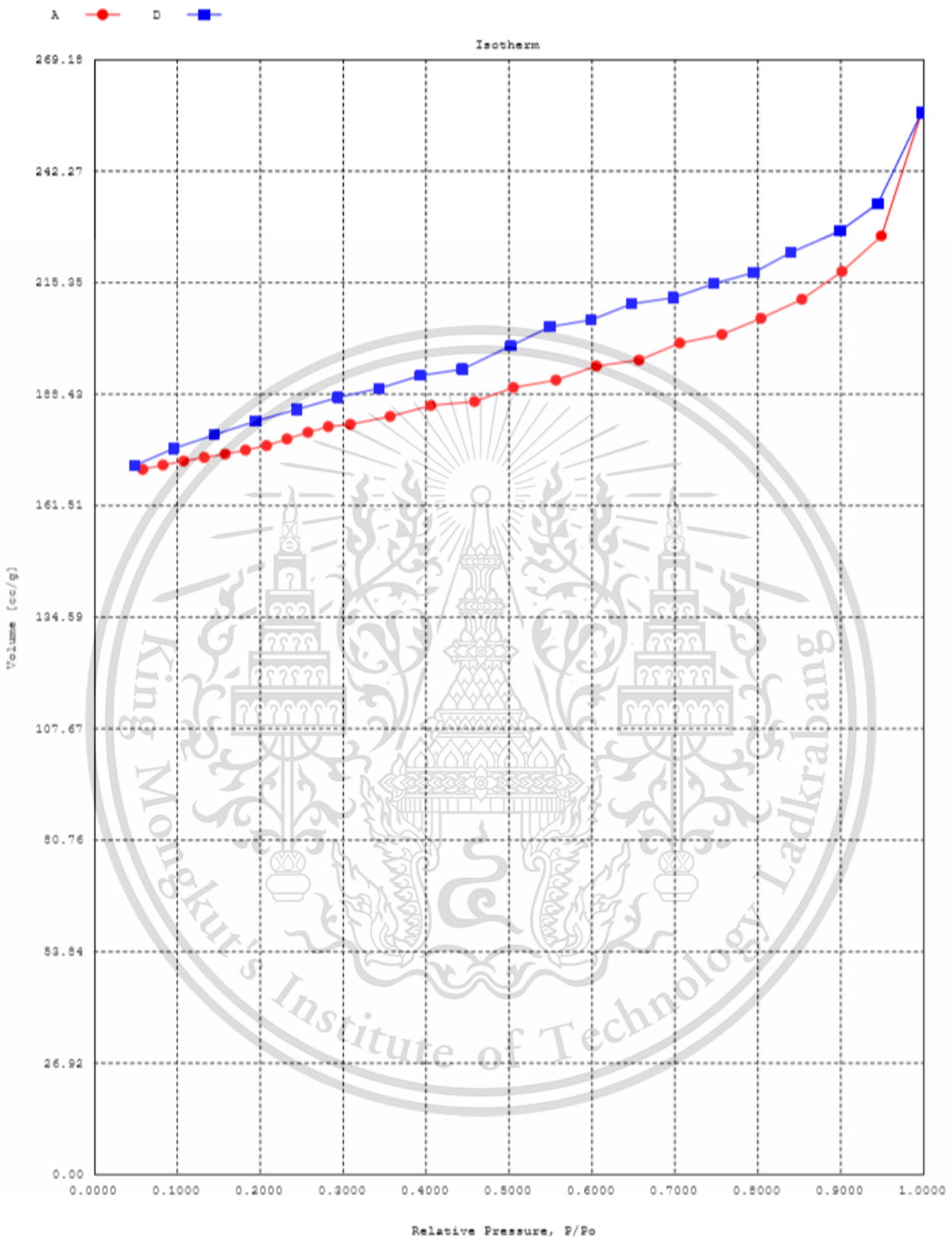

Figure D11 N_2 adsorption-desorption isotherm of 3.13%MgO-KNaX commercial.

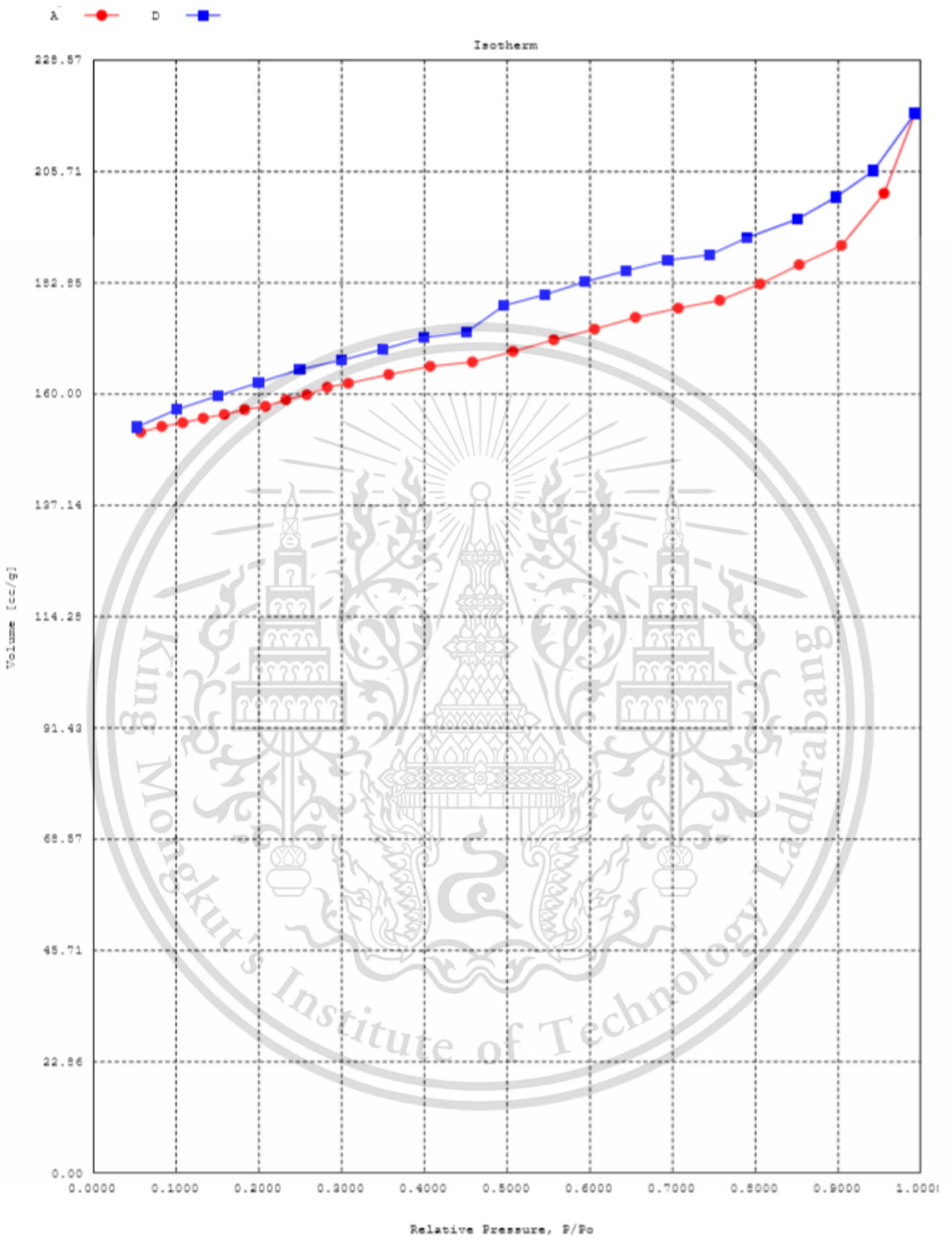

Figure D12 N_2 adsorption-desorption isotherm of 3.28%MgO-KNaX commercial.

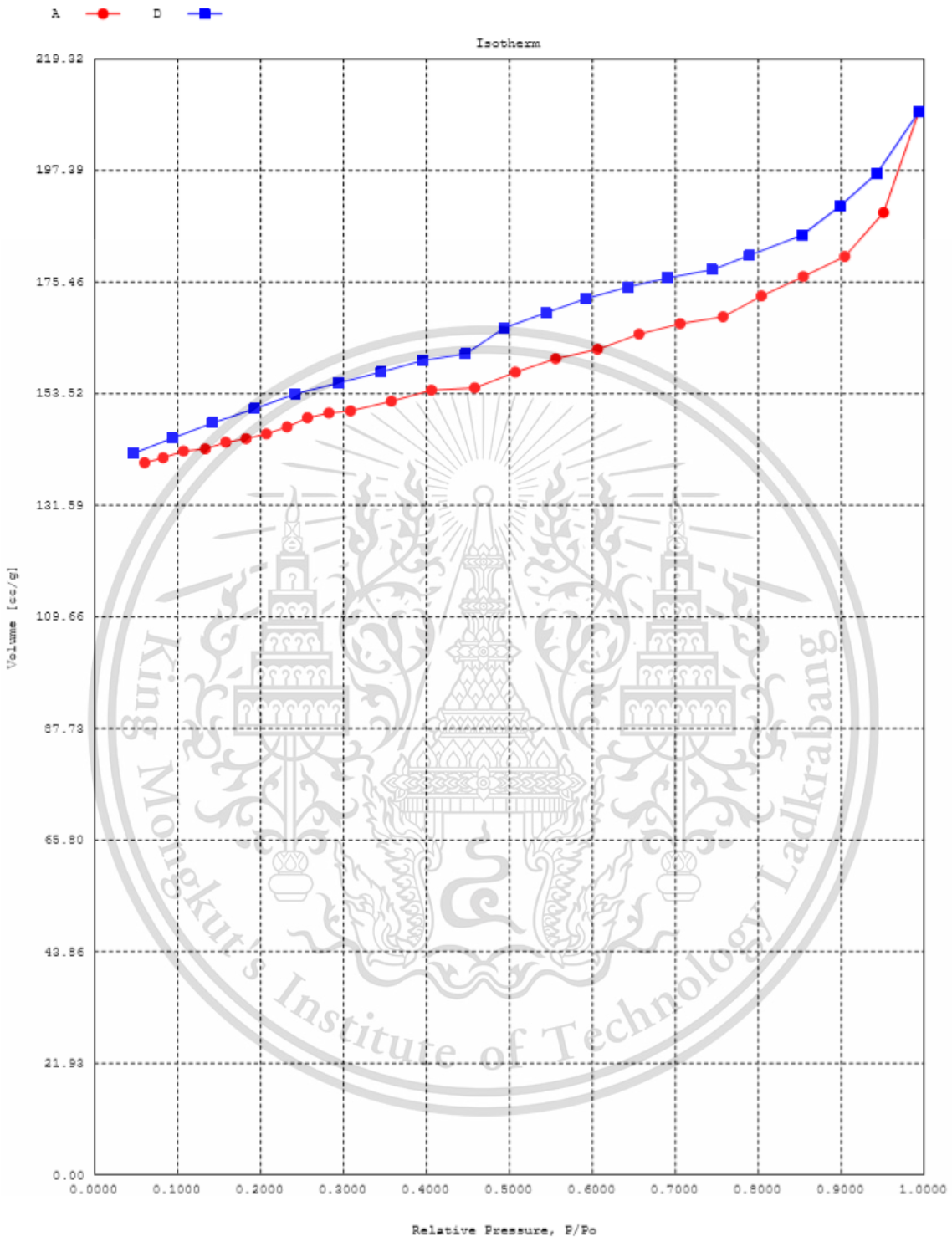

Figure D13 N_2 adsorption-desorption isotherm of 3.38%MgO-KNaX commercial.

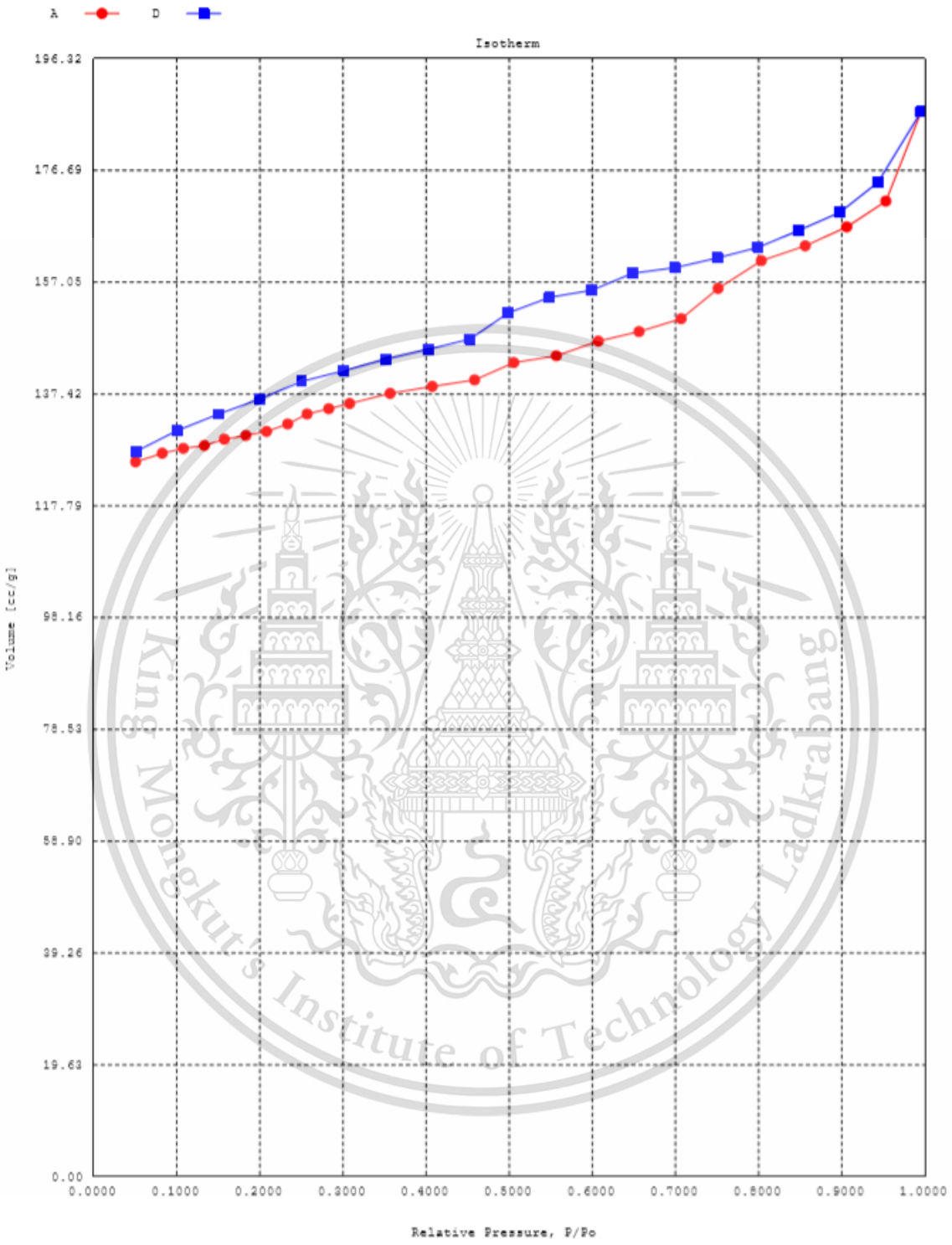

Figure D14 N_2 adsorption-desorption isotherm of 3.89%MgO-KNaX commercial.

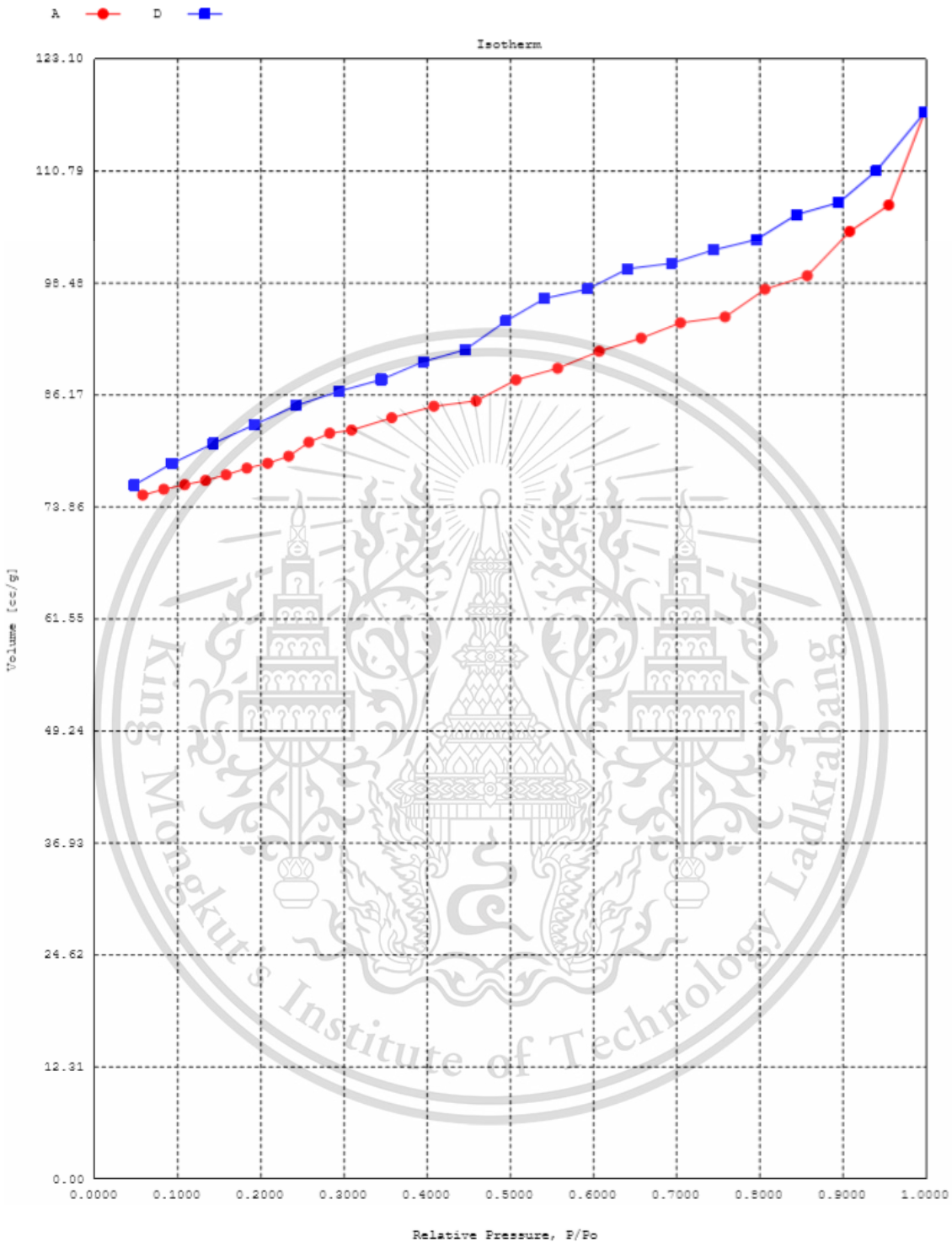

Figure D15 N_2 adsorption-desorption isotherm of 4.27%MgO-KNaX commercial.

X-ray Fluorescence analysis (XRF)

Table D1 Elemental analysis by X-ray Fluorescence technique.

Catalyst	% by weight					
	Si	Al	Si : Al	Na	K	Mg
NaX	18.20	13.50	1.35	13.10	0.00	0.00
KNaX	16.60	13.10	1.27	12.60	12.60	0.00
3.13%Mg-KNaX	15.20	12.30	1.24	1.32	15.00	3.13
3.28%Mg-KNaX	14.40	11.50	1.25	0.84	14.90	3.28
3.38%Mg-KNaX	14.80	12.00	1.23	1.04	16.10	3.38
3.89%Mg-KNaX	14.90	12.10	1.23	1.05	15.90	3.89
4.27%Mg-KNaX	14.60	12.30	1.19	1.00	15.60	4.27

Scanning electron microscopy with energy dispersive X-ray analysis (SEM-EDX)

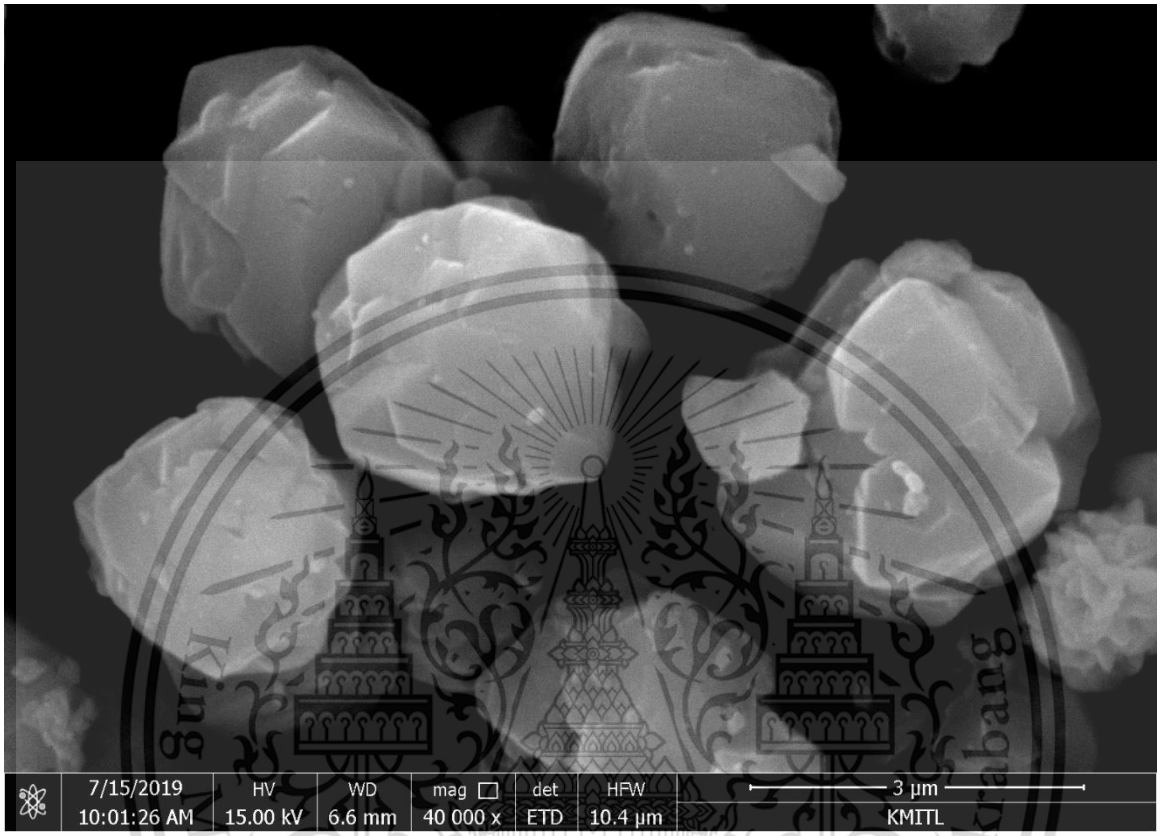

Figure D15 SEM image of KNaX

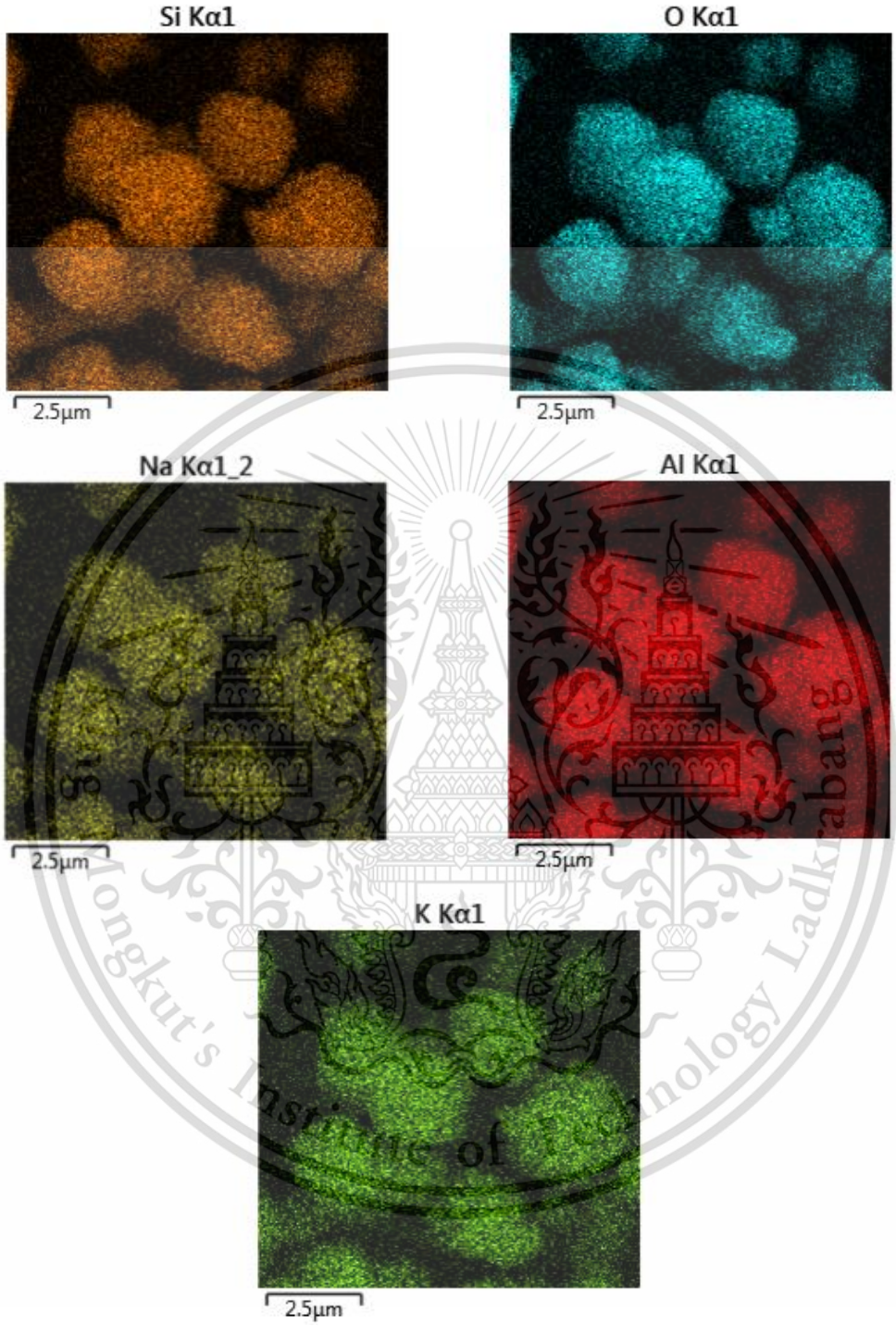

Figure D16 metal dispersion of KNaX

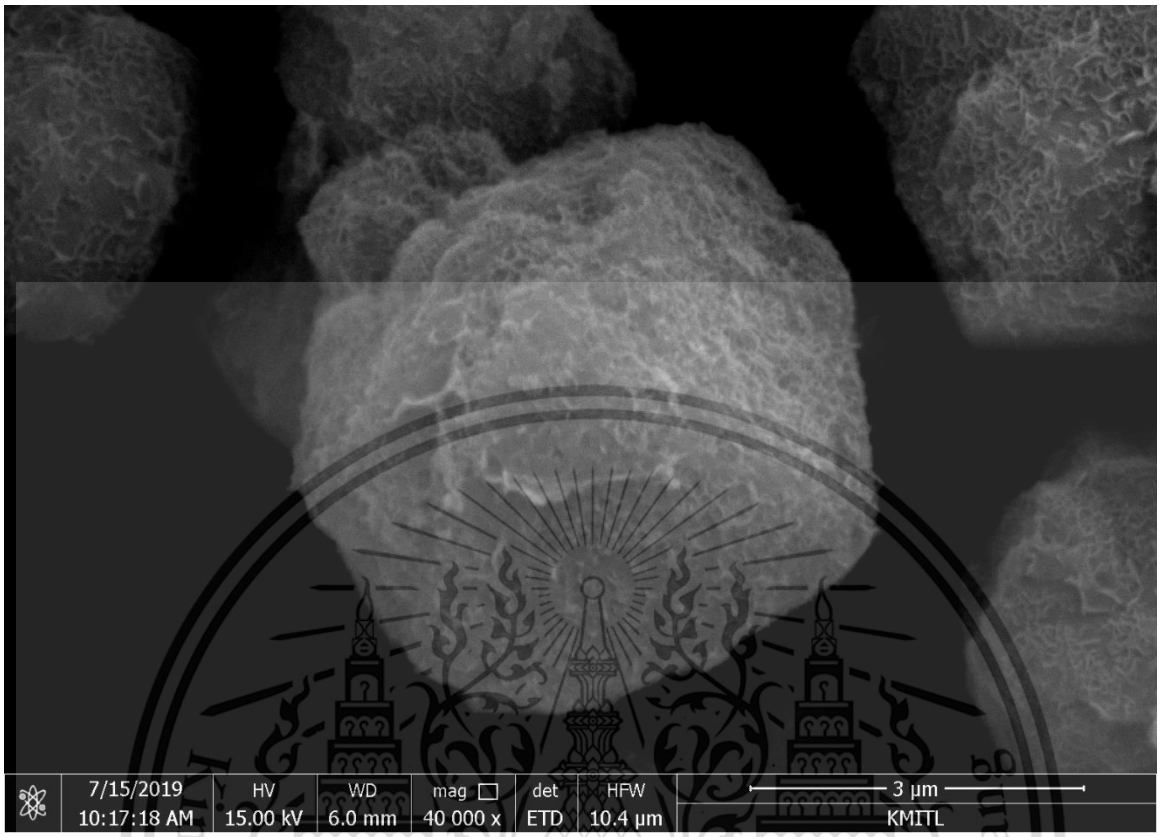

Figure D17 SEM image of 3.1Mg-KNaX

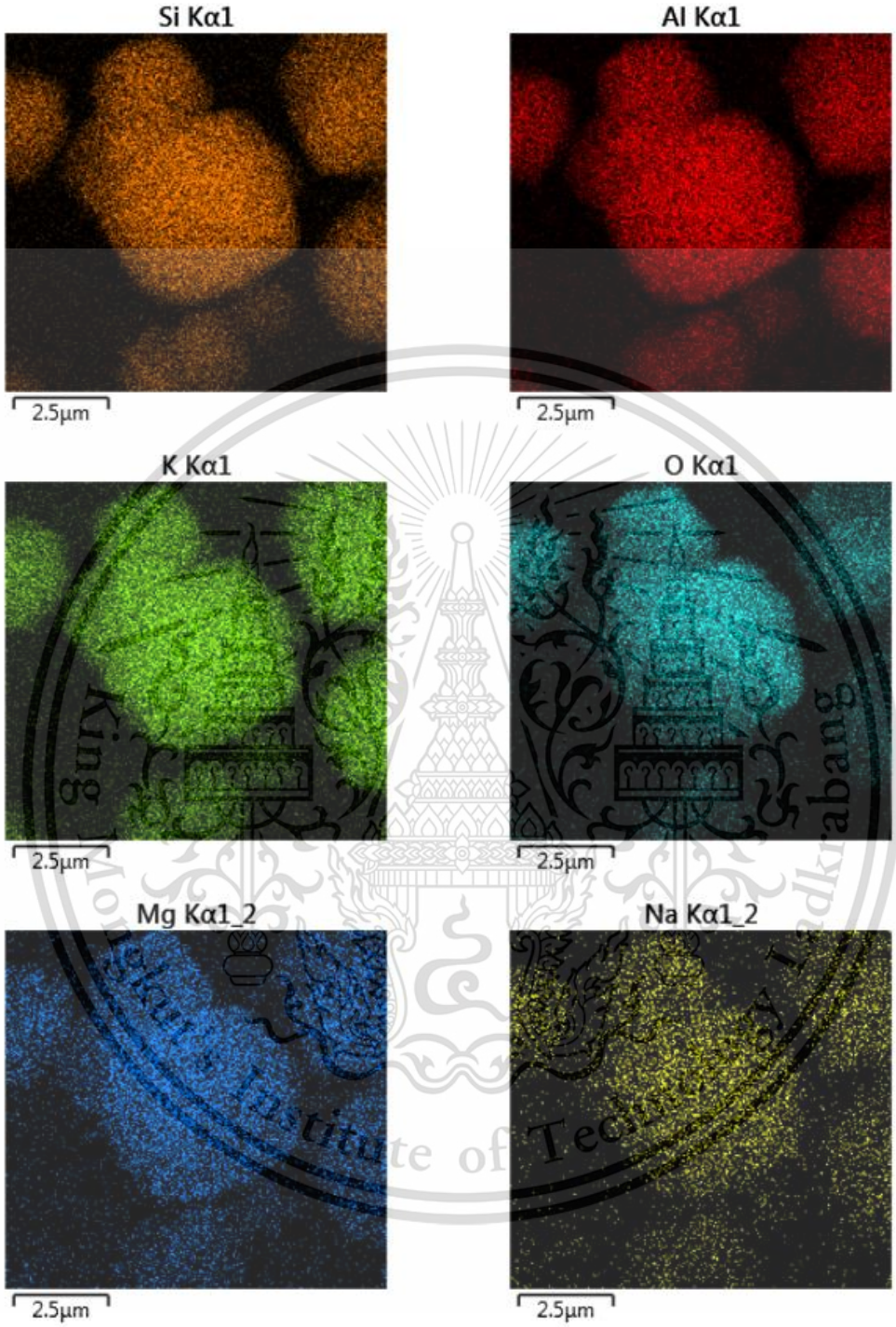

Figure D18 metal dispersion of 3.1Mg-KNaX

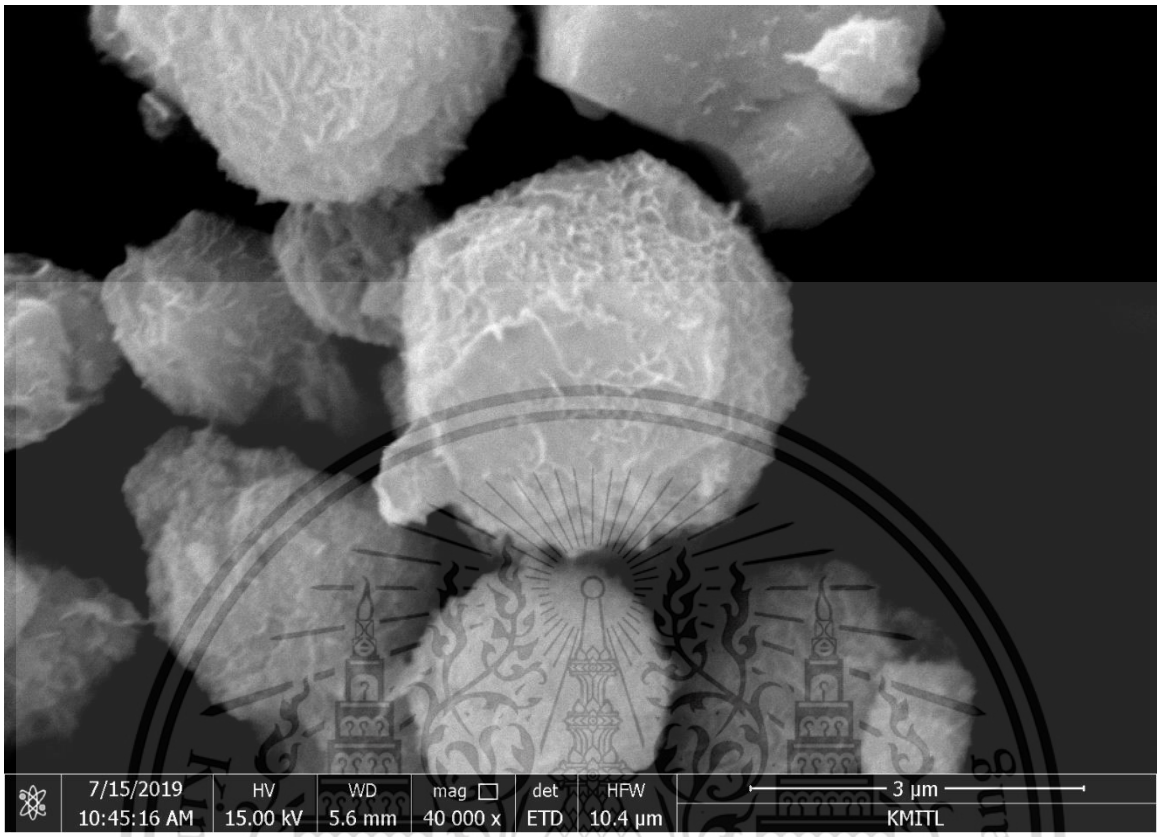

Figure D19 SEM image of 3.3Mg-KNaX

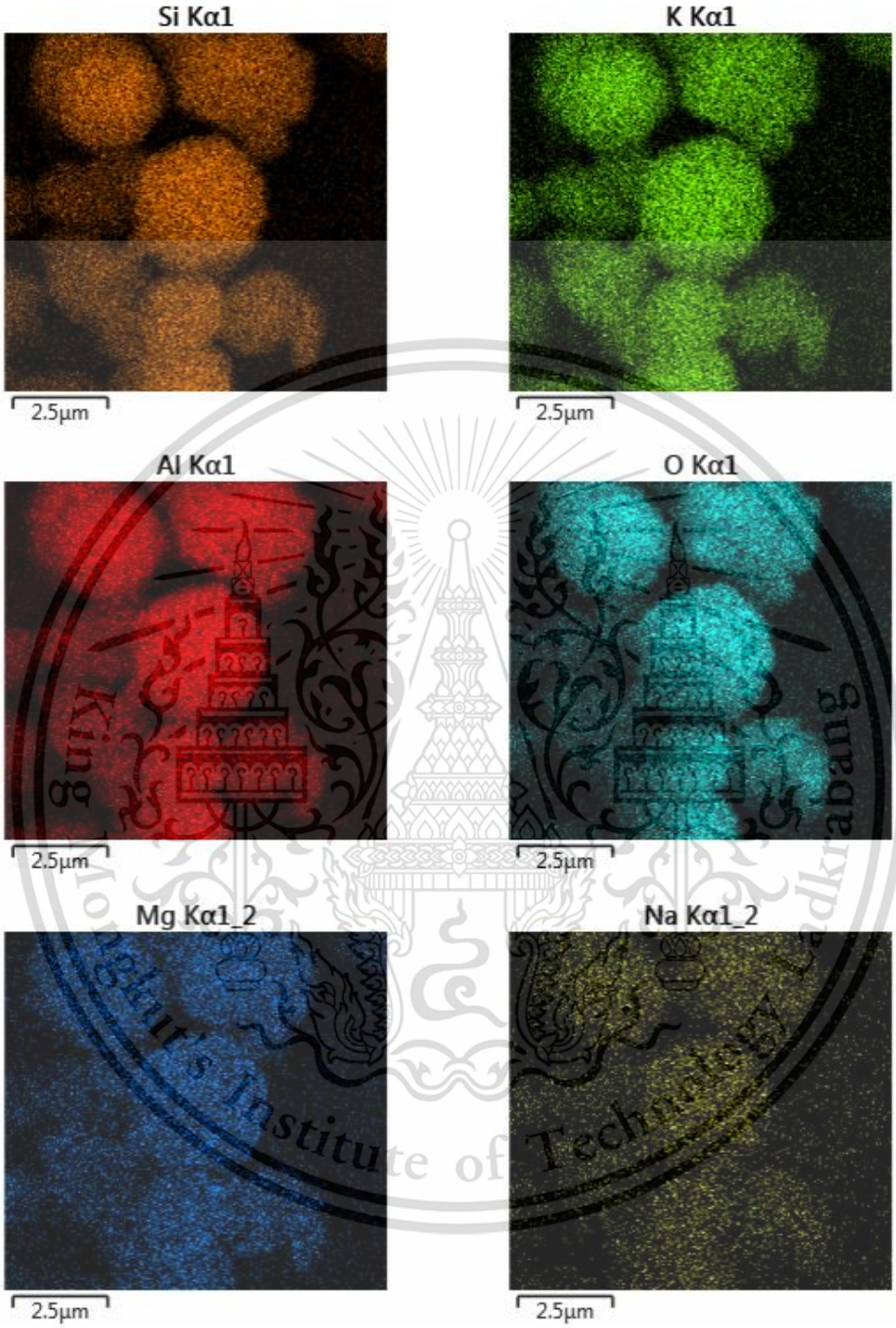

Figure D20 metal dispersion of 3.3Mg-KNaX

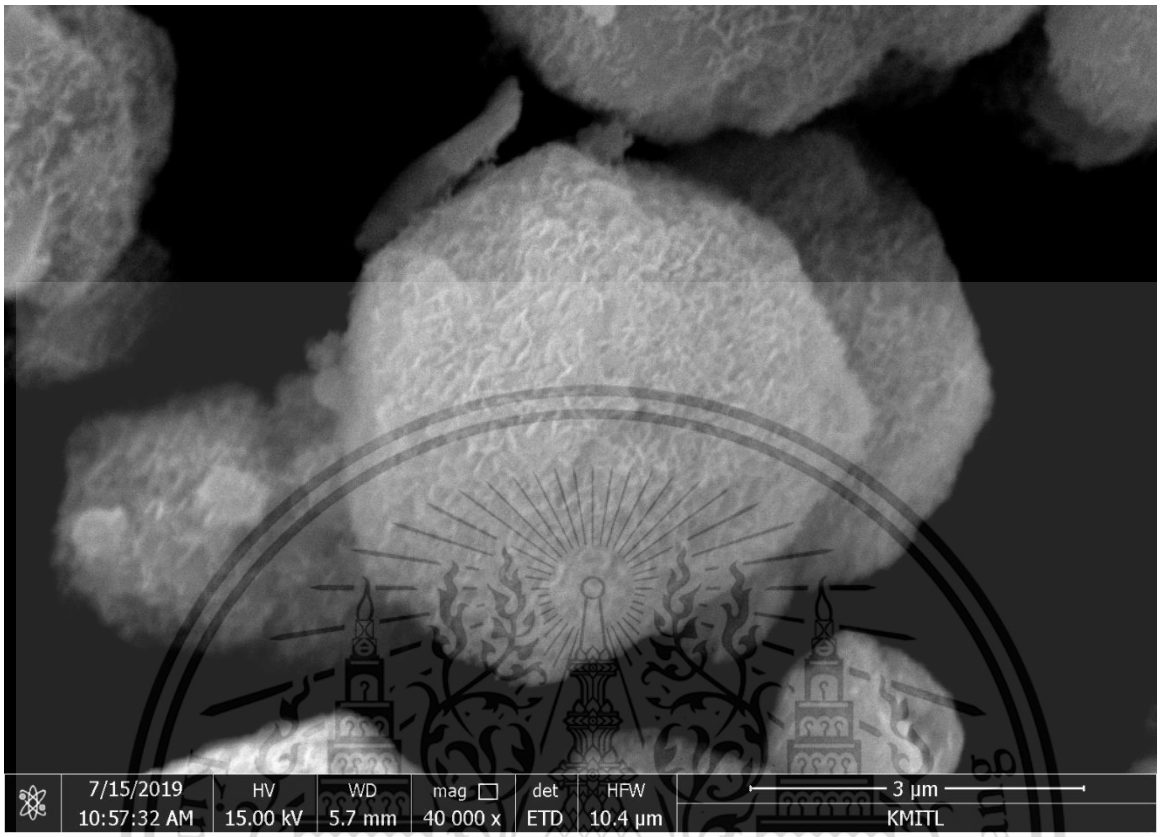

Figure D21 SEM image of 3.4Mg-KNaX

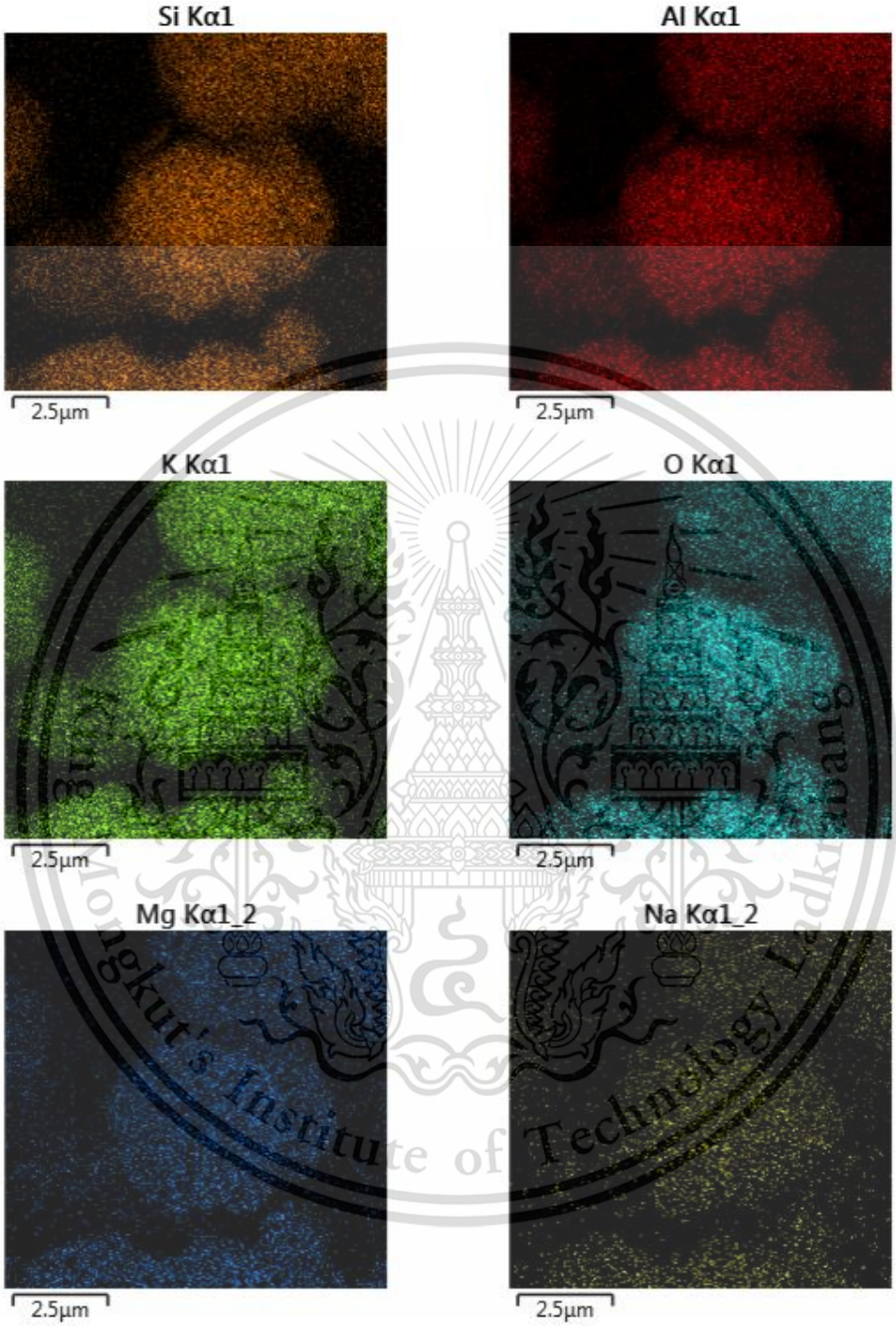

Figure D22 metal dispersion of 3.4Mg-KNaX

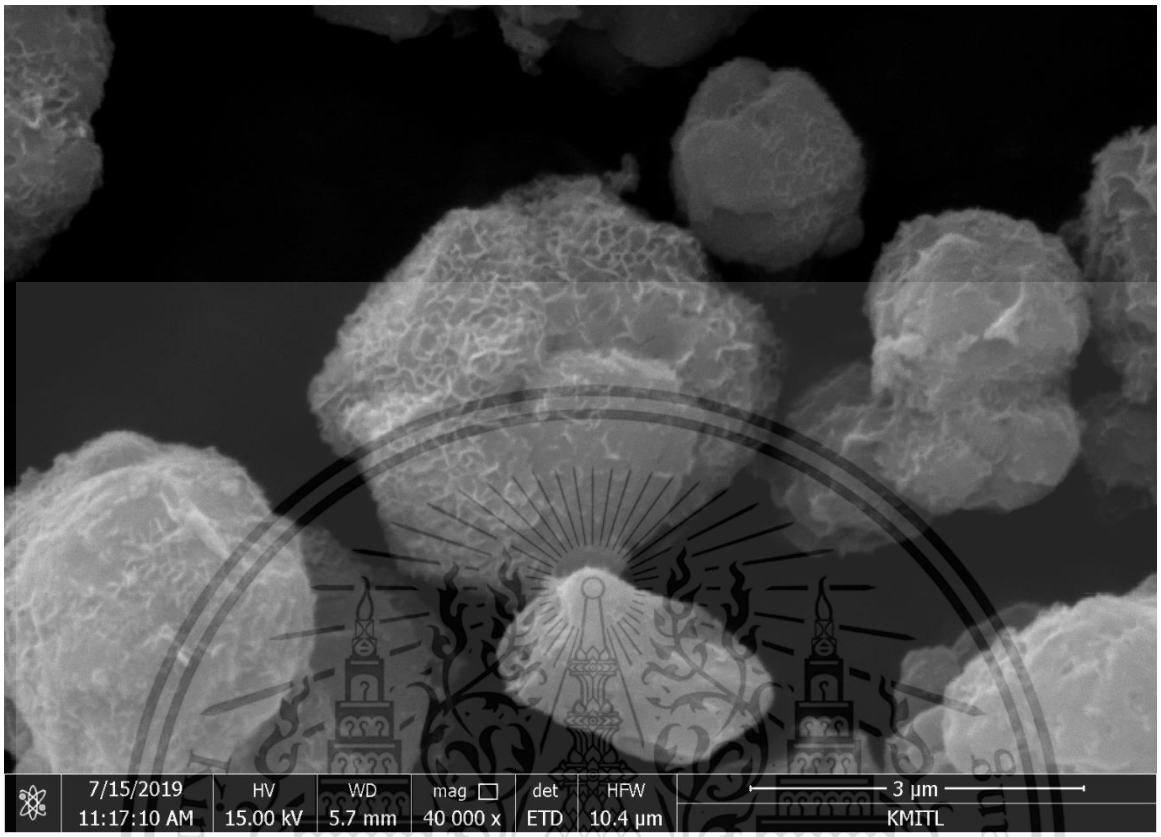

Figure D23 SEM image of 3.9Mg-KNaX

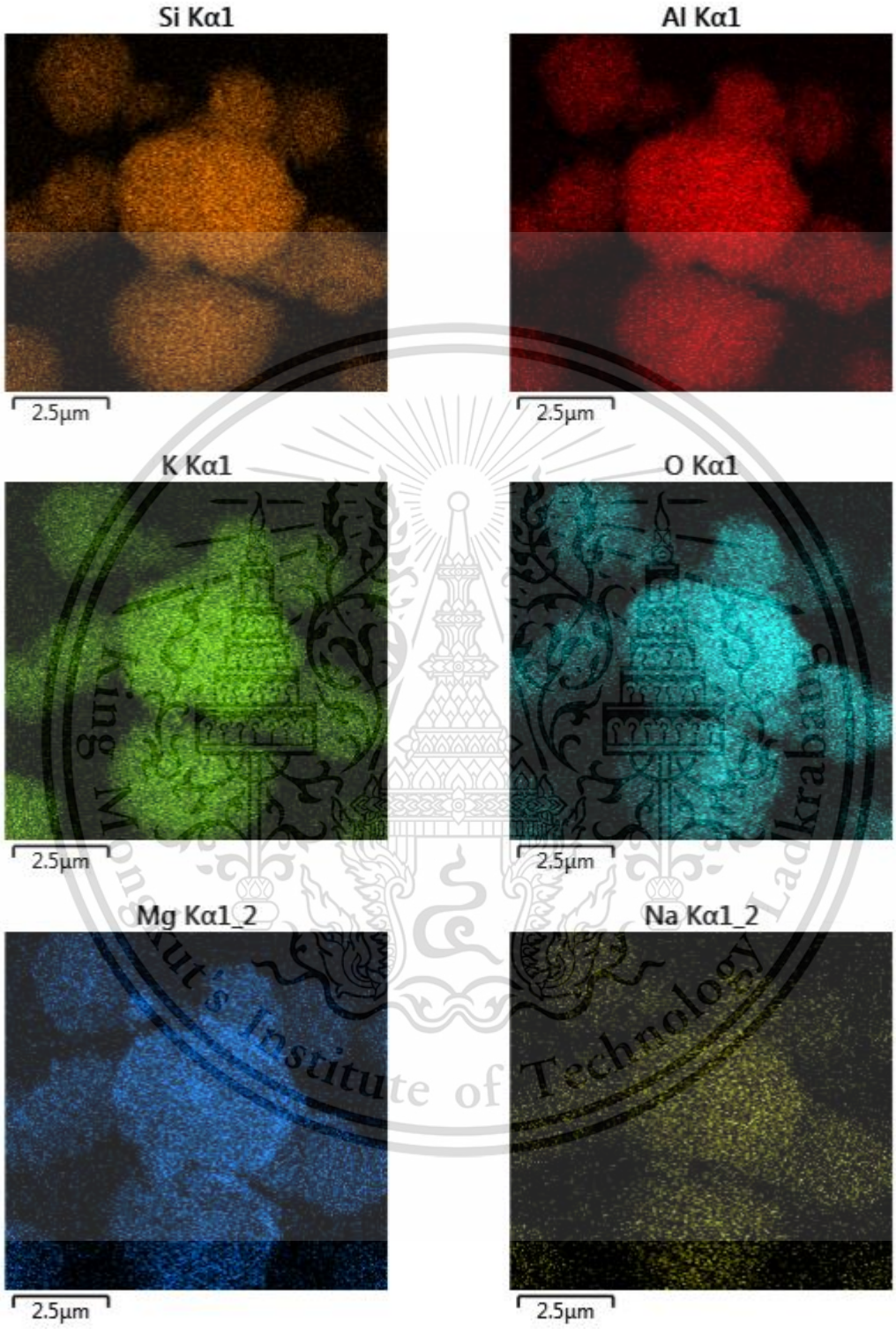

Figure D24 metal dispersion of 3.9Mg-KNaX

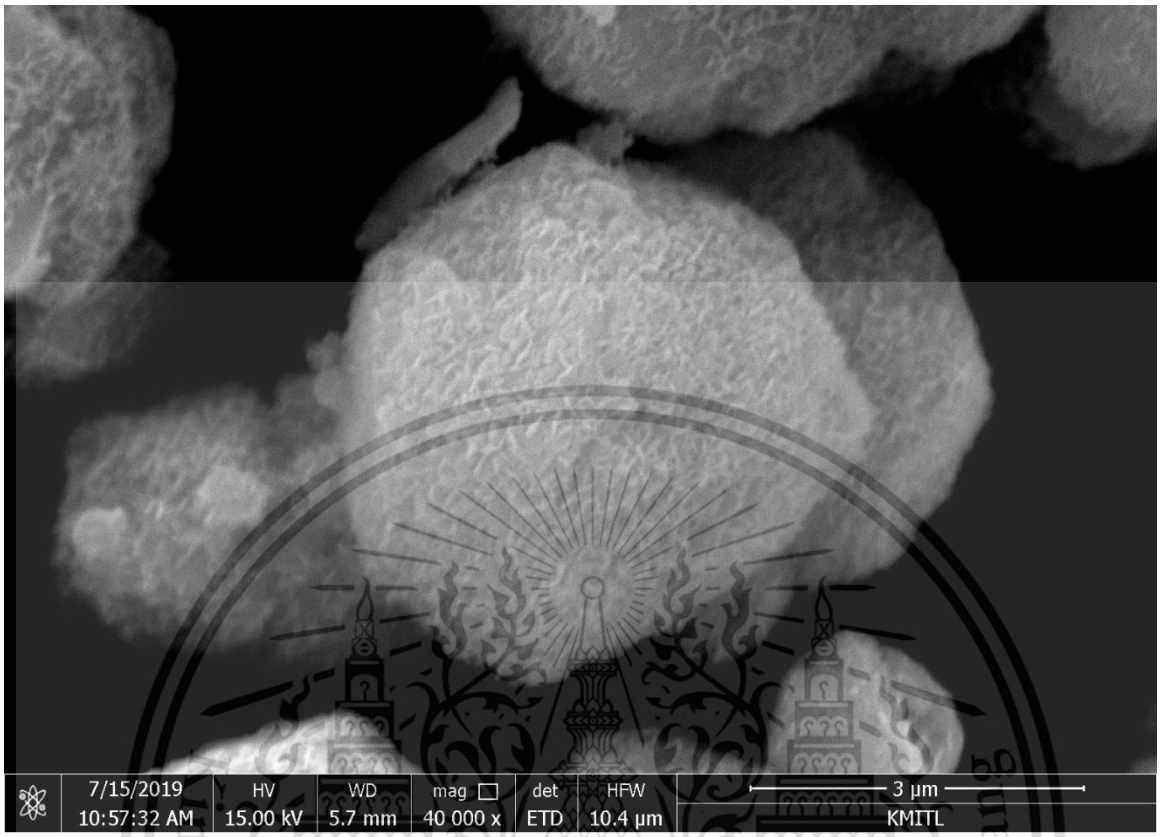

Figure D25 SEM image of 4.3Mg-KNaX

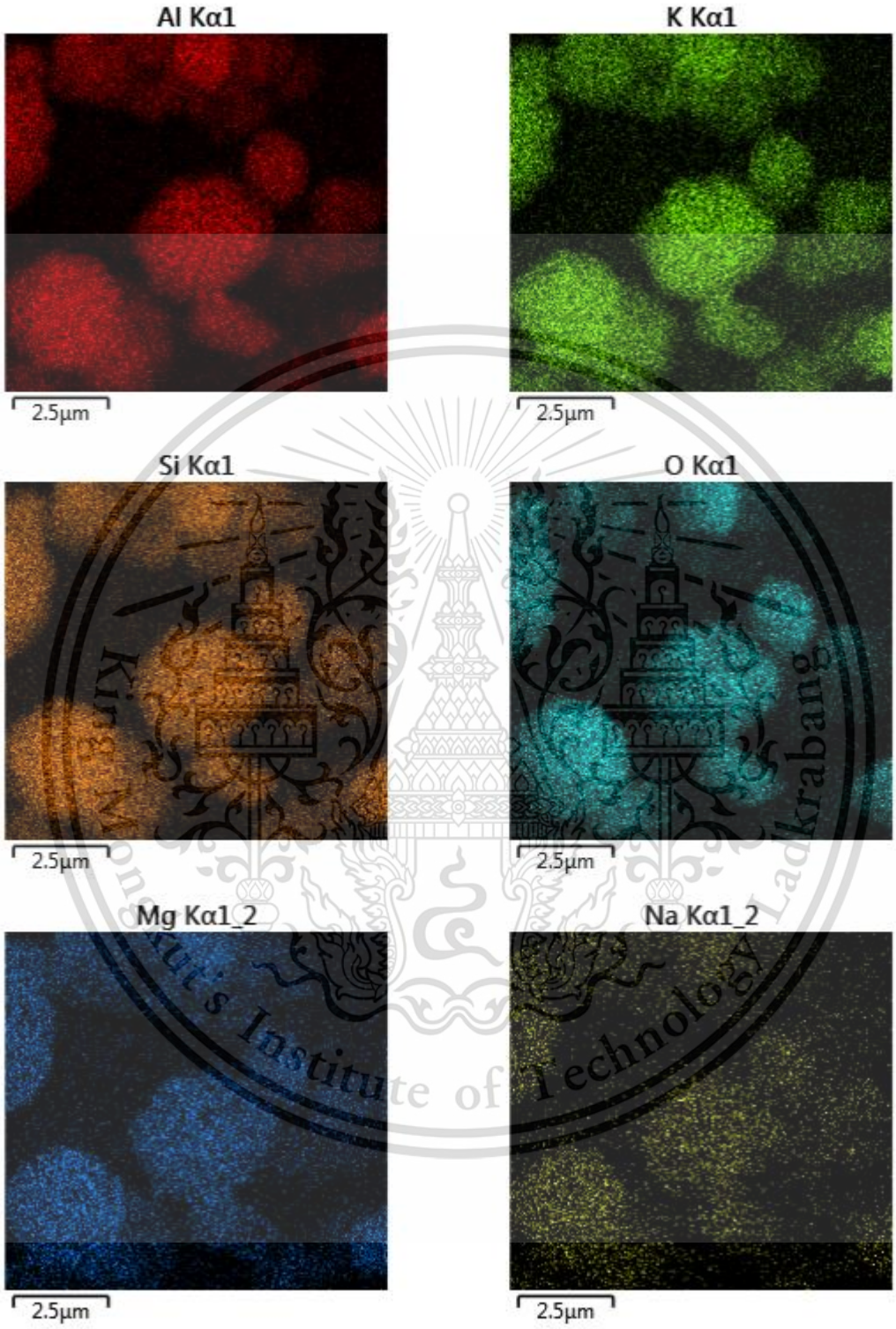

Figure D26 metal dispersion of 4.3Mg-KNaX

Temperature program desorption (NH_3-TPD)

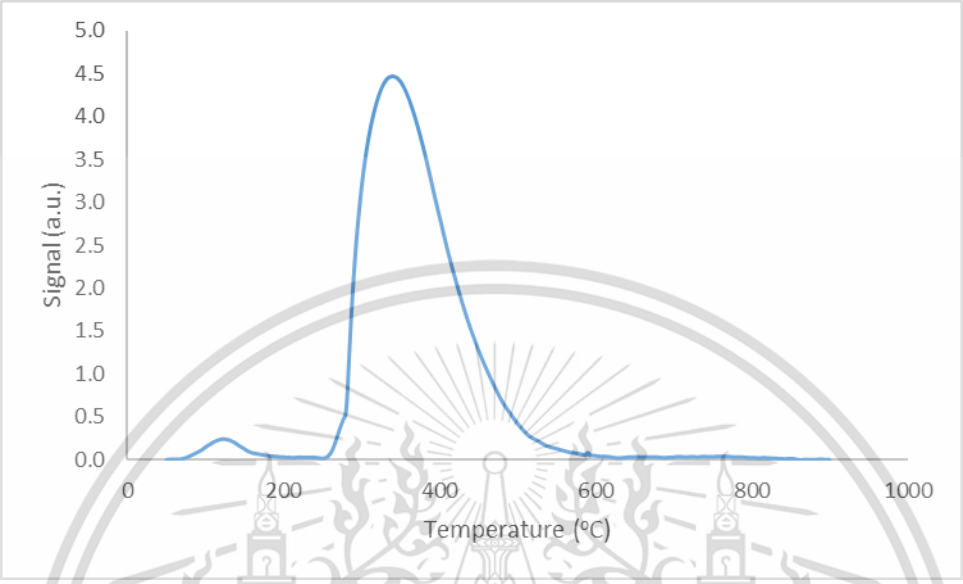

Figure D27 NH_3-temperature programmed desorption profile over NaX

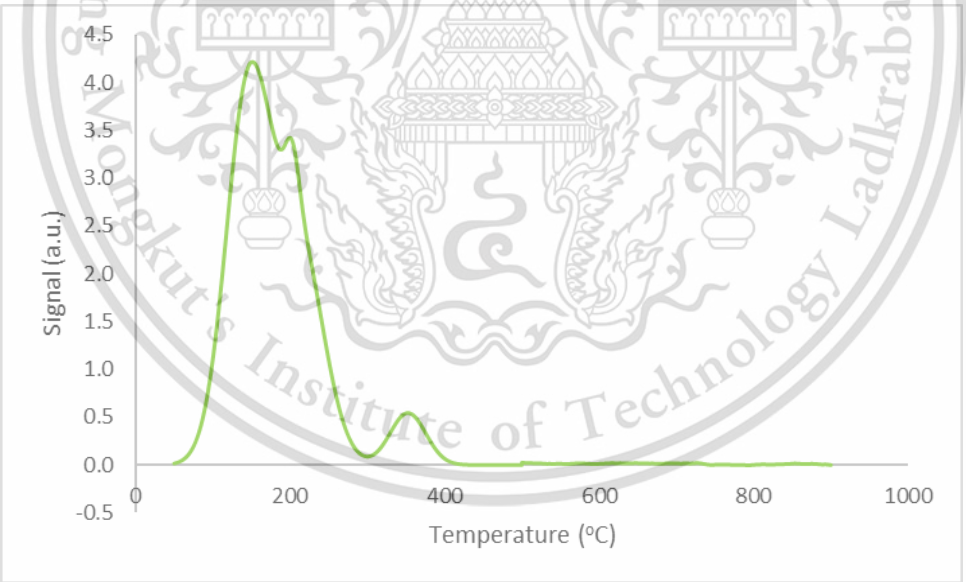

Figure D28 NH_3-temperature programmed desorption profile over KNaX

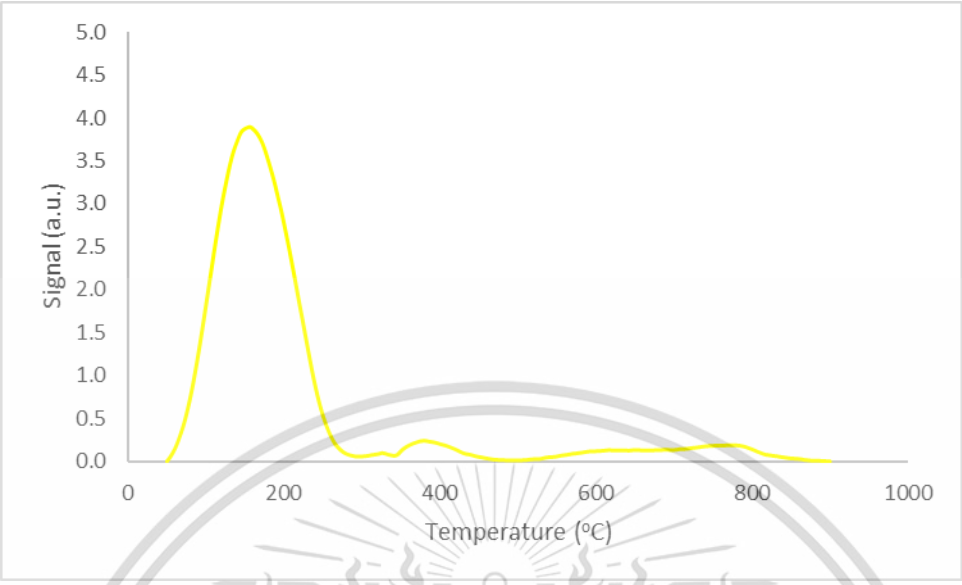

Figure D29 NH_3-temperature programmed desorption profile over 3.1Mg-KNaX

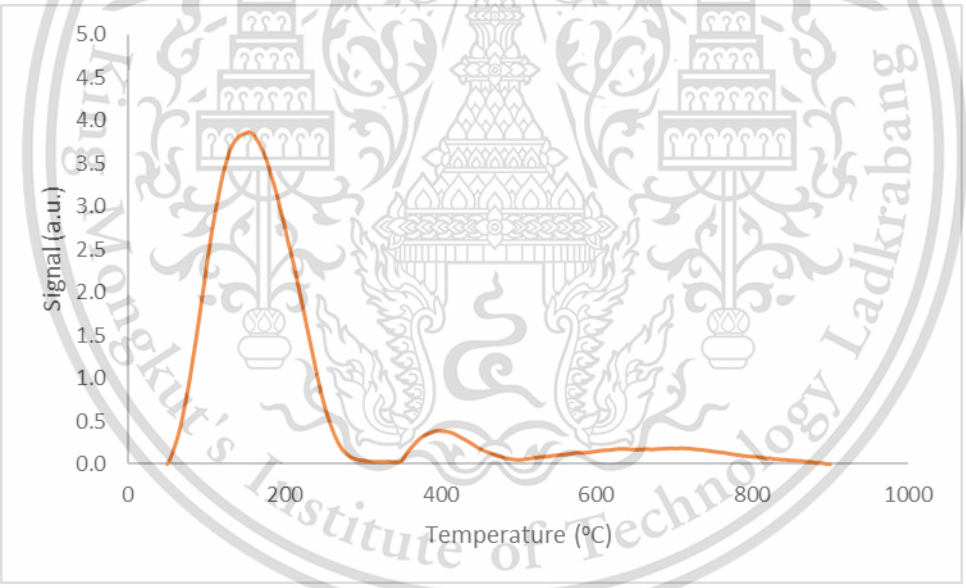

Figure D30 NH_3-temperature programmed desorption profile over 3.3Mg-KNaX

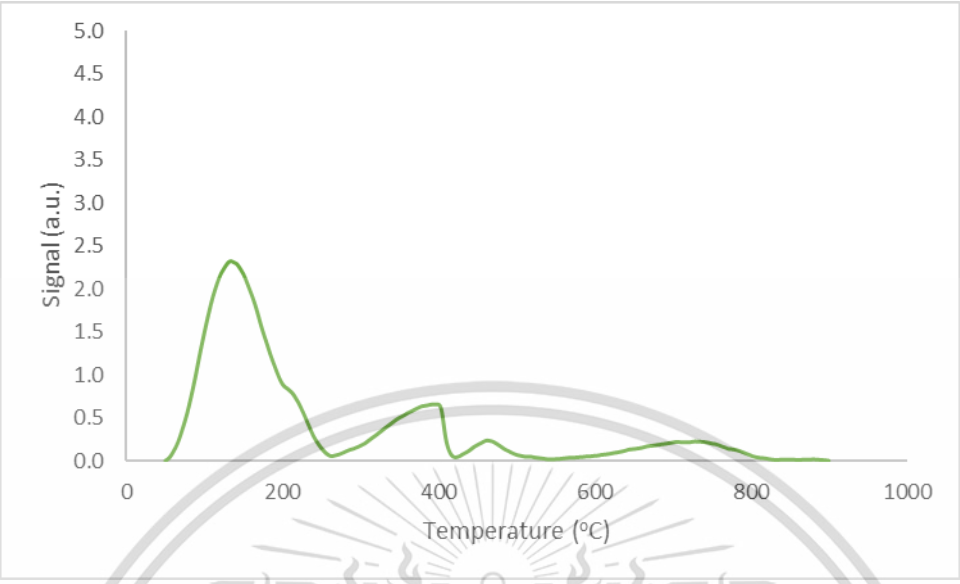

Figure D31 NH_3-temperature programmed desorption profile over 3.4Mg-KNaX

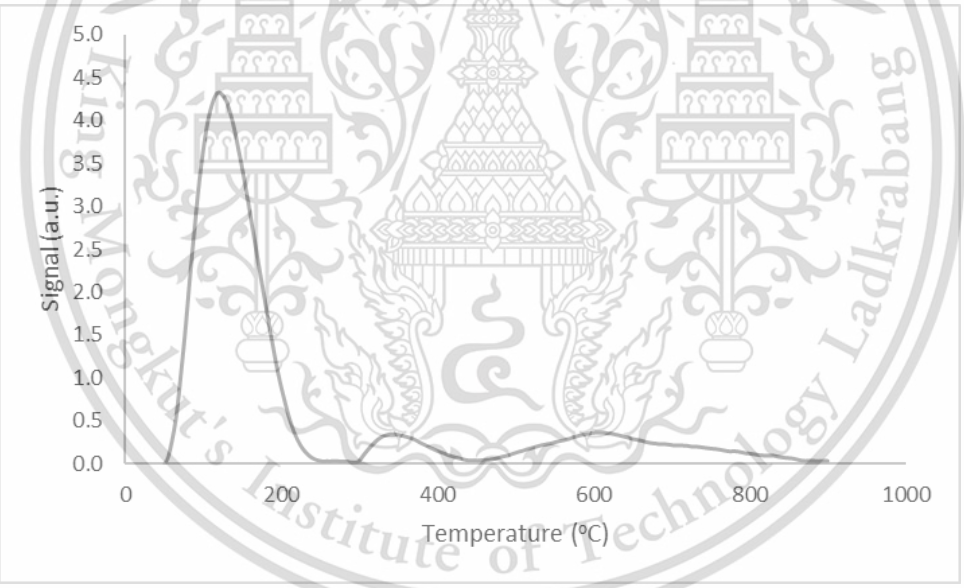

Figure D32 NH_3-temperature programmed desorption profile over 3.9Mg-KNaX

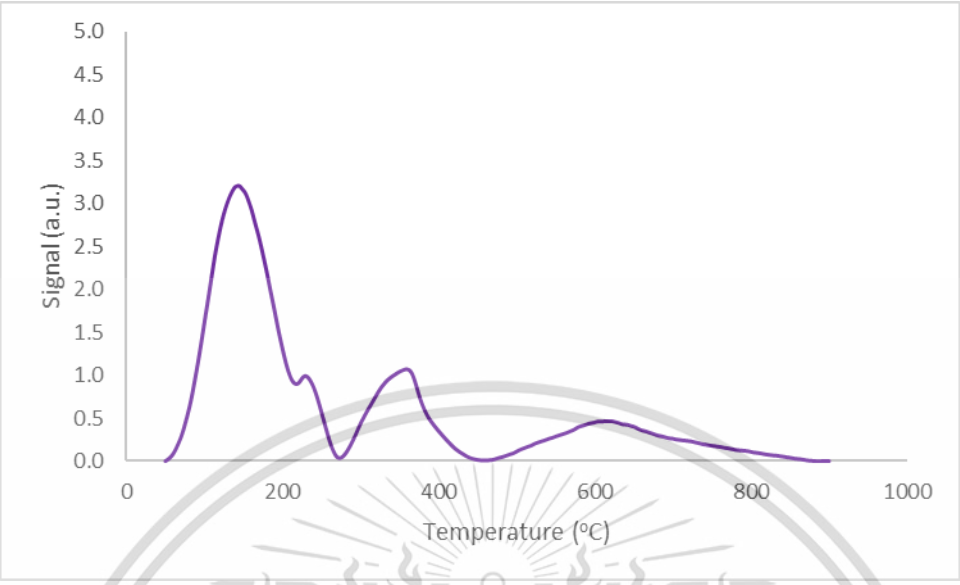

Figure D33 NH_3-temperature programmed desorption profile over 4.3Mg-KNaX

Temperature program desorption (CO_2-TPD)

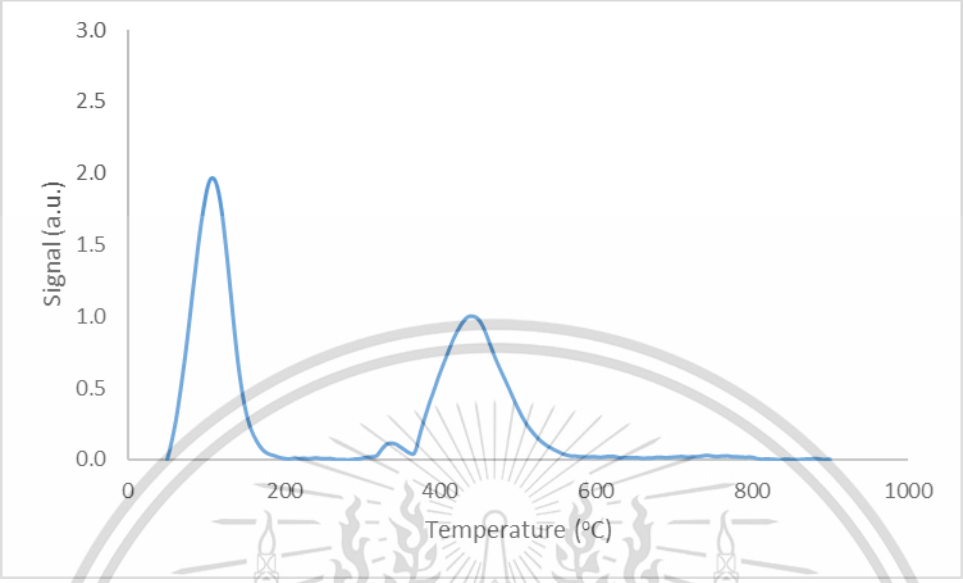

Figure D34 CO_2-temperature programmed desorption profile of NaX

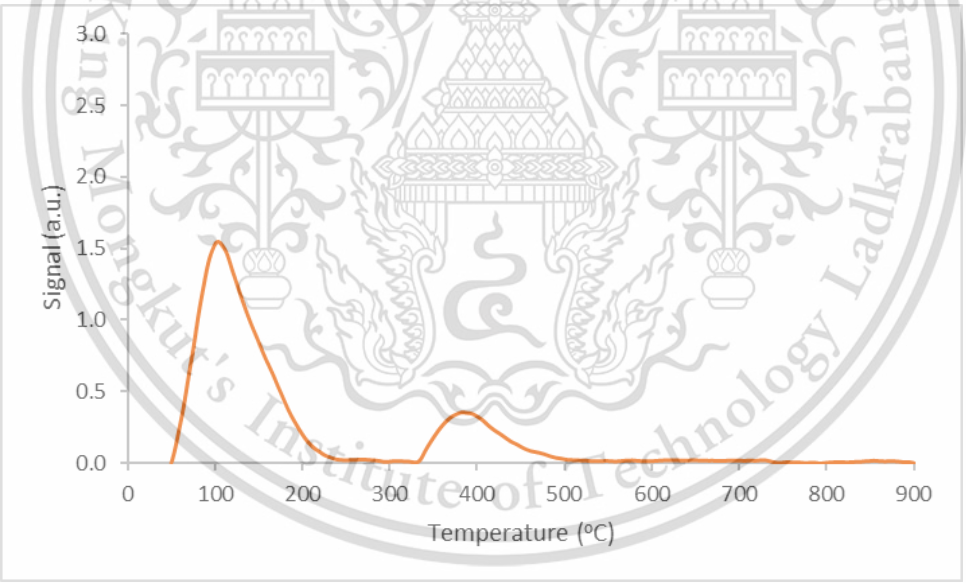

Figure D35 CO_2-temperature programmed desorption profile of KNaX

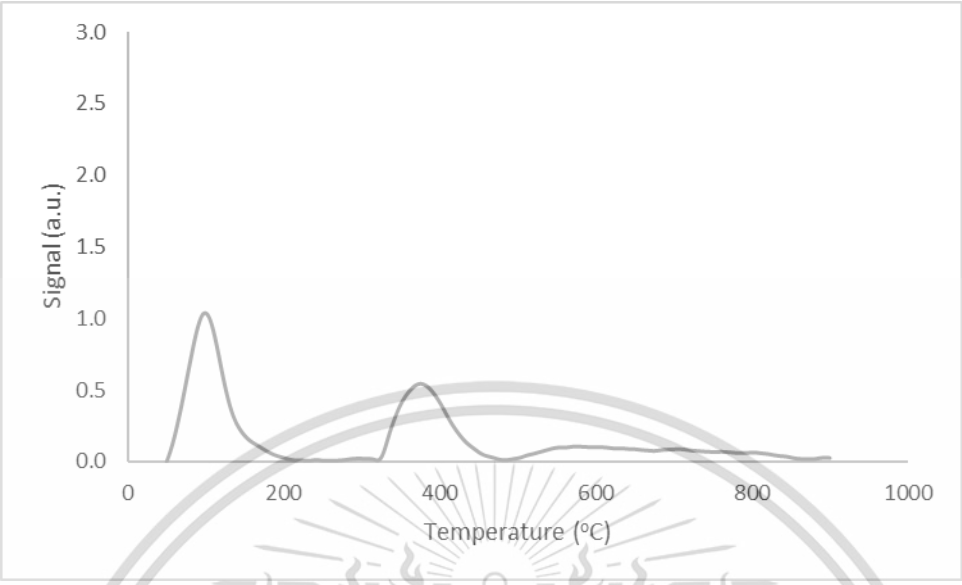

Figure D36 CO_2-temperature programmed desorption profile of 3.1Mg-KNaX

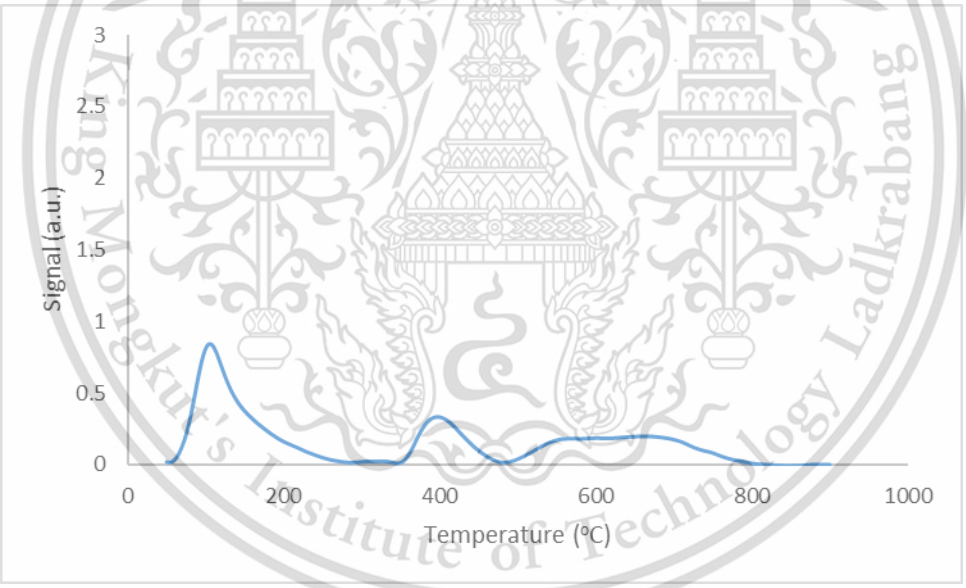

Figure D37 CO_2-temperature programmed desorption profile of 3.3Mg-KNaX

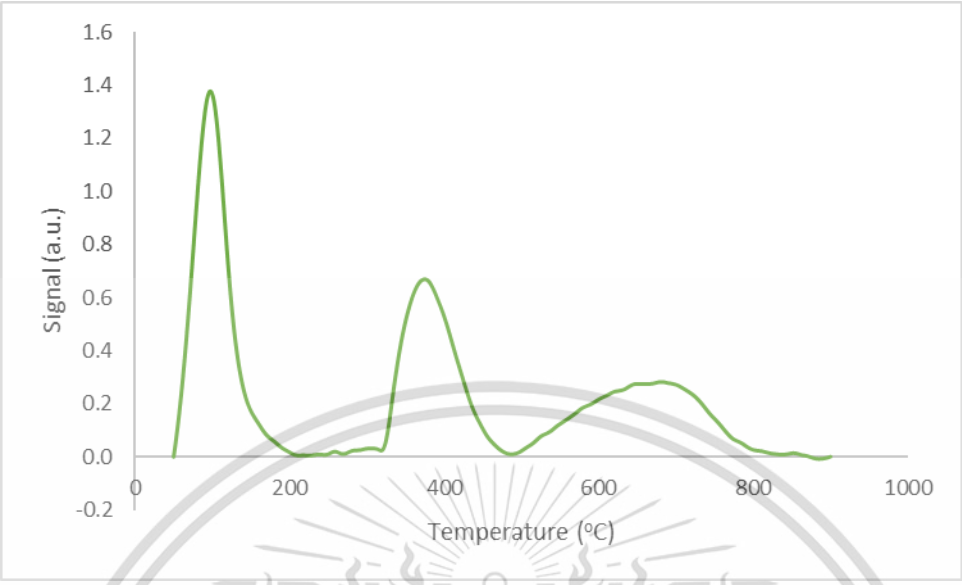

Figure D38 CO_2-temperature programmed desorption profile of 3.4Mg-KNaX

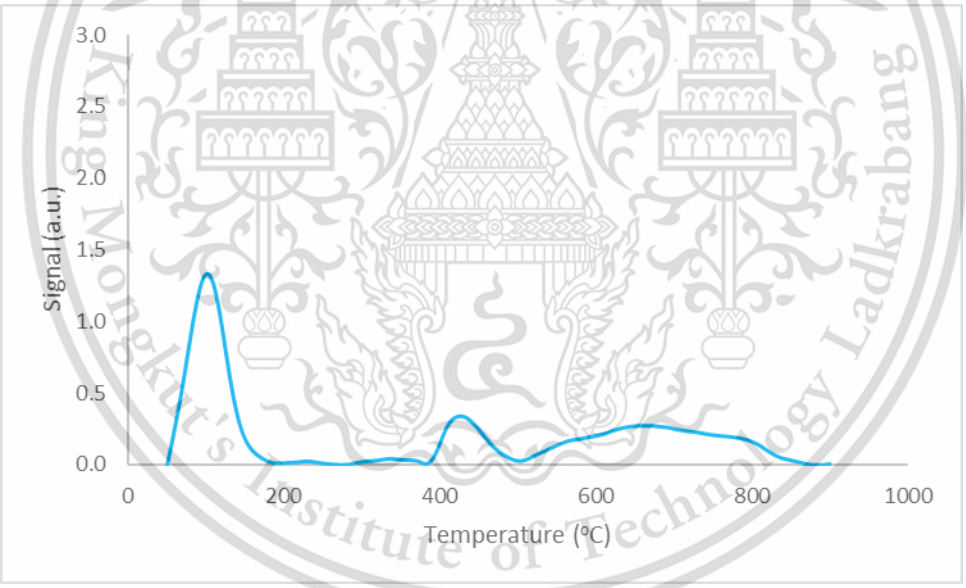

Figure D39 CO_2-temperature programmed desorption profile of 3.9Mg-KNaX

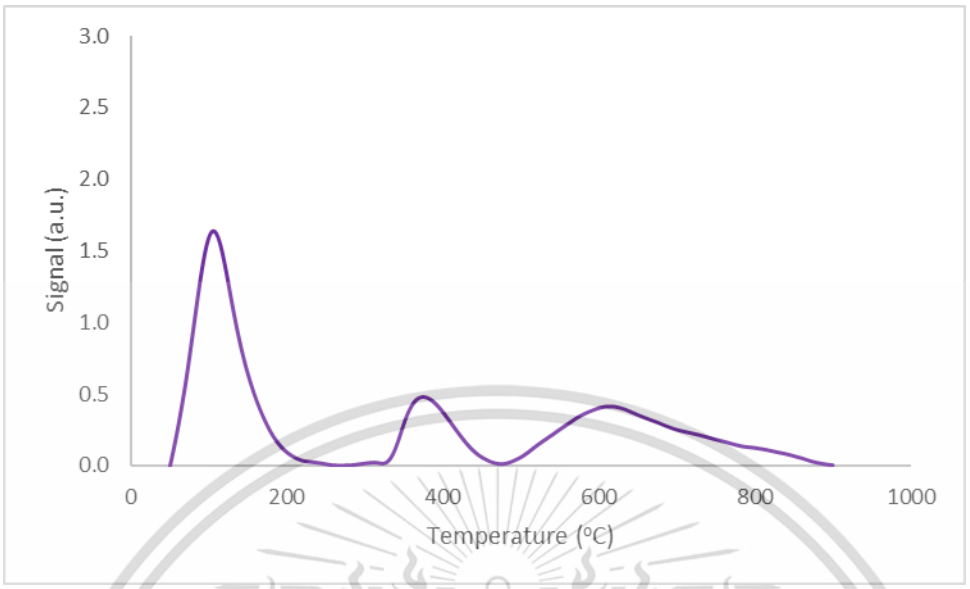

Figure D40 CO_2-temperature programmed desorption profile of 4.3Mg-KNaX

Author Biography

Name Mr. Pittawat Sukkeaw

Date of Birth Day Month Year 27 September 1994

Address 86 Village No.6, Rai Rot Subdistrict, Don Chedi District, Suphanburi Province, 72170

Education (Year) Bachelor of Science in 3.10

(University/ Institute) KING MONGKUT'S INSTITUTE OF TECHNOLOGY LADKRABANG

(Year) Master of Science in 3.31

(University/ Institute) KING MONGKUT'S INSTITUTE OF TECHNOLOGY LADKRABANG

Academic Publication

1. P. Sukkeaw, N. Numwong, T. Sooknoi. "Ethanol conversion to higher alcohols over magnesium oxide modified faujasite catalysts" The 2020 Pure and Applied Chemistry Chemistry International Conference (PACCON 2020), pp. CS30-35